An observation-based analysis of the contribution of aviation emissions to local air quality near Schiphol airport

MSc Thesis

M. Blanke

Technische Universiteit Delft

TU Delft

An observation-based analysis of the contribution of aviation emissions to local air quality near Schiphol airport

MSc Thesis

by

M. Blanke

in partial fulfillment of the requirements for the degree of

Master of Science
in Aerospace Engineering

at the Delft University of Technology,
to be defended publicly on Monday March 1, 2021 at 13:00.

Student number:	4224388	
Project duration:	February 3, 2020 – March 1, 2021	
Thesis committee:	Dr. I.C. Dedoussi	TU Delft, supervisor
	Prof. dr. ir. M. Snellen,	TU Delft, chairman
	Ir. P.C. Roling,	TU Delft

TU Delft Delft University of Technology

Preface

With this project my time at the TU Delft will come to an end. When starting my bachelor in Aerospace Engineering in 2012, I could not have imagined the amazing adventures that I have been able to experience during my time at this university. By finishing this project, it will be time to end this wonderful adventure and get ready for the next phase in life.

I am thankful to my faily supervisor Irene Dedoussi who has given me the opportunity to work on a topic that I felt truly connected to. Besides the interesting topic, I would also like to thank her for all the constructive meetings and feedback throughout the project.

Besides my supervisor, I would also like to thank my family, flatmates and girlfriend for their support during this project. As this project took place during the COVID-19 pandemic, some unexpected challenges arose. But thanks to their support I have still been able to enjoy these final moments as a student.

Mathieu Blanke
Delft, February 2021

Contents

List of Figures

List of Tables

Abbreviations

AEIC Aviation Emissions Inventory Code. 5, 6

AQ Air Quality. 1–5, 10–14, 18, 20–22, 24–29, 31, 32, 34, 38–40, 44, 46, 48, 54

BAU business as usual. 26, 40, 48, 49, 52

CO carbon monoxide. 3–7, 22, 23, 26, 32, 34, 35, 38, 39, 43, 44, 47–49, 52, 54, 84, 85

GAM generalized additive model. 22, 24

KNMI Koninklijk Nederlands Meteorologisch Instituut. 13

LME linear mixed effect model. 22, 24

LTO landing and take-off. 5, 42, 44

NDW Nationaal Dataportaal Wegverkeer. 13

NO nitrogen monoxide. 1, 12, 22, 23, 26–30, 32, 34–36, 38–40, 42, 44, 47–49, 52–54, 84–86

NO_2 nitrogen dioxide. 1, 11, 21–23, 26, 27, 29, 30, 32–40, 42, 44, 47–49, 52–54, 84–86

NO_x nitrogen oxides. 1, 3–7, 39, 53, 54

O_3 ozone. 1, 4, 26, 27, 29, 30, 32, 34, 35, 38, 39, 53, 54

PM_{10} particulate matter with an aerodynamic diameter smaller than or equal to 10 μm. 1, 3, 4, 22, 23, 26–30, 32–39, 42–44, 47, 49, 52–54, 84–86

$PM_{2.5}$ particulate matter with an aerodynamic diameter smaller than or equal to 2.5 μm. 1, 4–7, 22, 23, 26–30, 32, 34, 35, 38, 39, 43, 44, 47–49, 52–54, 84, 85

SD standard deviation. 11, 12

SO_2 sulfur dioxide. 3

Executive Summary

In Europe, three types of pollutants are responsible for the majority of air quality related health threats. These pollutants are nitrogen oxides, ozone (O_3) and particulate matter. Aviation is one of the sources of these pollutants and therefore concentrated areas of aviation activities, such as airports, can lead to elevated levels of local concentrations. Differences in lay-out, climate and operational activities complicate the implementation of one research method and conclusion to all airports. Therefore the need for separate case studies focusing on single airports arises. The aim of this study is to estimate the impact of Schiphol on local concentrations of nitrogen monoxide (NO), nitrogen dioxide (NO_2), O_3 and particulate matter with aerodynamic diameters smaller than 10 (PM_{10}) and 2.5 ($PM_{2.5}$) micrometer in the period of 2014 to 2020.

In order to reach this objective, three different methods were applied. Air quality measurements from 17 locations throughout the Netherlands were compared with measurements taken around Schiphol. This creates an overview of the effects of the direct environment of air quality monitors on observed concentrations. Additionally, wind conditions were linked to air quality measurements. By doing so, local sources of the pollutants of interest could be identified and quantitative estimates of the effects of these sources were made. The third method involved regression modelling. Linear mixed effects models were created for the various pollutants at the three monitoring sites around Schiphol. These models include air temperature, precipitation, wind conditions and hourly road traffic and air traffic parameters and were used to make quantitative estimates regarding the effects of Schiphol on local air quality.

Evaluation of the results of the three methods results in various conclusions. First, the methods were unsuitable to estimate Schiphol's effect on local concentrations of NO, as due to its short atmospheric lifetime fluctuations of concentrations at the air quality monitoring sites are expected to be a result of nearby road traffic. The results for NO_2 are more robust. From January 2014 to August 2020 concentrations of the three monitoring sites near Schiphol were 0.63 $\mu g/m^3$, or 2.7%, higher than the average of all monitoring stations used. Comparison of measurements taken upwind and downwind of the airport perimeter show an increase in NO_2 of at least 5 $\mu g/m^3$ between the three monitoring sites. Peaks can be as high as 10, 14 and 15 $\mu g/m^3$ based on the monitoring site and wind conditions. These peaks result in an increase of local concentrations of between 22 and 53% of the stations' average values from January 2014 to August 2020. Modelling showed that the medians of the observed NO_2 concentrations rose between 24 and 31% due to aircraft take-offs and landings, with peaks up to 48%.

The analysis of PM_{10} concluded that long range transport was the main source of this pollutant. Modelling estimated that aircraft take-offs and landings had a maximum effect of about 17% of local concentrations. But there are some uncertainties about these results, as road traffic parameters were not included in the model for PM_{10} and are likely to be included in the estimated effect. Similar results were found for $PM_{2.5}$, where the estimated median concentrations and relative effects due to aircraft take-offs and landings lie between 0.3 and 1.7 $\mu g/m^3$, which is 3 to 14.4% of the overall ambient concentrations. For O_3 no modelling could be performed and a qualitative negative correlation was found between nitrogen oxides and O_3 concentrations. No quantitative estimates could be made due to a lack of multiple monitoring sites around Schiphol and the availability of measurements.

As the data from 2020 offered information about the special situation due to the COVID-19 pandemic, the previous methods were also applied to data from this period only. This meant that data from March to August 2020 was analyzed separately. The analysis showed that local concentrations of NO and NO_2 decreased by 40 and 29%, respectively, compared with measurements taken in the same months between 2014 and 2019. Quantitative estimates based on regression modelling and the analysis of wind parameters showed that the reduction in flight activities between March and August 2020 led to a decrease of ambient NO_2 concentrations of about 4 to 5 $\mu g/m^3$. Median ambient concentrations of PM_{10} and $_{2.5}$ decreased by 1.2 and 0.9 $\mu g/m^3$, respectively. But these results are based on the regression models only, which means that the earlier mentioned

limitations are also applicable for these results.

By performing a case study on Schiphol airport this study resulted in qualitative and quantitative estimates regarding the impact of the airport on local air quality. Despite the obtained results, improvements can be made for future research. Air quality monitors located directly at the airport perimeter, more accurate flight data sets, improved models and larger data sets are opportunities for future research that will decrease the uncertainties of the results.

1

Introduction

In Europe air pollution is responsible for adverse human health effects and even premature deaths (EEA, 2020). Main contributors to this health threat are three types of pollutants. First, there are nitrogen oxides (NO_x). NO_x consists of nitrogen monoxide (NO) and nitrogen dioxide (NO_2). Both are gases and primary pollutants, which means that they are directly emitted by combustion processes that take place in aircraft engines. The second pollutant type is particulate matter. Particulate matter are particles or droplets with a small aerodynamic diameter. Two types of particulate matter are discussed in this study, namely particulate matter with an aerodynamic diameter smaller than or equal to 10 μm (PM_{10}) and particulate matter with an aerodynamic diameter smaller than or equal to 2.5 μm ($PM_{2.5}$). Both behave as primary and secondary pollutants. This means that they can be emitted directly, but are also formed by chemical reactions in the atmosphere. The final pollutant that will be analysed is ozone (O_3). O_3 is formed by chemical processes in the atmosphere. NO_x plays a major role in the formation and depletion of O_3 (Tiwari and Agrawal, 2018). With the presence of sunlight, NO_2 reacts to O_3 by photolysis, while O_3 can be depleted by NO.

The significance of these pollutants on human health in Europe is highlighted in a report by the European Environment Agency. In their latest report they concluded that elevated levels of $PM_{2.5}$, NO_2 and O_3 were responsible for 417,000, 55,000, and 20,600 premature deaths in Europe in 2018, respectively (EEA, 2020). In terms of aviation related effects, earlier research by Yim et al., 2015 estimated that the number of global yearly premature deaths due to long-term exposure of aviation induced $PM_{2.5}$ and O_3 is approximately 16,000. Previous studies by Unal et al., 2005 and Woody et al., 2016 have also shown that airports are sources of these pollutants that can have a significant impact on local Air Quality (AQ). Considering the resulting social costs of aviation emissions, AQ effects are dominant for areas near large airports (Wolfe et al., 2014) and can even become dominant at other locations if AQ effects due to cruise emissions are taken into account.

Considering these results, this study aims to broaden the understanding about the effects of an airport on local AQ. However, in literature there is a strong consensus that due to the variety in geography, meteorology, airport equipment, aircraft fleet and flight schedules a generic solution for all airports is not readily available (Kim et al., 2015, Koulidis et al., 2020). Due to this dissimilarity between airports the need for separate case studies taking different airports, pollutants and methodologies into account arises. Therefore this research comprises a case study about Schiphol airport. The aim of this study is to estimate the impact of Schiphol on the local AQ in the period of 2014 to 2020.

Once completed the results of this study offer new information about the effects of Schiphol airport on local concentrations of NO_x, O_3, $PM_{2.5}$ and PM_{10}. In order to generate this information a combination of methods that have not been combined before is used. On top of that road traffic data was available and introduced in this study. Previous observation-based studies did not include this parameter, while the presence of roads in the vicinity of airports are often referred to as a source of uncertainties in the final results. Thus, not only will this study combine various methods to estimate the effects of Schiphol on local AQ, but additionally the effects of adding road traffic information to these methods is investigated.

The main research question is defined as follows: is it possible to estimate the contribution of Schiphol Airport to the local concentrations of NO_x, O_3, $PM_{2.5}$ and PM_{10} and what would be these contributions? In order to answer the main question, three sub-questions were defined. The first sub-question considers the measured pollution levels and is formulated as: what are the concentrations measured for the different pollutant species at the ground stations in the area around Schiphol and how do these compare to other locations within the Netherlands? The aim of answering this question is to get a better understanding of the AQ around Schiphol compared to other locations within the Netherlands.

The second sub-question aims to broaden the understanding of the processes that influence AQ at the three monitoring sites near Schiphol. Instead of just looking at AQ over time, the airport's surroundings are analysed in more detail. Formally the second sub-question is: can we find correlations between the available wind data sets and the measured air quality at the three ground measurement stations closest to Schiphol?

The final sub-question is added to analyse whether it is possible to combine the available data sets in order to quantitatively estimate the contribution of Schiphol to the local AQ. The question is defined as follows: is it possible to quantitatively determine the contribution of Schiphol Airport on the local air quality and if so, what would be these contributions for the four species of interest at each measurement station?

Different methods will be applied in order to answer these research questions. But before the methodology is explained in chapter 3, chapter 2 provides a summary of existing literature. Additionally some expectations are created using predicted emissions for Schiphol in 2005 and a simple box model method. These expectations are used to compare with the results of the methods from chapter 3. These results are presented in chapters 4, 5 and 6. Finally, chapter 7 discusses the results of applying the same methods as discussed in chapter 3 on the special situation that arose due to the COVID-19 pandemic in 2020. The conclusion and recommendations for future research are presented in chapter 8.

2

Background and expectations

Before explaining the methodology and results of this research in detail, this chapter will provide an overview of the current understanding about the research topic. This will be done based on existing literature. The results of previous studies, combined with some preliminary calculations based on a simple air quality model also present opportunities to generate some expected results. These expectations were used as a way to test the reliability of this study's results. Section 2.1 summarises the existing literature, while section 2.2 explains reference values used for this study and the method to create these values.

2.1. Existing literature

Airports are located in different climates all around the world. On top of that every airport is unique as it can feature its very own lay-out suitable for its main activities. As a result various case studies have been performed to analyse the effects of the airports on local AQ. This section presents these observation-based studies, including their methodologies and results.

Two studies taking AQ measurements and wind parameters into account were performed by Yu et al., 2004 and Carslaw et al., 2006. Their studies examined the concentrations of pollutants such as sulfur dioxide (SO_2), NO_x, PM_{10}, and carbon monoxide (CO) measured in the vicinity of the airport. The main part of these studies investigated the effect of wind speed and direction on the measured values. The correlation between wind parameters and observed concentrations could then be analysed. This was done by locating potential nearby pollution sources, setting up hypotheses about how these could affect the concentrations at the measurement locations and finally comparing these hypotheses with the results. The study by Yu et al., 2004 concluded that emissions from ground vehicles that supply the airport dominate the emissions from aircraft for CO and NO_x at Los Angeles International Airport. However, the same study found that near Hong Kong International Airport, aircraft operations seem to contribute significantly to ambient concentrations of CO and PM_{10}.

The study by Carslaw et al., 2006 applied a similar methodology to a case study at Heathrow Airport. However, the correlation was graphically presented by the use of polar plots. A polar plot can be compared with a wind rose as it is a two-dimensional coordinate system whose coordinates are defined by a distance from a reference point and an angle from a reference direction. The reference point is the origin of the graph, while the reference direction is North. In the study by Carslaw et al., 2006, the wind direction is represented by the angle and the radius represents wind speed. The corresponding average pollutant concentration at each coordinate is shown by a color scale. These plots, in combination with a map create a convenient method to identify the wind directions responsible for increased pollution levels and vice versa. Additionally, they have shown that when multiple AQ monitoring sites are present at different locations around the airport's perimeter background subtraction is possible. By subtracting measurements taken upwind of the airport from downwind measurements, the potential quantitative effect of the area in between these stations on observed concentrations can be approximated. Of course, this does not necessarily contain only the direct effect of airport related pollution, as other pollution sources could be present as well. Nevertheless, it offers a simple method to estimate the effect of the airport based on wind parameters and air quality measurements only. The case study at Heathrow Airport concluded that even though the airport is an important emission source,

it is not the main contributor to local concentrations of NO_x. They found that at the airport fence about 27% of the measured NO_x level is due to airport operations, while these numbers are estimated to have an upper limit of 15% at 1-1.5 km from the airport. These are considered upper limits as more detailed conclusions are difficult to draw due to the presence of other sources such as road traffic. Schiphol also has several busy highways located right next to and even splitting the airport's grounds. Thus, this limitation could also play an important role in this case study.

Another observation-based study was performed by Dodson et al., 2009. Their study analyzed black carbon (part of $PM_{2.5}$) levels measured in the vicinity of T.F. Green airport (RI, USA) by using AQ measurements of four fixed AQ monitoring sites at different locations around the airport. Their approach contained the implementation of a regression model to estimate the quantitative effect of several parameters on the AQ measurements. Besides meteorological parameters such as wind speed, wind direction, temperature, and mixing height, aircraft take-offs and landings were also included in the model. This study demonstrated that such a regression-based approach with detailed meteorological and pollution source parameters can provide valuable insights about the source contributions to black carbon near an airport. One of the limitations of the study by Dodson et al., 2009 was the lack of road-traffic parameters in the model, even though this could be an important source of black carbon emissions. During this thesis study, the regression modelling method from Dodson et al., 2009 will be extended to other pollutants as well. Moreover, over the full measurement period of the AQ monitors hourly road traffic information is available. Therefore, a road traffic parameter will be added to the models.

Most studies concluded that even though airport contributions to local AQ concentrations can be identified, other sources are the main contributors to higher local NO_2 levels. An example is the study by Popoola et al., 2018, in which they concluded that at Heathrow airport approximately 75% of the annual mean concentrations were caused by non-airport related sources. Additionally, Diez et al., 2012 also concluded that other sources are dominant over airport effects. Nevertheless, near a departure runway at Los Angeles International Airport significantly higher concentrations of NO_x and a drop in O_3 were found approximately 1-2 minutes after flight departures. A review paper written by Masiol and Harrison, 2014 supports this statement. Taking these results into account suggests that at the monitoring sites around Schiphol similar effects will be observed. In order to further improve expectations, the next section introduces a simple air quality model that was used to generate some quantitative predictions applicable for Schiphol.

Even though this method can be used for , CO and $PM_{2.5}$, it does not produce expected values for O_3 and PM_{10}. PM_{10} is actually not considered one of the main species relevant for aviation related AQ effects. A previous study by Dassen et al., 2006 about the effects of Schiphol on local concentrations of PM_{10} estimated that in 2020 Schiphol would be responsible for maximally 3% of the ambient PM_{10} concentrations. This is an absolute concentration of about 1 $\mu g/m^3$. As no other reference values can be calculated or found in existing literature, this will be taken as a reference value for this pollutant.

For O_3 it will also be hard to determine the direct relationship between aircraft emissions and local concentrations as it is not emitted directly. Nevertheless, two studies by Pison and Menut, 2004 and Song et al., 2015 have modeled the effects of airport operations on local O_3 levels in Paris and South Korea, respectively. Both studies found that in the vicinity of the airports O_3 concentrations decreased significantly, while at background sites further downwind from the airport O_3 levels increased. Around the airports in Paris the largest decrease of O_3 was between 5.3 and 6.5 $\mu g/m^3$, while around the airports in South Korea the reductions were between 4 and 7 $\mu g/m^3$. The values in South Korea meant decreases of local concentrations from 18 to 33%. The main reason for the decrease was the fast O_3 titration by NO emissions from aircraft, this effect was largest at night. In both studies it was found that ozone concentrations increased at rural background sites. The maximum elevations of ozone levels at two background sites near Paris were 3.8 and 6.5 $\mu g/m^3$.

The most recent studies analyzing the effects of Schiphol on local AQ are Dassen et al., 2006 and Janssen et al., 2019. The first analyzed the impact of Schiphol on local concentrations of PM_{10} and has already been mentioned in this section. The latter, on the other hand, was commissioned by the Dutch ministry of health, welfare and sport and investigated the health effects of ultrafine particles on people living in the vicinity of Schiphol. No further studies investigating the pollutants discussed in this thesis have been found, as a result this project will aid the understanding of the airport's effect on ambient AQ.

2.2. Expectations based on estimated emissions and a box model

Based on the Aviation Emissions Inventory Code (AEIC) emission model created by Simone et al., 2013, the emissions of NO_x, $PM_{2.5}$ and CO produced by ground support equipment and aircraft taking off and landing at Schiphol can be estimated. The model uses the method from Stettler et al., 2011 to estimate landing and take-off (LTO) emissions based on a flight schedule from 2005 provided by the Official Airline Guide (OAG, 2005). This section will explain how the emissions calculated using this model were converted to expected effects of aircraft movements at the AQ monitoring sites. These expectations will be used in chapters 4, 5 and 6 to check the results of those chapters with the expected order of magnitude.

2.2.1. Methodology

The emissions calculated by the AEIC model are taken as the input for this method. So, once these emissions are known they have to be translated into expected concentrations observed at the three measurement stations surrounding the airport. This will be done using the simple box model (Seinfeld and Pandis, 2016). The box model is the most basic air quality modeling algorithm and its mathematical formulation is given by equation 2.1.

$$\frac{dc}{dt} = \frac{Q}{H} + R + \frac{S}{H} + \frac{u}{\Delta x}(c_0 - c) \tag{2.1}$$

The box model assumes that emissions are equally distributed over a fictitious box with dimensions Δx, Δy and H, which respectively represent the sides and height of the box as shown in figure 2.1. Q is the mass emission rate per area in $kgm^{-2}h^{-1}$ and is determined by dividing the estimated emissions predicted by the AEIC model by the ground area of the box and the amount of seconds in an hour. u is the wind speed in m/s. In order to keep the model simple, the chemical production rate (R) and removal rate (S) are set to 0 and steady state is assumed ($\frac{dc}{dt} = 0$). Finally, c and c_0 are the pollutant concentration in the control volume and the background level, respectively. As the model should determine the elevated concentrations in the area due to airport activities, the actual value of interest is $c_0 - c$. Assuming steady-state and ignoring chemical production and loss, the equation to determine the values of interest becomes:

$$c - c_0 = \frac{Q\Delta x}{Hu} \tag{2.2}$$

The height of the box (H) represents the assumed mixing height. In order to choose a relevant value for this parameter existing literature was consulted. The mixing height defines the height above the surface over which it is expected that a pollutant will be dispersed. The mixing height can vary strongly throughout the day. Lowest values (about $100m$) are typically observed during the night, while daytime values range between 1000 and $2000m$ (Davies, 2012). The mixing height is inversely related to the estimated concentration in equation 2.2. In order to keep estimates conservative, i.e. to create a maximum estimate, the minimum daytime value of $1000m$ will be used in this model.

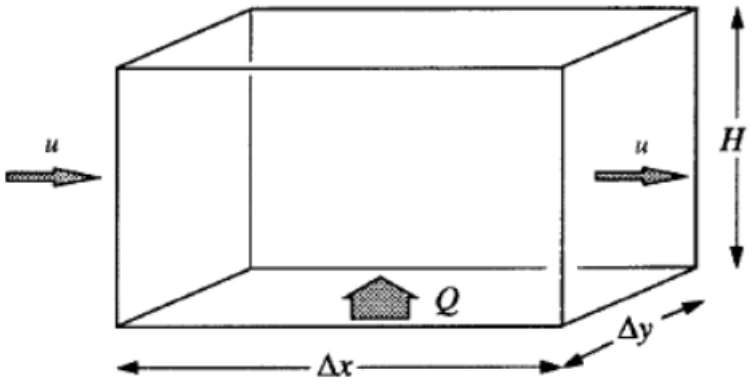

Figure 2.1: Graphical representation of the box model. (Seinfeld and Pandis, 2016)

Finally, the box has to be placed on top of the area of interest. Figure 2.2 shows the areas used in the model as well as the relevant wind directions. For stations Badhoevedorp and Oude Meer (see table 3.6 and figure 3.5) the entire black box is used and the wind is assumed to come from the directions shown by $u2$ and $u1$, respectively. As the station at Hoofddorp is located in the large box used for the other stations, another solution had to be found. For this reason an alternative area was used to create reference values at this location. First, the blue area and winds from $u3$ were considered. However, the hourly emission values from the model assume all airport activities, while for this example the Polderbaan is outside of the area. A quick correction for the emission values was therefore put in place. This correction was done based on some usage data. According to a report by To70, 2016 about 32% of the landings and take-offs at Schiphol occur at the Polderbaan. On top of that, from the emission data from the AEIC model it seems that aircraft movements are responsible for about 89% of the total NO_x emissions at Schiphol. Ground support equipment is responsible for the other 11%. So, in order to get a basic correction the emissions are multiplied by $1-(0.89*0.32)$, i.e. 0.72. For winds from the direction of $u1$ this same methodology, but inversed, can be applied.

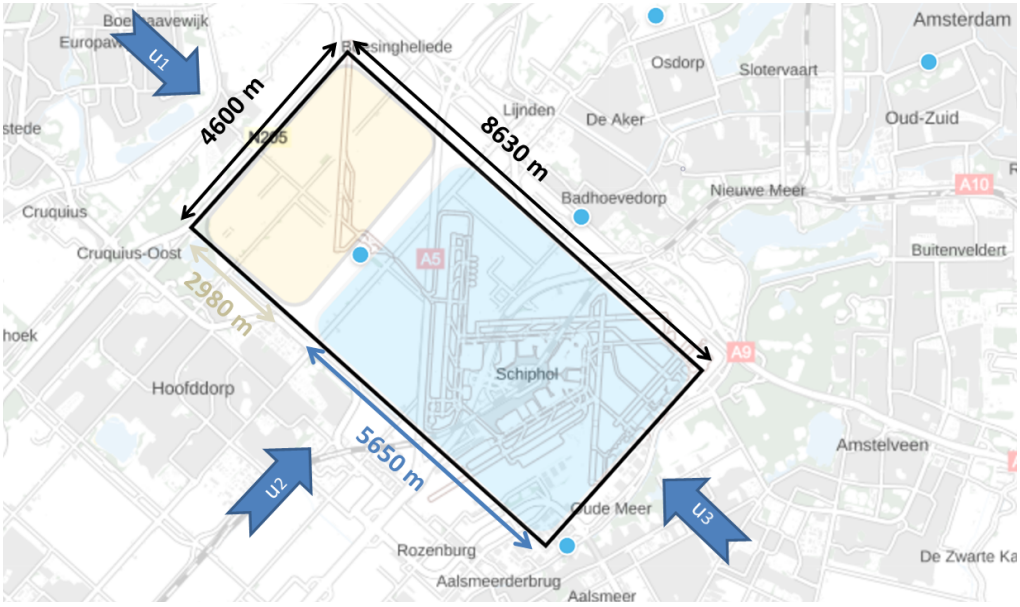

Figure 2.2: The areas used for the box model including their dimensions and the wind directions. The base map is taken from www.luchtmeetnet.nl.

2.2.2. Results

With the methodology explained earlier expected concentrations of NO_x, $PM_{2.5}$ and CO are calculated and shown in figures 2.4, 2.5 and 2.6, respectively. In order to efficiently show the results the expected concentrations are shown based on the number of flights per hour and the time of day for different wind speeds. Wind speeds of up to $10 m/s$ were taken into account, because the predicted values converge at high wind speeds. Additionally, in the period from January 2014 until August 2020 just 4% of the measurements showed wind speeds higher than $10 m/s$. The distribution of wind speeds measured at Schiphol are shown in figure 2.3.

To start with NO_x, figure 2.4 shows that there are some variations with respect to the expected values per station. The largest effect of the airport is expected at Hoofddorp and can be approximately 40 $\mu g/m^3$ during the peak at 2 o'clock at low wind speeds. The majority of anticipated values lie between 0 and 10 $\mu g/m^3$. These values are expected to be observed at the majority of times, as 94% of the wind measurements are higher than 1 m/s. The aforementioned predictions were based on winds from the South-East, which is the direction of the main terminal and five of Schiphol's six runways. Additional approximations were calculated for winds from the opposite direction. In this case, the expectations range between 0 and 3 $\mu g/m^3$. At Badhoevedorp and Oude Meer the expected effects are slightly lower. For the latter the highest value is about 30 $\mu g/m^3$, while this is 17 $\mu g/m^3$ at Badhoevedorp. But similar to the predictions for Hoofddorp, the majority of the expectations are lower and range between 0 and 10 $\mu g/m^3$ and 0 and 5 $\mu g/m^3$ at Oude Meer and Badhoeve-

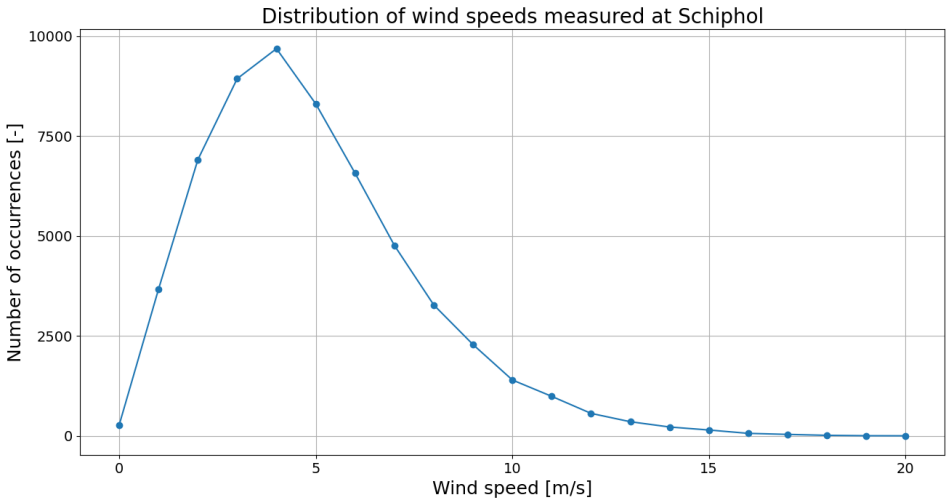

Figure 2.3: Wind speeds measured at Schiphol between 1 January 2014 and 31 August 2020. Data from KNMI, 2020.

dorp, respectively.

Similar to the graphs of NO_x, the results for both $PM_{2.5}$ and CO show a high maximum prediction at low wind speeds while the values converge at wind speeds above 3 m/s. For $PM_{2.5}$ the highest concentration expected is about 0.11 $\mu g/m^3$, while the majority of expectations lie between 0 and 0.02 $\mu g/m^3$. The predictions for CO from figure 2.6 show a maximum of 14 $\mu g/m^3$ while the majority of predictions range from 0 to 4 $\mu g/m^3$. These predictions are only generated for Badhoevedorp, because this is the only station that monitors these species.

According to the predictions there are some differences between the expected effects at the different locations that measure NO_x. These results should however be used with caution. First of all the emissions were estimated using a flight schedule and aircraft composition from 2005, while this study focuses on the situation from 2014 to 2020. Additionally ground support equipment is part of the emission estimates, which also adds uncertainties as equipment and procedures might have changed. Moreover, assumptions had to be made regarding the emissions of ground support equipment during aircraft ground handling. Besides caveats regarding the predicted emissions that were used, the box model approach also required some assumptions. For example, the model assumes a uniform distribution of emissions over the entire volume. Therefore local concentrations could be higher or lower than the expected values, as in reality emissions at different locations within the box's ground area will affect measurement stations differently. This is true for all pollutants discussed in this study.

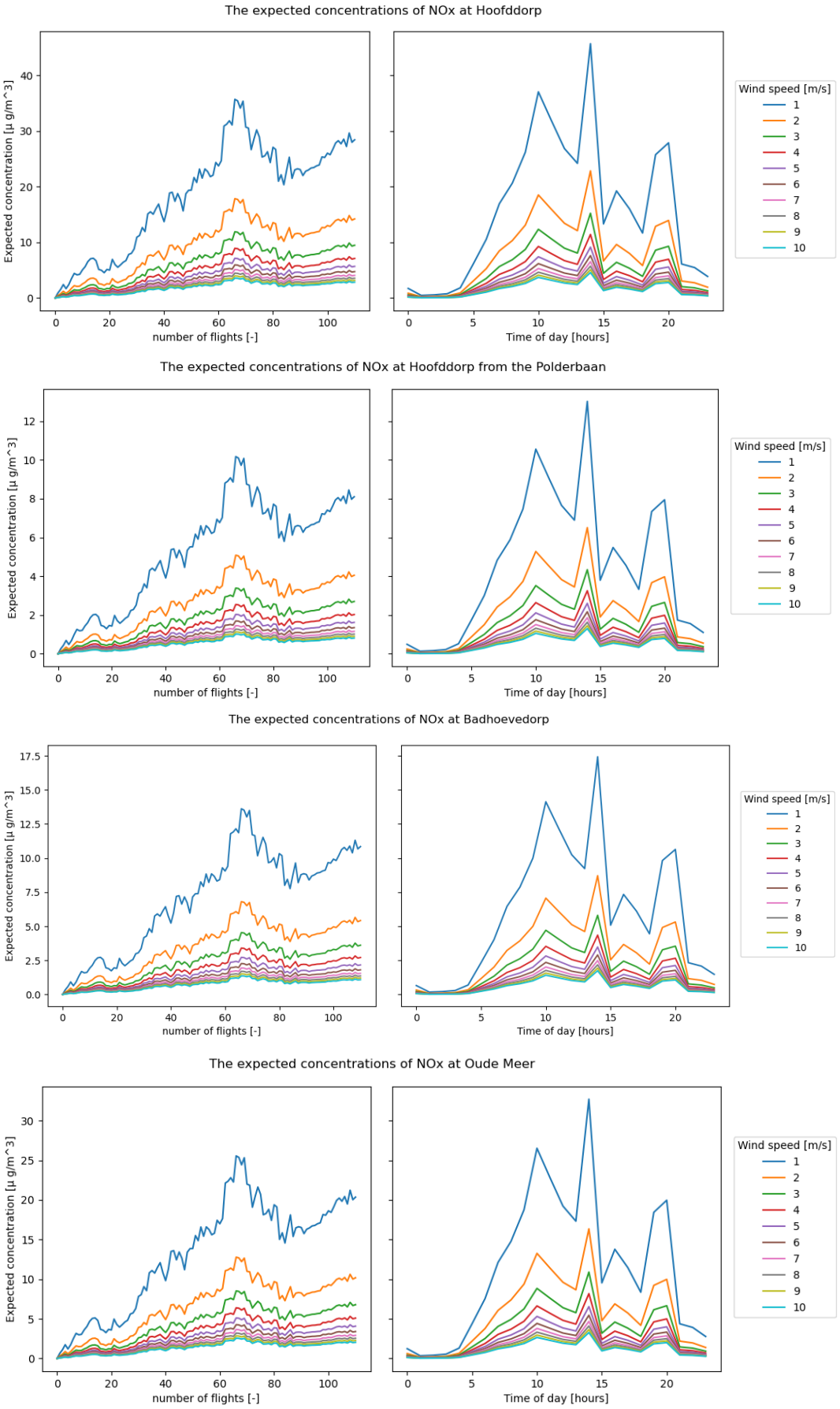

Figure 2.4: The expected effects of the airport on ambient concentrations of NO_x.

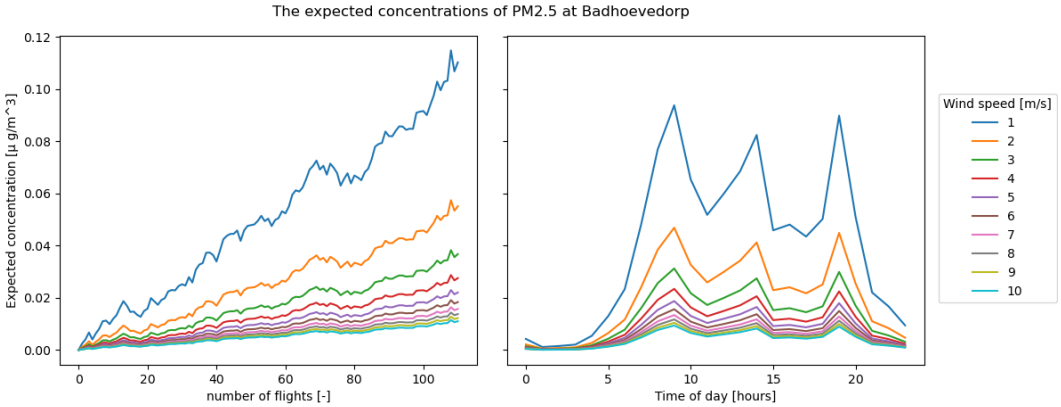

Figure 2.5: The expected effects of the airport on ambient concentrations of $PM_{2.5}$.

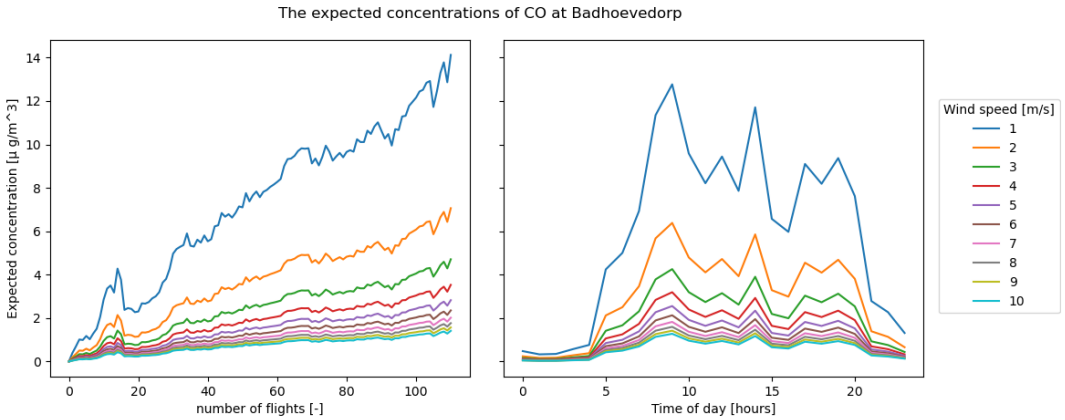

Figure 2.6: The expected effects of the airport on ambient concentrations of CO.

3

Methodology

This chapter explains the methods used throughout the thesis. As the research is divided into three research questions, three different methods are used to answer the sub-question. Before these three methods are explained, the data preparation is explained in section 3.1. Subsequently sections 3.2, 3.3 and 3.4 present the methods used to answer the three sub-questions.

3.1. Data preparation

Throughout this observation-based research conclusions are drawn based on an analysis of the available data sets. It is therefore crucial that these data sets are as complete and reliable as possible. This section explains the methodologies used to ensure the data is reliable and complete. AQ data will be discussed first, after which the meteorological data is presented. Finally road- and air traffic data sets are introduced.

3.1.1. Raw air quality data

The AQ data is downloaded from luchtmeetnet.nl (RIVM et al., 2020). This website contains the measurements from AQ monitors (figure 3.1) located throughout the Netherlands. All monitoring results are obtained under the ISO 17025 accreditation of GGD Amsterdam (Jonge de, 2020). The measurement equipment and the corresponding accuracies are presented in table 3.1. The measurements from these monitors are used for purposes that require reliable data. The information is used to check compliance with European regulations. Additionally the data is made publicly available for scientific research and forms the basis for models that generate AQ predictions. As a result the data is being checked using various methods before and after it is published.

Figure 3.1: Air quality monitors at Oude Meer (left) and Hoofddorp (right).

Table 3.1: Air quality measurement equipment and accuracies. (Jonge de, 2020)

Pollutant	**Equipment**	**Accuracy [95% confidence interval]**
$PM_{2.5}$	Met One BAM1020	17.2%
PM_{10}	Met One BAM1020	11.8%
CO	API T300	12.2%
O_3	Thermo 49i	9.7%
NO and NO_2	Thermo 42i and API200e	10.1% and 9.4%

Nevertheless, despite the pre-processing done by the governmental organisations that manage the measurement stations, some data processing is required. AQ measurements from 1 January 2014 till 31 August 2020 were downloaded and information about the number of data points of the raw data can be found in table 3.2. These data sets still contained outliers. An example of such an outlier was present in the data from the AQ monitor in Badhoevedorp. The data set showed a NO_2 value of 100,001 $\mu g/m^3$, while the median of that data set is equal to 22.8 $\mu g/m^3$ and the second highest value is only 178.3 $\mu g/m^3$. The impacts of such a measurement cannot be neglected. For example, the mean and standard deviation of the data set (with a length of 58,884 data points) change from 29.4 and 412 to 27.7 and 18.6, respectively. Thus, this example showed the importance of checking the data sets and taking out outliers. As most data sets consisted of six and a half years worth of hourly measurements, it was difficult to determine manually whether all data points were reliable and likely to show the true state of the AQ at that time. For this reason this process was automated.

3.1.2. Outlier detection and removal for air quality data

The most frequently used method for outlier detection in AQ data sets is the z-score method (Feng et al., 2004, Durre et al., 2010). This method uses the mean and standard deviation of the data set to determine the z value for each data point. The z-score is calculated using equation 3.1, where $z(i)$ and $f(i)$ are the z score and the measured value of the i^{th} data point, $\overline{f}$ is the mean of the data set and σ is the standard deviation (SD). If the value of $z(i)$ exceeds a certain threshold, the data point is removed.

$$z(i) = \frac{\left| f(i) - \overline{f} \right|}{\sigma} \tag{3.1}$$

The z-score method is quick and robust, but it also assumed that the data follows a normal distribution. However, it turns out that the distribution of the AQ measurements is closer to a log-normal distribution as all measurements are (or should be) positive. In order to overcome this limitation one could log-transform the data sets and apply the z-score method. This method was applied to the available AQ data sets. Inspection of the resulting data sets showed that the majority of outliers were values below the averages of the data sets. Research by van Zoest et al., 2018 also mentioned that this method would result in an implausible number of outliers below the mean. However, the outliers of interest are mainly those with high values, as these are related to air pollution events or errors.

The method that was chosen for outlier detection in the AQ data sets of this study was presented by Wu et al., 2018. In their research they developed an automated outlier detection method for the official measurements of the China National Environmental Monitoring Center. Data sets with hourly measurements of six different air pollutants ($PM_{2.5}$, PM_{10}, SO_2, $NO_{2.}$, CO and O_3) were used to develop their outlier detection methods. The algorithm developed by Wu et al., 2018 to determine outliers with large errors is used as part of the data pre-processing in this research. This algorithm is based on a modified z-score method and probability theory. Before the algorithm from Wu et al., 2018 is applied, all measurements with a value below zero are removed from the data sets. This is done as negative concentrations are not expected to represent true events. Then, several steps have to be performed in order to determine whether measurements are potential outliers.

First, for a measurement at time i the expected value is estimated. This step is essential as instead of assessing the measurements directly, the residuals between observed and estimated values are evaluated to determine whether a measurement is a potential outlier. The estimated values are determined by a median filter as shown in equation 3.2. In this equation $F_m(i)$ is the expected value at time i, $f(i+k)$ is the measured value at

time $i+k$, M represents the median function and $i-n$ and $i+n$ are the start and end of the sliding window, respectively.

$$F_m(i) = M\big(f(i+k)\big), \qquad k \in [-n, n] \tag{3.2}$$

The total number of data point to determine the median, e.g. $2n+1$, is set to one month (721 data points). Once the expected values are known, the residuals R are determined by subtracting the expected value at time i from the measured concentration at time i ($f(i)$) as shown in equation 3.3.

$$R_m(i) = f(i) - F_m(i) \tag{3.3}$$

Similar to the z-score method, the standard deviation needs to be determined as well. Instead of using the overall SD of the actual AQ measurements, the standard deviation of the residual (S_m) at time i is calculated using the median absolute deviation of a normal distribution as shown by equation 3.4. Again, the window $2n+1$ equals 721.

$$S_m(i) = 1.4826 M\left(|R_m(i+k)|\right), \qquad k \in [-n, n] \tag{3.4}$$

Once the residuals and the standard deviation of the residuals are known the final steps are to determine the Z value of the measurement at time i and the probability of Z. The value of Z is determined by dividing the residual at time i by the calculated standard deviation at time i, as shown by equation 3.5.

$$Z(i) = \frac{R_m(i)}{S_m(i)} \tag{3.5}$$

Finally, the outlier selection is done by evaluation of the probability of $Z(i)$ using equation 3.6. Through a sensitivity analysis, Wu et al., 2018 found that 10^{-15} is a suitable probability threshold. If the probability is lower than this threshold value, the data point is considered an outlier and it is removed from the data set.

$$P(i) = \frac{1}{\sqrt{2\pi}} e^{-\frac{1}{2}Z(i)^2} \tag{3.6}$$

After evaluation of this method by plotting the AQ measurements and outliers using various thresholds, the same probability threshold of 10^{-15} was chosen. This method is considered suitable for all species of this research, except for nitrogen monoxide. As the NO measurements show large deviations which are probably the result of nearby pollution events, too many measurements are discarded if this method is used despite decreasing the probability threshold.

In order to make the method suitable for NO, several changes to the previous method were tried and evaluated. For example, the probability threshold was lowered in steps from 10^{-15} to 10^{-30}. Additionally the windows over which the median filters from equations 3.2 and 3.4 were lowered to a period of twelve hours. Still, the results showed a large number of outliers and were likely to delete valid measurements from the data sets.

After some evaluation on why so many data points were deleted, it was found that that the low median in combination with sudden peaks led to high residual values. As most measurements showed low concentrations, the median was low compared to higher values measured at potential pollution events. While one of the properties of a median is that it is less sensitive to measurements with large deviations, due to the expected fluctuations of the NO concentrations as a result of pollution events most of the sudden deviations should not be discarded. This can be done by adjusting equation 3.2 to the expected behaviour of the data set. It was found that replacing the median filters and median absolute deviation from equations 3.2 and 3.4 by a mean filter and the mean absolute deviation, respectively, immediately resulted in far better results. Extreme outliers were deleted, while lower peaks are maintained. Therefore, these simple changes were implemented in the algorithm for NO.

3.1.3. Results of outlier detection for air quality data

Table 3.2 shows the difference in the number of outliers using the traditional z-score method and the method from Wu et al., 2018. It has to be noted, though, that due to the median filters of equations 3.2 and 3.4 the first and last months of the data set are deleted. Thus, the comparison from table 3.2 has been made based on the number of measurements marked as outliers in the range of measurements that are still in the data sets

Table 3.2: The average number of data points per pollutant at the air quality monitoring sites from table 3.6, including the percentage of data points that are discarded by two outlier detection methods.

Pollutant	Average number of measurements per AQ monitor	% outliers z-score method	% outliers alternative method
NO	53,723	2.40	0.25
NO_2	56,126	1.71	0.05
PM_{10}	52,225	1.73	0.13
$PM_{2.5}$	50,223	1.85	0.22
O_3	51,368	0.77	0.00
CO	57,273	1.43	0.51

of both methods. Despite eliminating two months of AQ measurements, the resulting data set is considered better for this research as fewer peaks are removed. These peaks are potentially correlated with pollution events, which is something that this research is interested in. Consequently, by using this more selective outlier detection method the risk of losing valuable data points is reduced.

3.1.4. Meteorological data

Besides source information another important factor that influences air quality are the atmospheric conditions. Parameters regarding wind speed, wind direction, temperature and precipitation cannot be neglected when evaluating the AQ measurements. For example, wind speed and direction influence the flow of air that is send towards the measurement location. Other parameters, such as temperature and precipitation, impact the atmospheric chemistry and deposition of pollutants.

The meteorological information is taken from the Koninklijk Nederlands Meteorologisch Instituut (KNMI, 2020). The KNMI operates an automatic measurement station within the airport's perimeter. The available parameters that are measured at this station, including the accuracy and averaging period, are shown in table 3.3. No data was deleted from the data sets and continuous information was available from January 2014 until August 2020. The exact location of the measurement station is shown in figure 3.2. Only one KNMI operated automated weather station with publicly available data is present at Schiphol. Consequently, all meteorological parameters used to create regression models are based on the same measurements. This could be an issue if the values of these parameters are significantly different at the AQ monitoring sites. However, as hourly values are used it is assumed that by averaging the conditions over the previous hour, relative (short term) differences in meteorological parameters per site are decreased.

Table 3.3: An overview of the available meteorological information.

What	Accuracy	Measurement period	Frequency	Sensor specifics
Wind direction	Per 10 degrees	Last 10 minutes of the hour	Hourly	
Wind speed	Per 0.1 m/s	Averaged over the hour	Hourly	
Temperature	Per 0.1 degrees Celsius	Averaged over the hour	Hourly	Measured at 1.5 m above the ground.
Precipitation duration	Per 0.1 hour (6 minutes)	Last hour	Hourly	
Precipitation amount	Per 0.1 mm	Total over the last hour	Hourly	
Rain	Binary variable	Last hour	Hourly	

3.1.5. Hourly road traffic data

Compared to previous studies, the availability of detailed road traffic data provides new opportunities to determine the effect of this source on local air pollution levels. Road traffic data is made available by the Nationaal Dataportaal Wegverkeer (NDW), which is an initiative started by a collaboration of Dutch road authorities and operates the data based of national road traffic information. Based on their database, hourly road traffic intensities can be obtained. This means that the total amount of vehicles that pass the locations of interest, as explained later in this section, are stored in the road traffic data set. This includes vehicles travelling in both directions.

In order to download the data a Dexter account was used. Dexter is the data exploration and exporter tool from NDW, 2020. Through this portal desired locations and time ranges for road traffic information can be selected. Figure 3.2 shows the measurement locations relevant for this study and table 3.4 provides more

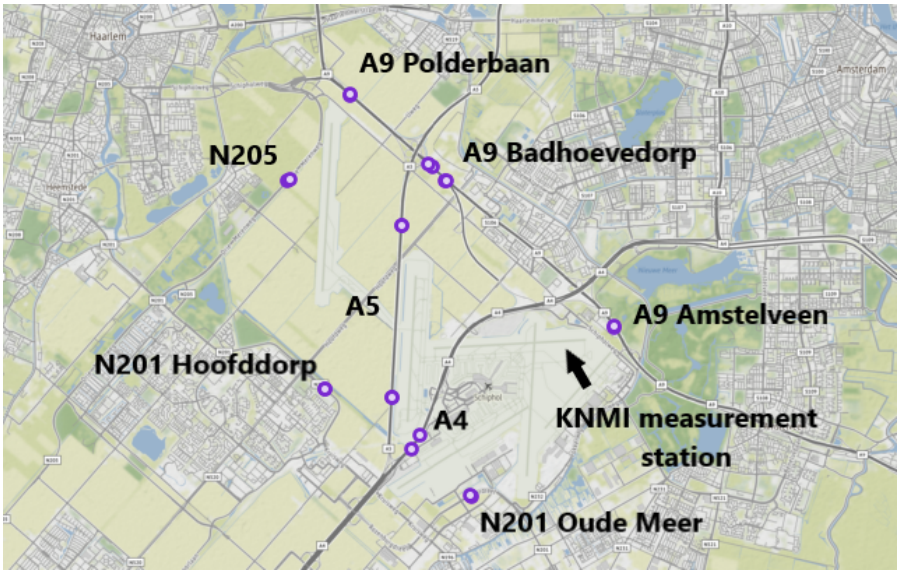

Figure 3.2: Locations of air traffic measurements shown as dots. The black arrow shows the location of the KNMI weather station used to generate meteorological information. The base map is taken from the NDW, 2020 Dexter tool.

detailed information about the measurements. Hourly traffic intensities from January 2014 until August 2020 were obtained. The locations presented in figure 3.2 were chosen based on their relative position to the AQ monitoring sites and the availability of continuous data. Especially locations at the A9 had to be selected with care, as the road was relocated from the old location through Badhoevedorp to a new location closer to the airport. Similarly, only one location at the A4 was taken as other locations did not offer continuous measurements over the selected time period.

Before the data can be used for further research, the data sets were filtered for errors and missing information. If there were issues with the measurement equipment, such as malfunctioning sensors or maintenance works, this was registered in an extra column. All measurements taken at a timestamp that showed some discrepancy were discarded. The percentage of data lost per measurement station can be found in table 3.4. The hours covered column shows the percentage of hours in the year that have valid traffic intensity information. From the table it follows that during the most critical years, being the ones with air traffic data, the completeness of road traffic information is 98.9% or higher for all main roads (A roads). Later on during this study, it was found that too many road parameters in the final models did not increase model accuracy. Consequently chapter 6 only refers to parameters A4, A5 and A9. These values are the average traffic intensities measured at these highways. Thus, in order to get the A5 parameter the average of traffic intensities from both measurement locations are taken. The same is true for the A9, while at the A4 only one location was used and no averaging was required.

3.1.6. Hourly take-offs and landings at Schiphol

If one aims to estimate the effects of Schiphol on local AQ based on a model, activity data from the airport is required. Without this data being publicly available from official sources, alternatives had to be assessed. This sections presents the available options and the final method that was used to create the flight data set used for this research.

Official sources that could provide data on air traffic are Schiphol and Luchtverkeersleiding Nederland. The latter does not publish any numbers. On the airport's website, however, monthly reports with traffic information are published. These reports offer overall aircraft movements per month and make a distinction between (passenger) commercial flights, cargo flights and general aviation. Even though this information provides exact numbers, the monthly frequency was not considered high enough. But even though the monthly reports were not used for the analysis of AQ measurements, the numbers were used for validation of the air traffic data set.

Table 3.4: An overview of the available road traffic data. The number of data points are hourly measurements throughout the year. The final column, hours covered, is taken relative to the total number of hours in the year. For 2020, measurements until August are considered. All data is taken from NDW, 2020.

Station	Year	# Data points	# Errors	# Final data points	Hours covered
A4	*2014*	*8,759*	*1,828*	*6,931*	*79.1%*
	2015	*8,759*	*218*	*8,541*	*97.5%*
	2016	*8,783*	*168*	*8,615*	*98.1%*
	2017	*8,759*	*92*	*8,667*	*98.9%*
	2018	*8,759*	*97*	*8,662*	*98.9%*
	2019	*8,759*	*13*	*8,746*	*99.8%*
	2020	*5,855*	*42*	*5,813*	*99.3%*
A5	*2014*	*8,759*	*1,766*	*6,993*	*79.8%*
	2015	*8,759*	*464*	*8,295*	*94.7%*
	2016	*8,783*	*50*	*8,733*	*99.4%*
	2017	*8,759*	*27*	*8,732*	*99.7%*
	2018	*8,759*	*81*	*8,678*	*99.1%*
	2019	*8,759*	*13*	*8,746*	*99.8%*
	2020	*5,855*	*34*	*5,821*	*99.4%*
A9 Polderbaan	*2014*	*8,759*	*1,725*	*7,034*	*80.3%*
	2015	*8,759*	*83*	*8,676*	*99.0%*
	2016	*8,783*	*167*	*8,616*	*98.1%*
	2017	*8,759*	*53*	*8,706*	*99.4%*
	2018	*8,759*	*62*	*8,697*	*99.3%*
	2019	*8,759*	*54*	*8,705*	*99.4%*
	2020	*5,855*	*48*	*5,807*	*99.2%*
A9 Amstelveen	*2014*	*8,759*	*1,731*	*7,028*	*80.2%*
	2015	*8,759*	*156*	*8,603*	*98.2%*
	2016	*8,783*	*499*	*8,284*	*94.3%*
	2017	*8,759*	*33*	*8,726*	*99.6%*
	2018	*8,759*	*56*	*8,703*	*99.3%*
	2019	*8,759*	*13*	*8,746*	*99.8%*
	2020	*5,855*	*34*	*5,821*	*99.4%*

Station	Year	# Final data points	# Errors	# Final data points	Hours covered
A9 Badhoevedorp	*2014*	*8,759*	*1,720*	*7,039*	*80.4%*
	2015	*8,759*	*716*	*8,043*	*91.8%*
	2016	*8,783*	*49*	*8,734*	*99.4%*
	2017	*8,759*	*31*	*8,728*	*99.6%*
	2018	*8,759*	*58*	*8,701*	*99.3%*
	2019	*8,759*	*22*	*8,737*	*99.7%*
	2020	*5,855*	*51*	*5,804*	*99.1%*
N201 Hoofddorp	*2014*	*8,759*	*50*	*8,709*	*99.4%*
	2015	*8,759*	*66*	*8,693*	*99.2%*
	2016	*8,783*	*391*	*8,392*	*95.5%*
	2017	*8,759*	*4*	*8,755*	*99.9%*
	2018	*8,759*	*33*	*8,726*	*99.6%*
	2019	*8,759*	*10*	*8,749*	*99.9%*
	2020	*5,855*	*33*	*5,822*	*99.4%*
N201 Oude Meer	*2014*	*7,354*	*94*	*7,260*	*82.9%*
	2015	*8,759*	*24*	*8,735*	*99.7%*
	2016	*8,783*	*372*	*8,411*	*95.8%*
	2017	*8,759*	*1,799*	*6,960*	*79.5%*
	2018	*8,759*	*764*	*7,995*	*91.3%*
	2019	*8,759*	*1,052*	*7,707*	*88.0%*
	2020	*5,855*	*33*	*5,822*	*99.4%*
N205	*2014*	*8,759*	*7*	*8,752*	*99.9%*
	2015	*8,759*	*114*	*8,645*	*98.7%*
	2016	*8,783*	*235*	*8,548*	*97.3%*
	2017	*8,759*	*7*	*8,752*	*99.9%*
	2018	*8,759*	*36*	*8,723*	*99.6%*
	2019	*8,759*	*31*	*8,728*	*99.6%*
	2020	*5,855*	*33*	*5,822*	*99.4%*

Without sufficient data from official sources, a potential alternative is the use of information from ADS-B signals transmitted by aircraft. An estimate from Flightradar24, 2020 shows that in Europe approximately 80% of all commercial aircraft are equipped with an ADS-B transmitter. Thus, this could be a valuable source of activity data from Schiphol. Due to the COVID-19 situation a data set with hourly flights was made publicly available at zenodo.org (Olive et al., 2020, based on previous work from Schäfer et al., 2014 and Olive, 2019). The number of take-offs and landings from Schiphol are obtained from this data set by looking for the ICAO code of Schiphol in the origin and destination columns of the data set. Adding the timestamp information then results in hourly arrivals and departures at Schiphol. Comparing the monthly number of take-offs and landings from this data set with the earlier mentioned official monthly reports from Schiphol, an average accuracy of 76.3% is achieved. An overview of monthly numbers can be found in table 3.5. Even though 76% already approaches the estimated maximum accuracy of 80%, a second method regarding ADS-B based aircraft data was evaluated.

The alternative method is based on research by Sun et al., 2017. An advantage of this source is the availability of data from January 2018 to August 2020, whereas the data from Olive et al., 2020 is only available from 2019 to 2020. Sun et al., 2017 have developed an algorithm to decode raw ADS-B signals obtained by the receiver at the TU Delft campus. Based on these decoded messages they were able to automatically detect various flights and corresponding flight phases per message. An example of a flight that was identified using this method is shown in figure 3.3. In order to translate flights and corresponding flight phases to hourly landings and take-offs at Schiphol, a final filtering algorithm was written.

This algorithm consists of three phases. First, it filters out all flights that did not send any messages below 2500 ft. Secondly, all flights without a climb or descent phase are discarded. Finally, the script runs through the remaining flights in order to determine whether these could have originated or ended at Schiphol. Again, this final part consists of several steps.

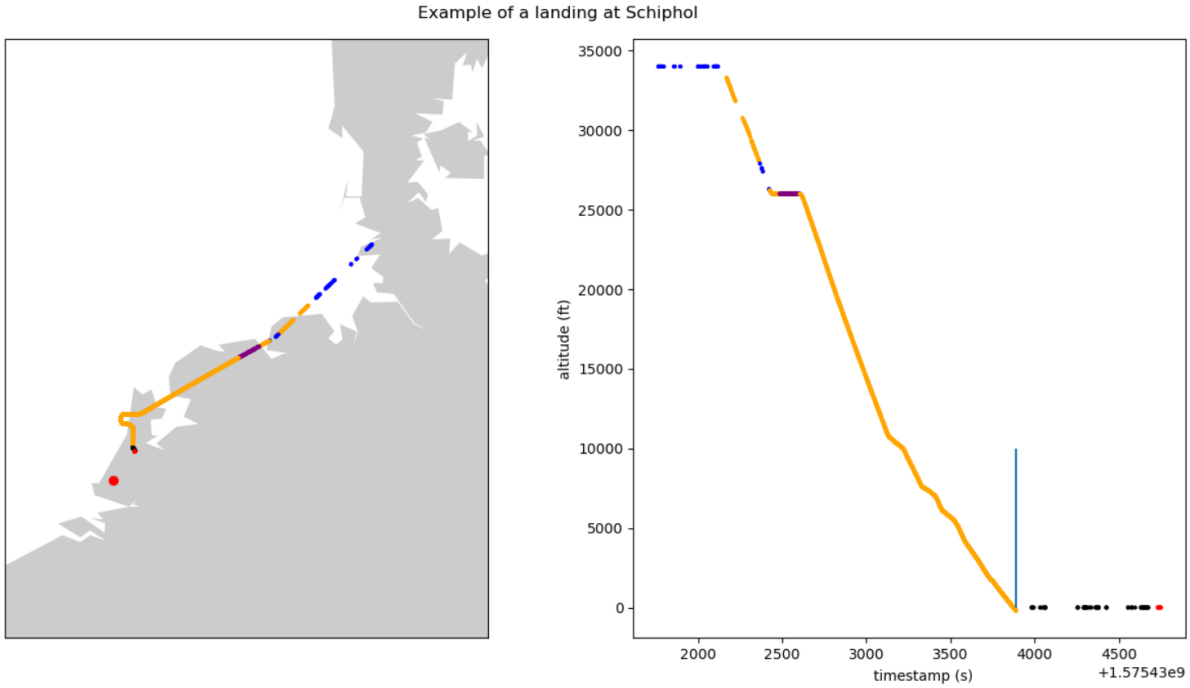

(a) Example of a flight landing at Schiphol. The timestamp value is the number of seconds since 1 January 1970, UTC time.

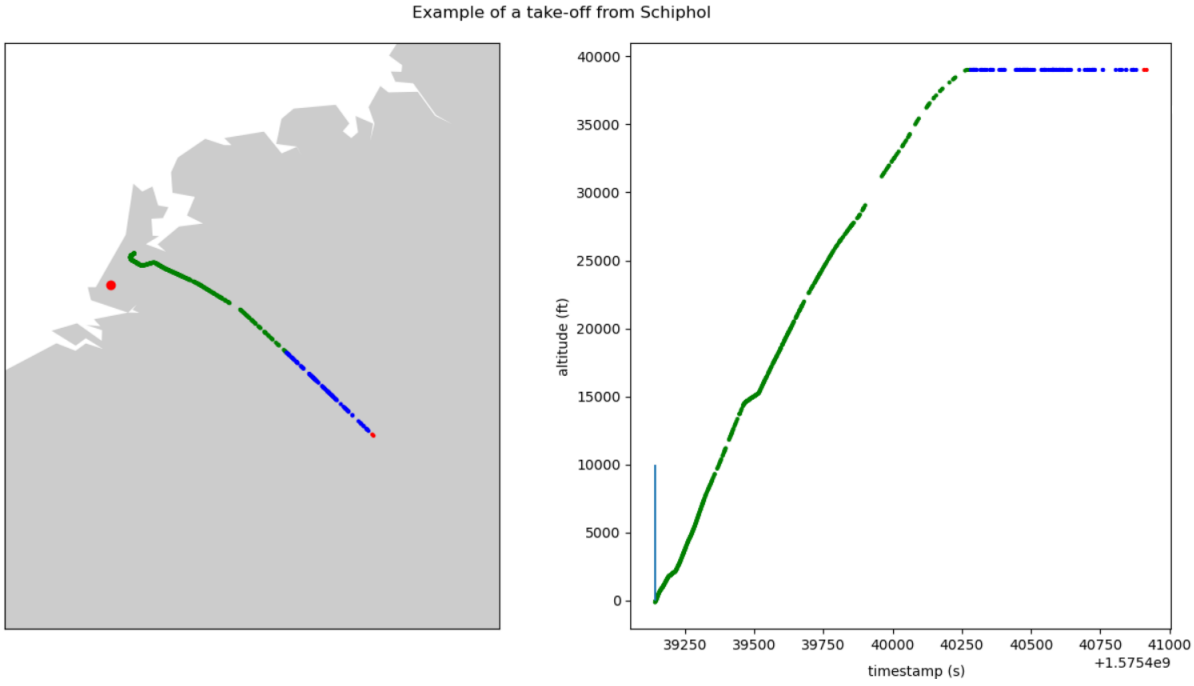

(b) Example of a flight taking-off from Schiphol. The timestamp value is the number of seconds since 1 January 1970, UTC time.

Figure 3.3: Two examples of the visualisation method used to test various parameters in the flight activity algorithm. Blue dots represent cruise flight, yellow dots are descent, purple stands for level flight, green is climb, black is ground and red is not applicable. The big red dot on the map shows the location of the receiver (Delft). The vertical blue line in the right graph shows the time stamp stored in the flight data set.

Per flight the program runs through the time sorted messages using the schematic from figure 3.4. Per message, the flight phase can be defined as ground, climb, descent, cruise, level, or non applicable (unidentified). If the flight phase is climb or descent, the program checks whether the message was sent within a specified area around Schiphol and the altitude is lower than 1500 ft. If this is true, there are two options: for a climbing flight the time stamp of that message is taken as the departure time. If the flight phase is descent, the

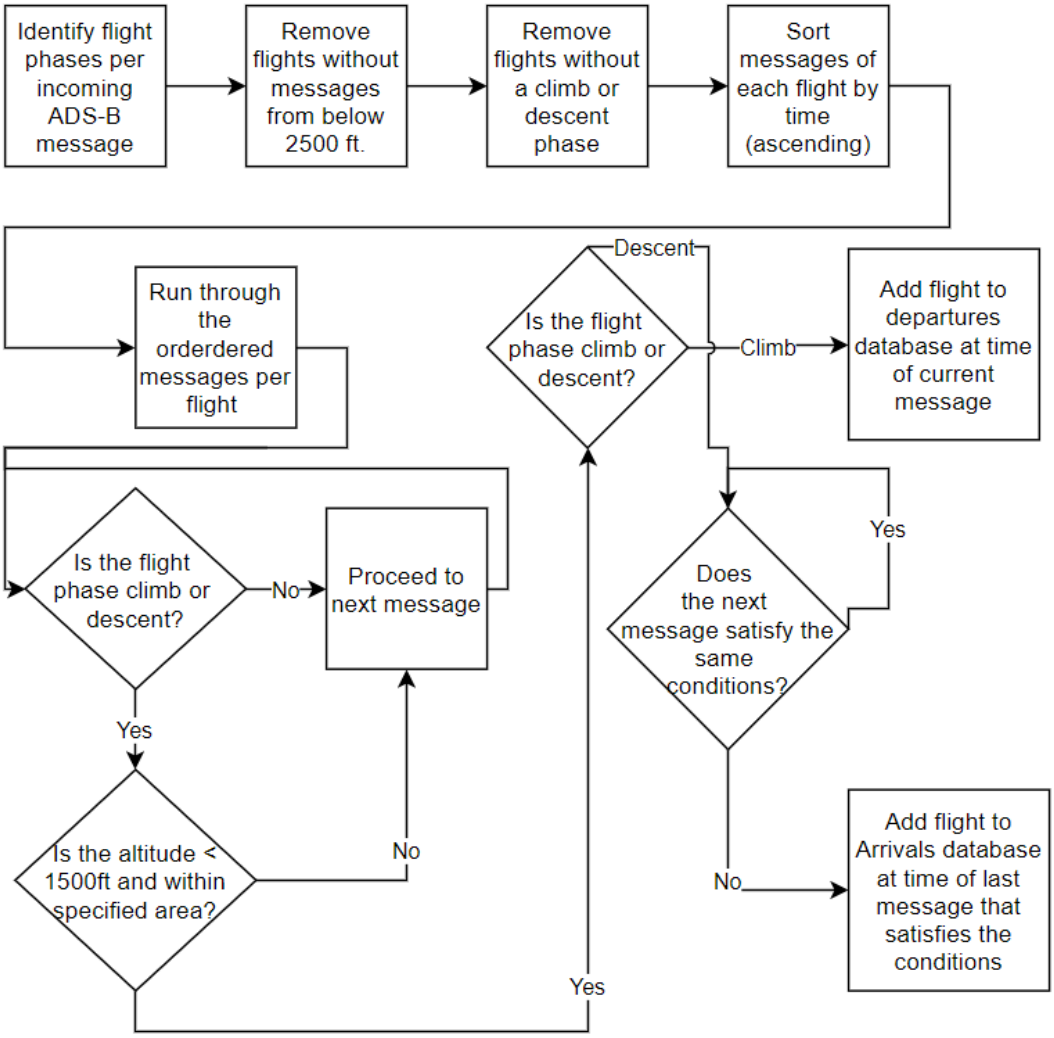

Figure 3.4: A schematic of the algorithm used to create the flight data set.

program tests whether the next message also satisfies the same criteria. If that is true, the loop continues. If the next message does not meet these criteria, or there is no next message, the timestamp of that message is considered the arrival time of the flight. The parameters for the area and altitude are chosen based on a trial and error process. By evaluating graphs similar to figure 3.3, the results of the program were checked. For several days the graphs of all flights were evaluated and it was checked whether the correct flights were added to the final data set. Based on this process, the reference area was defined as latitudes between 52.24 and 52.42 and a longitude greater than 4.64 and smaller than 4.88. The altitude requirement mentioned earlier was set using this same method. The results of are shown in table 3.5

When the results of this final method are compared to the official data from Schiphol, it turns out that this method is able to identify 82.6% of the aircraft movements from Schiphol. This is 5.3 % better than the open source data base mentioned earlier. There are some gaps in the data set due to downtime of the receiver, but the presence of 2018 data and a higher accuracy still makes this data set more interesting than the open source database. Consequently, for the remainder of this thesis the data set based on the TU Delft receiver is used.

Table 3.5: Aircraft activity based on several sources. The open source flight information was taken from Olive et al., 2020. The total flight movements, used as a reference to compare the other sources, are taken from the airport's official website (Schiphol, 2020).

		Results using TU Delft receiver			*Open source database*					
Year	**Month**	**Take-offs**	**Landings**	**Accuracy [%]**	**Take-offs**	**Landings**	**Accuracy [%]**	**Total flight movements**	**Difference in accuracy**	**Comments**
2018	**1**	15,383	15,147	**79.5**				38,385		
	2	14,510	14,325	**79.2**				36,428		
	3	16,922	16,728	**80.7**				41,675		
	4	17,860	17,602	**81.8**				43,349		
	5	17,424	17,088	**74.4**				46,399		30 and 31 May are missing.
	6	18,491	18,129	**80.9**				45,278		No data on morning 1st of June.
	7	19,657	19,304	**82.4**				47,274		
	8	19,870	19,413	**83.4**				47,095		
	9	19,267	18,830	**83.2**				45,786		
	10	19,521	19,164	**82.8**				46,709		
	11	16,423	16,176	**81.7**				39,899		
	12	16,351	16,186	**82.4**				39,495		
2019	**1**	15,885	15,587	**81.7**	14,334	12,353	**69.3**	38,524	**12.4**	
	2	15,237	14,815	**82.2**	14,429	12,141	**72.7**	36,566	**9.5**	
	3	16,584	16,050	**79.1**	16,290	14,871	**75.5**	41,282	**3.6**	Missing information on 23rd.
	4	18,131	17,774	**82.5**	17,218	16,731	**78.0**	43,540	**4.5**	
	5	13,725	13,563	**58.7**	18,363	17,461	**77.0**	46,511	**-18.4**	No data from receiver after 22nd.
	6	0	0	**0.0**	17,654	15,661	**73.6**	45,249	**-73.6**	No data from receiver.
	7	603	538	**2.5**	18,370	17,447	**66.2**	46,428	**-63.7**	Only last two days available.
	8	19,441	19,137	**82.7**	18,194	16,066	**73.4**	46,662	**9.3**	
	9	19,126	18,872	**83.0**	17,195	16,020	**72.6**	45,758	**10.5**	
	10	19,242	18,978	**82.8**	18,365	18,868	**80.6**	46,190	**2.1**	
	11	16,272	15,825	**81.6**	15,587	15,142	**78.2**	39,322	**3.5**	
	12	16,739	15,739	**81.7**	15,197	13,666	**72.6**	39,779	**9.1**	
2020	**1**	12,897	12,580	**65.5**	15,121	13,554	**73.8**	38,879	**-8.2**	January 24 until 29 are missing.
	2	15,578	15,060	**84.1**	14,768	13,767	**78.3**	36,442	**5.8**	
	3	11,509	11,317	**86.4**	10,945	10,169	**79.9**	26,412	**6.5**	
	4	2,023	1,928	**79.8**	1,801	1,935	**75.4**	4,954	**4.3**	
	5	2,992	2,869	**86.8**	2,653	2,889	**82.1**	6,750	**4.7**	
	6	4,180	4,003	**88.8**	3,830	3,863	**83.4**	9,220	**5.3**	
	7	7,945	7,776	**91.3**	7,313	6,821	**82.1**	17,219	**9.2**	
	8	10,862	10,551	**87.0**	10,142	9,650	**80.4**	24,612	**6.6**	

3.1.7. An overview of the available data sets and their use throughout this study

The data sets that are presented in section 3.1 are used to answer the three research questions. As air traffic is not available over the entire period from January 2014 to August 2020, the regression modelling could only be performed on data from January 2018 to August 2020. The other data sets are available from January 2014 to August 2020. Therefore only the regression modelling will take a shorter time period into account. An example data set is added in appendix A.

3.2. Comparison of observations from different air quality monitoring sites

The first sub-question is formulated in order to compare the AQ in the vicinity of Schiphol with other locations within the Netherlands. This section introduces the AQ monitoring locations used to answer this question and explains why these sites were chosen.

Even though there are only three AQ monitoring stations in the vicinity of Schiphol, data from seventeen stations is used for this research. By doing so, the concentrations of various air pollutants can be compared at different locations. As the measurement stations are static and are thus likely to be affected by its direct environment, the effect of the direct environment should be visible by comparison of data from different monitoring sites. The seventeen monitoring sites are divided into four groups based on their direct surroundings. First, there are the three stations located in the vicinity op Schiphol. Additionally, there are five urban background stations, five rural background stations and four stations that are located right next to main roads. An overview of the names of all stations and their characteristics is provided in table 3.6. Additionally, a map of the measurement locations is shown in figure 3.5.

In order to create relevant reference values the background stations are chosen at different locations within the Netherlands. For example, urban background is considered for Amsterdam, The Hague, Rotterdam and Utrecht. The rural background levels are taken based on locations in North-Holland, South-Holland, Flevoland,

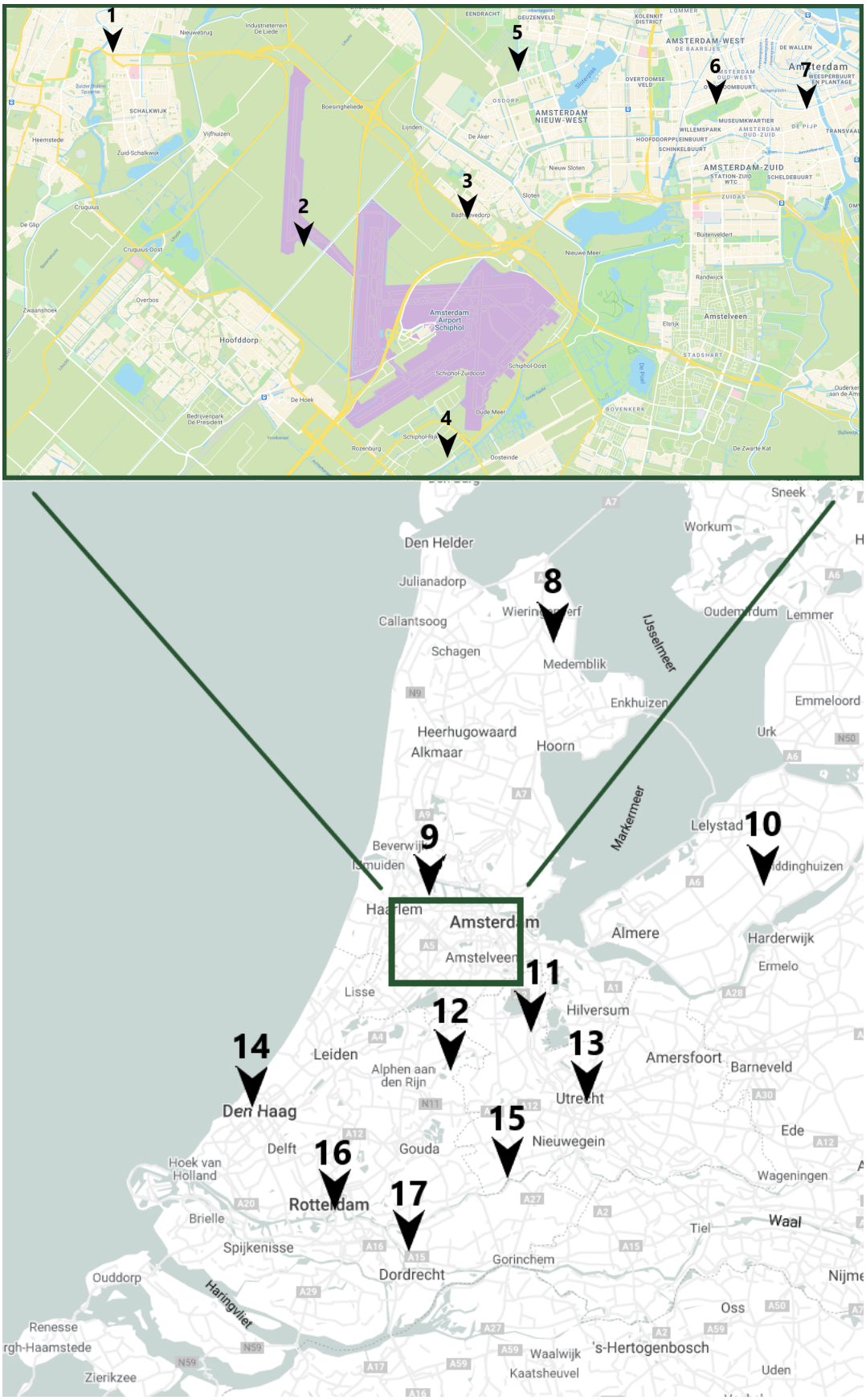

Figure 3.5: Locations of all air quality monitoring sites used in this study. (Base maps from Google Maps)

Table 3.6: An overview of the air quality monitoring sites. The numbers correspond to the locations shown in figure 3.5

#	Name	Pollutants	Type
1	Haarlem	NO, NO_2, O_3, PM_{10}	Road
2	Hoofddorp	NO, NO_2, O_3, PM_{10}	Schiphol
3	Badhoevedorp	NO, NO_2, PM_{10}, $PM_{2.5}$, CO	Schiphol
4	Oude Meer	NO, NO_2, PM_{10}	Schiphol
5	Ookmeer	NO, NO_2	Urban background
6	Vondelpark	NO, NO_2, O_3, PM_{10}, $PM_{2.5}$	Urban background
7	Stadhouderskade	NO, NO_2, PM_{10}, $PM_{2.5}$	Road
8	Wieringerwerf	NO, NO_2, O_3, PM_{10}, $PM_{2.5}$	Rural background
9	Spaarnwoude	NO, NO_2, PM_{10}, $PM_{2.5}$	Rural background
10	Biddinghuizen	NO, NO_2, PM_{10}, $PM_{2.5}$	Rural background
11	Breukelen	NO, NO_2, O_3, PM_{10}, $PM_{2.5}$	Road
12	Zegveld	NO, NO_2, O_3, PM_{10}	Rural background
13	Utrecht	NO, NO_2, O_3, $PM_{2.5}$	Urban background
14	Den Haag	NO, NO_2, O_3, PM_{10}, $PM_{2.5}$	Urban background
15	Cabauw	NO, NO_2, O_3, PM_{10}, $PM_{2.5}$	Rural background
16	Rotterdam	NO, NO_2, O_3, PM_{10}, $PM_{2.5}$	Urban background
17	Alblasserdam	NO, NO_2, PM10	Road

and Utrecht. The maximum distance from a background station to the airport is 55 kilometers. The last classification contains near-road monitoring stations. As the name suggests these are located in the direct vicinity of main roads with high traffic intensities. Two of the traffic stations are near highways, while the other two are located near large provincial roads in Haarlem and Amsterdam. The labeling of stations is based on inspection of their direct surroundings and the official labeling used by Luchtmeetnet. The observations from the different monitoring sites are presented and compared in chapter 4.

3.3. Air quality measurements versus wind conditions

The first parameters to be linked to AQ measurements are wind speed and direction. Previous studies that investigated the effects of airports on local air quality have already shown that correlations between wind parameters and AQ measurements are useful to assess airport contributions to ambient AQ levels. Therefore, this section describes the methods used to investigate the correlation between these parameters. The goal of this analysis is to determine both qualitatively as quantitatively if the airport has an effect on ambient AQ.

3.3.1. Data visualization

In order to perform this analysis, the data sets of AQ measurements and wind parameters had to be connected. The information comes from different sources, but was put together in a single dataframe. Python version 3.8.2 in combination with the pandas 1.1.1 module was used to extract the downloaded information from the .csv files and match the timestamps of all data sets. The data sets that are combined are the ones for AQ data from section 3.1 and meteorological data from section 3.1.4. Both data sets consist of hourly monitoring results. However, the AQ data is not necessarily available for all hours in this period. As a result, times where no or only data from one data set was available are discarded. Once the pandas dataframes are created, the information is displayed in polar plots. Polar plots are useful graphical tools that can show the effects of two predictive parameters on a third dependent variable. In order to do so an existing package in R (4.0.2) is used. Carslaw and Ropkins, 2012 have created the Openair package, which offers functions to analyse AQ data. The polarPlot() function from this package will be used to create the figures shown in chapter 5.

These figures consist of bivariate polar plots and these will be used for qualitative and quantitative analyses. In order to create the polar plots shown in this research, several parameters have been changed from the default settings. First, the statistic used to determine the values for each box and the estimated values in between is performed using the non-parametric wind regression approach of Henry et al., 2009 that used kernel smoothers. Additionally, the limit wind speed was reduced to 15 m/s. Wind speeds larger than this value are scarce (figure 2.3), resulting in values in the graphs that could be based on just a few data points. Consequently, these points in the graphs with large uncertainties are taken out.

3.3.2. Analysis methods

The graphs that were introduced in the previous section will be used for two different types of analyses. First, polar plots based on measurements from January 2014 until August 2020 are created for all pollutants for the three AQ monitoring stations around Schiphol. These polar plots are based on measurements taken between 6am and 10pm. The time frame for the first part is chosen based on flight activities at Schiphol. The second method includes background subtraction. Application of background subtraction provides a method to analyze shifts in measured concentrations that could have been a result of airport operations. More specifically, similar to the box model approach that was explained in chapter 2, air is assumed to move across the

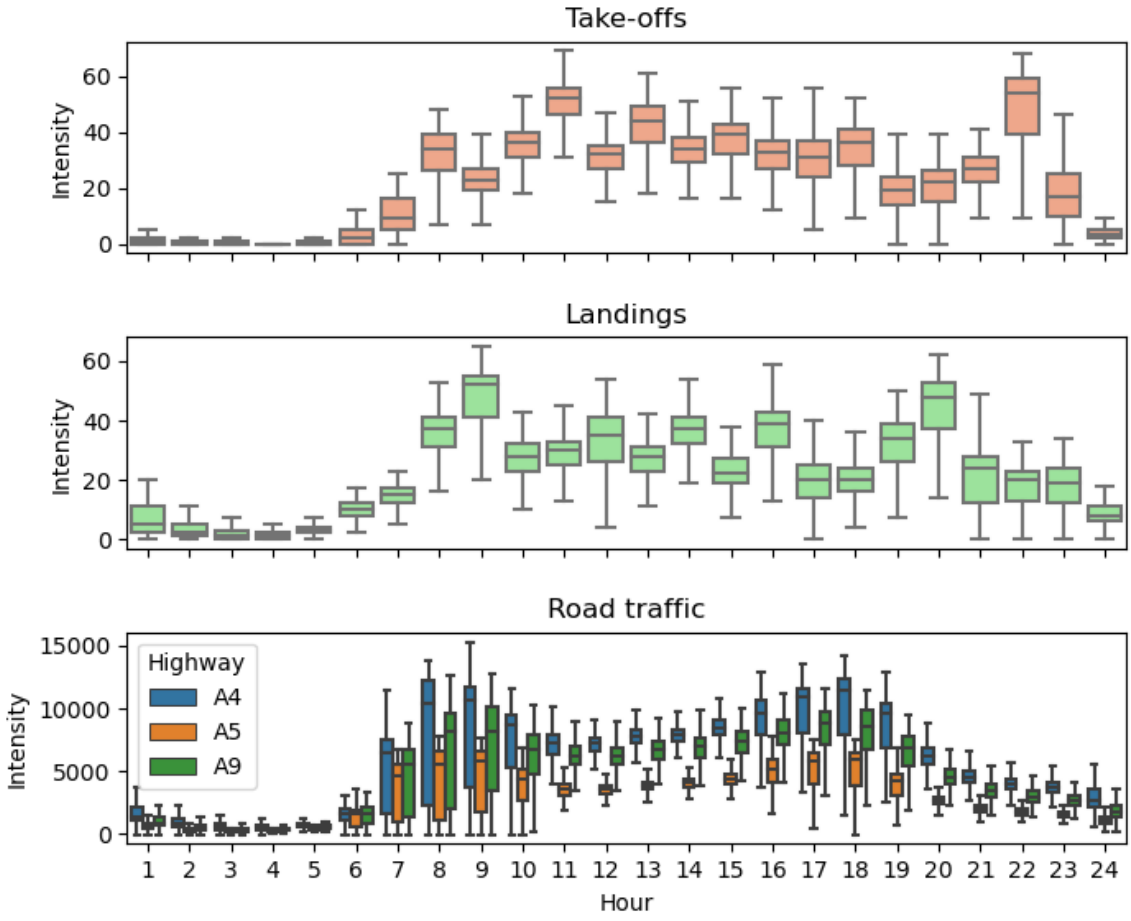

Figure 3.6: Flight activities and road traffic intensities per hour of day. The road traffic intensities are total vehicles at the highway in both directions.

airport. How this happens depends on the wind speed and direction. Based on properties of the area that the air moves across, concentrations of the various pollutants can change. For example, if a source of NO_2 is present in the area and one measures local concentrations of this pollutant downwind and upwind of this source, measurement downwind are likely to show higher concentrations of NO_2. Making use of this principle, several combinations of upwind and downwind monitoring sites are formed and shown in table 3.7. The differences in concentrations measured at the upwind and downwind sites are visualized in polar plots. Considering the combinations of AQ monitoring sites and wind parameters, the results for measurements taken between 6am and 10pm are analyzed. Additionally, the time sensitivity of the results of the two different methods is investigated. This is done by generating similar polar plots as discussed before for every hour of the day. Adding this time sensitivity analysis can provide further information about local pollution sources, as the hourly polar plots will be linked to the patterns from figure 3.6.

Table 3.7: Combinations of measurement stations used for background subtraction.

Wind direction	**Wind direction interval** [°]	**downwind station**	**upwind station**
South	90 - 270	Badhoevedorp	Oude Meer
North	270 - 90	Oude Meer	Badhoevedorp
South East	55 - 235	Hoofddorp	Oude Meer

3.4. Regression modelling

The third research questions aims to estimate the quantitative effect of Schiphol on local AQ. In order to answer this question regression modelling is used. In order to create a model to infer correlations between Schiphol and local AQ three steps are required. First, the correct model type should be chosen. Subsequently the data should be prepared properly and samples for fitting and testing the model should be created. Finally, the model should be created and the results have to be analysed and tested. How these three steps are performed in this study is explained in this section.

3.4.1. Model selection

The data sets that are combined in the model represent three types of information. First, there are meteorological conditions that describe local wind, temperature and precipitation at the time of measurement. Additionally there is information available about source activities such as the amount of road traffic at highways and the estimated number of aircraft take-offs and landings. Finally there are the AQ measurements, which are the model's response variables. In order to properly link these parameters in a representative model, the correct model type should be chosen. This is done based on the expected relationships between parameters, which determines the model's shape, and an evaluation of the effects of adding parameters on the model's accuracy. The remainder of this subsection will explain the model selection process in more detail.

If the predictive parameters are expected to show a linear interaction with the response variable, a simple linear regression model could be used. For sources such as road and air traffic a linear relationship might hold. For example, additional emissions due to an increase of flights or cars by an x amount can be approximated by multiplying x by the average emissions of these sources. Parameters that are not expected to show such linear behaviour are wind speed and direction. In chapter 5 the relationship between wind and AQ measurements is discussed extensively. From this analysis it followed that for various combinations of stations and pollutants the wind relationships showed different patterns. As a result, it is not straight forward to determine the appropriate shape of the relationship.

A possible solution for the model type was proposed by Dodson et al., 2009. Their study showed several similarities with this research. In both cases hourly meteorological and air traffic information was available and the pollutant's ambient concentrations were measured at different locations around the airport. The model chosen in their research was a combination of a linear mixed effect model (LME) and a generalized additive model (GAM). A LME is an extension to simple linear models that allow the implementation of both fixed and random effects. These models can be useful for hierarchical data or data sets that are non-independent. Additionally, GAMs are additive models that can be used to analyze non-linear relationships between the predictor and response variables. An advantage of combining these two methods is that it allows more flexibility than linear regression, but it is not as abstract as most machine learning techniques. More importantly, Dodson et al., 2009 also showed that this is a valid method to estimate the quantitative correlation between the airport and locally observed black carbon concentrations. Based on this conclusion a similar model structure is developed here. Additionally, the availability of road traffic information for this case study should overcome one of the limitations of the previous study. Once completed, the application of this approach for the case study of Schiphol does not only provide quantitative estimates of airport contributions to NO, NO_2, PM_{10}, $PM_{2.5}$, and CO, but it also evaluates the implementation of road traffic as a parameter in such models. On top of that it also tests the applicability of this method to other air pollutants.

The remainder of this section explains the methods used to develop the models for analyzing the effects of aircraft take-offs and landings on local concentrations of the pollutants of interest. This process consists of three steps (Zuur et al., 2009). First, the distribution of the response variable should be determined. Once the distribution is known, the model shape is defined and the variables of interest are added to the model's equation. Finally, the need for a link function that connects the expectations from the predictor values to the dependent variable should be analyzed. These three steps are further explained in the next subsections.

3.4.2. Distribution of response variables

In linear regression and additive modelling it is assumed that the response variable is normally distributed. For generalized linear modelling and GAMs, on the other hand, the distribution is non-Gaussian (Zuur et al., 2009). Which distribution is required for the models depends on the distribution of the response values. In

this case, these are the measured concentrations of the pollutants. The distributions for NO, NO_2, PM_{10}, $PM_{2.5}$, and CO measured at Badhoevedorp are shown in figure 3.7. The distributions of NO, NO_2 and PM_{10} from figure 3.7 show the same patterns as those of Hoofddorp and Oude Meer.

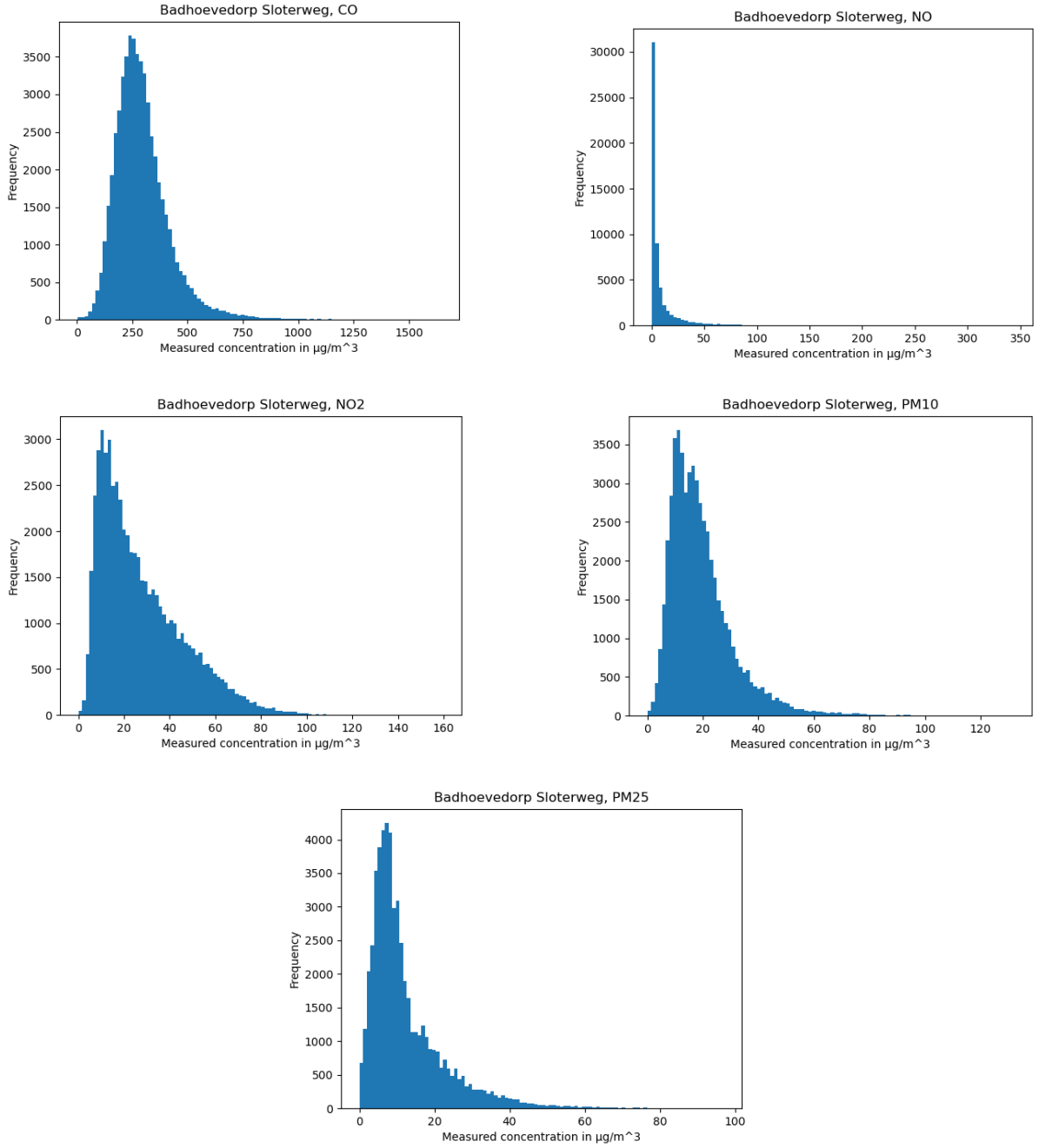

Figure 3.7: The distributions of AQ measurements at Badhoevedorp.

From figure 3.7 it follows that all distributions are asymmetric and skewed to the right. This is the smallest for CO, but this distribution is still slightly skewed to the right. Based on this distribution and the fact that the data is considered continuous, the gamma distribution is considered the appropriate distribution and will be used in the models of all species.

3.4.3. Model structure and candidate variables

With the distributions known, the second step is to determine the covariates and set up the function. Choosing the final models that will be used to estimate the effect of aircraft take-offs and landings on pollutant concentrations at the AQ monitoring sites will be based on a trial and error method. This means that several models are tested and based on their performance one configuration is considered the best fit. This configuration will then be used to estimate the effect of airport parameters on the pollutant concentrations. Five different combinations of model parameters were tested, these models and the reason for including them will be discussed here.

As mentioned before, a combination of GAM and LME models is used. The smooth terms, e.g. the GAM part of the model, was introduced using thin-plate splines (Wood, 2003). The smooth part is a function of wind vectors in m/s in East-West (x) and North-South (y) directions. Other parameters are implemented as fixed terms in the LME model. The function is shown in equation 3.7.

$$Y = \beta_0 + \mathbf{X}\beta + f(w_x, w_y) + \epsilon \tag{3.7}$$

The predictor (Y) is the measured concentration ($\mu g/m^3$), β_0 is the intercept ($\mu g/m^3$), β is a matrix with the regression coefficients, X is a vector including the values of all linear parameters, $f(w_x, w_y)$ is the smooth function based on the wind vectors and finally ϵ is the random error term. This model structure is similar to the one proposed by Dodson et al., 2009. However, the covariate vector X includes different terms.

In order to have a reference, the first model only contained meteorological parameters. These parameters include temperature (°C), wind speed and direction as two vectors (m/s) as mentioned earlier and the amount of precipitation in the last hour (mm). Once this reference is created the hourly number of landings and take-offs are added in the second model. Subsequently hourly road traffic intensities, expressed as the amount of vehicles that use the road per hour, are added.

If one has a close look at the map of Schiphol (figure 3.5), it can be observed that the airport, roads and AQ monitoring stations are intertwined over the area. As there is data available from all roads separately, including them as individual parameters might improve the model's accuracy. Tests with models that include separate parameters for local (N) roads did not improve performance. No statistically significant relations were found between these parameters and AQ measurements. Therefore, only highways are taken into account during the remainder of the analysis. In order to test which parameters should be used, models with only one road parameter where compared to those with parameters for the A4, A5 and A9 separately. The parameters A4, A5 and A9 contain the hourly number of vehicles using these roads in both directions. If a single road parameter is used, its value is the average of the intensities of the individual road traffic intensities or the nearest highway only. In the latter models the A4, A5, and A9 were used for Oude Meer, Hoofddorp, and Badhoevedorp, respectively.

All the variations of X are shown in table 3.8. Before these models were compared, some other variations were tested. For example, chapter 5 concluded that a significant time sensitivity is present in the hourly polar plots. Based on this conclusion a shorter test run was performed in which the hour term was added to the model's smooth function. In all cases this resulted in significantly worse performance, therefore this structure was not used as one of the final candidate models. Another early test compared the application of a link function, after comparing inverse, log and identity links the log link was chosen. Thus, for all models a gamma distribution with a logarithmic link function. All modelling is done using the nlme (Pinheiro et al., 2020) and mgcv (Wood, 2017) packages in R.

3.4.4. Fitting and evaluating model performance

For each combination of AQ monitoring site and pollutant, models with different parameters and structures had to be created and evaluated. Models are fitted on data from July 2018 to August 2020 and the model's predictive performance is tested in a separate subset of data from January to June 2018. Additionally, the temporal autocorrelation of the data sets was determined. Autocorrelation is the dependency of the current value on the variable's previous value. The air quality measurements are taken on an hourly basis and the

Table 3.8: An overview of the parameters in the linear regression part (X in equation 3.7) of the different models

Model	Temperature	Precipitation	Wind vectors	Take-offs	Landings	All aircraft	A4	A5	A9	Average roads
1	√	√	√							
2	√	√	√	√	√					
3	√	√	√	√	√		√	√	√	
4	√	√	√	√	√					√
5	√	√	√	√	√		√*	√**	√***	
6	√	√	√			√				
7	√	√	√			√				√

* Only at Oude Meer ** Only at Hoofddorp *** Only at Badhoevedorp

measurement taken at one hour is likely to be related to the concentration that was present the hour before. Thus, the previous measurement would then be related to the current measurement. Taking this into account, autocorrelation is expected. If indeed this can be seen in the data set, this should be accounted for when fitting the model. Once this is done, the model itself should be fitted and finally the results are evaluated. When all steps are completed, the most appropriate model can be chosen. This process is repeated for all pollutants measured at stations Hoofddorp, Badhoevedorp and Oude Meer.

One method to determine the autocorrelation in a data set involves the calculation of spearman's rank correlation coefficient (R_s) (Dodge, 2008). This coefficient can be used to determine the statistical correlation between the rankings of two variables. If this correlation is strong, R_s approaches 1 or -1, while a weak correlation results in a R_s closer to 0. R_s values approaching -1 and 1 represent almost perfect negative and positive relations between the variables, respectively. The coefficient is calculated using formula 3.8.

$$R_s = \frac{Cov(X,Y)}{\sigma_X \sigma_Y} \tag{3.8}$$

where,

$$Cov(X,Y) = \frac{\sum_{i=1}^{n}(X_i - \overline{X})(Y_i - \overline{Y})}{n-1}$$

$$\sigma_X = \sqrt{\frac{\sum_{i=1}^{n}\left(X_i - \overline{X}\right)^2}{n}} \qquad \text{and} \qquad \sigma_Y = \sqrt{\frac{\sum_{i=1}^{n}\left(Y_i - \overline{Y}\right)^2}{n}}$$

In these formulas X and Y are two series of data points, the subscript i represents the i^{th} data point of the series and $\overline{X}$ and $\overline{Y}$ are the means of X and Y, respectively. The variable n is the length of X and Y. In the case of AQ measurements the autocorrelation refers to the temporal relationship correlation between subsequent observations in the same series. Therefore a 1-hour lag autocorrelation is calculated. This means that the data set is compared with a data set shifted by one. Thus, if the original series is represented by X, then Y_i is X_{i+1}. The one-hour lag spearman rank correlation coefficients are presented in table 3.9, all values are statistically relevant.

Table 3.9: The spearman rank correlation coefficients for the air quality measurement data sets.

	NO	**NO_2**	**PM_{10}**	**$PM_{2.5}$**	**CO**
Hoofddorp	0.86	0.88	0.85		
Badhoevedorp	0.89	0.91	0.86	0.89	0.92
Oude Meer	0.88	0.90	0.85		

Since all values in 3.9 are larger than 0.8, all data sets show strong temporal autocorrelation. As a result it will be necessary to account for this when fitting and testing the models. One way to do this is by using a moving block bootstrap similar to the one used by Dodson et al., 2009. Application of the moving block bootstrap involves a resampling of the data set and repetitively fitting the model through it. The steps of this method are:

1. Determine the moving block size k. In this case a moving block of 24 hours was taken in order to keep daily patterns.

2. Create blocks of length k with overlap to choose from in the next step. Creating blocks with overlap means that the same data point can be used in multiple blocks, i.e. if X is the data set of length n and the block length is 3, then the first block consists of data points X_1, X_2, X_3, the second block contains points X_2, X_3, X_4, and the final block is X_{n-2}, X_{n-1}, X_n.

3. In order to create a new data set n/k blocks are randomly chosen. These are combined in the order they were picked and form the new data set.

The previous steps have created a shuffled data set that is used to fit the models. The models that were fitted were explained in section 3.4.3. The aim of fitting these different models is to compare their accuracy and choose the one that performs best. Therefore, the next steps are:

4. Fit a candidate model from section 3.4.3.

5. Use this fitted model to predict the hourly concentrations of a subset of the original data that was not used for the fitting. Which part is used will be discussed later in this section.

6. The predictions of the previous step are compared to the true values. For each time point, the squared prediction error is calculated using

$$\text{Squared prediction error} = \left(X_{true} - X_{predicted}\right)^2 \tag{3.9}$$

   Per bootstrap repetition these prediction errors are averaged.

7. Steps 3 to 6 are repeated 1000 times and the values from step 6 are averaged for all 1000 repetitions. This results in one final value that can be used to compare the candidate models' performance. A comparison was made between the results of 500 and 1000 bootstrap replicates, but this only resulted in small changes of the squared prediction error and it did not affect the models that should be chosen. Consequently, based on these results and the large computational time 1000 bootstrap replicates were applied.

This procedure is followed for all combinations of stations and corresponding pollutants around Schiphol, except for O_3. The subset used for fitting the models is based on measurements from July 2018 until August 2020. For steps 5 and 6 data from January to June 2018 was used. This division was made such that the fitting contained information about both business as usual (BAU) conditions as well as the effects due to COVID-19 measures taken by the Dutch government. After completing the aforementioned steps the appropriate model for each station and pollutant is chosen. Once the appropriate models are known, the next step is to estimate the effects of the airport parameters on the predicted pollutant concentrations.

3.4.5. Estimate airport contributions to ambient AQ

As a result of the model structure the effects of the airport on ambient AQ cannot be directly deduced from the model's parameters. Therefore, the estimated effect of the number of take-offs and landings is examined by using the best model from section 3.4.3 according to the procedure of the previous section. This is done by fitting the model through the entire data set and predicting local concentrations of NO, NO_2, PM_{10}, $PM_{2.5}$, and CO at the corresponding monitoring sites for the true conditions and with the values of take-offs and landings set to zero. At every hour in the data set this results in a predicted value with and without aircraft contributions.

These predictions can be compared and finally the absolute and relative effects of the take-off and landing parameters can be estimated. Since the time period of available measurements contains a special period with a significant decrease in flight activities compared to the years before, predictions will be made for the BAU case and the special period due to the COVID-19 lockdown. The BAU period contains data from 1 January 2018 until 26 March 2020, while the special case is the period from 27 March 2020 until 31 August 2020. By evaluating these periods separately potential effects of the COVID-19 measures taken by the Dutch government can be assessed.

4

Measurement locations and their effect on locally observed air quality

This chapter compares the AQ around Schiphol with other locations within the Netherlands. By doing so, this chapter provides an overview of the measured concentrations of NO, NO_2, O_3 PM_{10}, and $PM_{2.5}$ at various locations throughout the Netherlands. The methods and monitoring sites discussed in section 3.2 are used. To start, in section 4.1 the measurement results from the four different background sites are discussed. Subsequently section 4.2 presents the measurement results from the AQ monitoring stations closest to Schiphol. This chapter ends with a short conclusion regarding the measurement results and some discussion about the relevance of these results for the remainder of this research.

4.1. Analysis of measurements from different types of monitoring sites

The comparison is done based on hourly measurements from January 2014 until August 2020, unless explicitly mentioned otherwise. The averages of the measurements of NO, NO_2, PM_{10}, $PM_{2.5}$, and O_3 over the entire measurement period were calculated and are shown in table 4.1.

Table 4.1 shows that the averages vary strongly per background type and pollutant species. From the data it follows that observed concentrations of nitrogen oxides and $PM_{2.5}$ are lowest at urban and rural locations, while the opposite is true for O_3. For NO the difference in average concentrations is largest. Additionally the variance of the data is large for road stations, whereas rural and urban sites show more stable levels (figure 4.1). The stations near Schiphol show a higher median value than urban and rural sites, with a large variance in the data. NO is a primary pollutant that is directly emitted by car exhausts and aircraft engines with an atmospheric lifetime of minutes. Therefore, the significantly larger variance and average value could be explained by times of increased source activity, while at background sites in cities and rural areas the longer distance to sources could explain the lower average and variance.

Similar to NO, NO_2 is also a primary pollutant as a result of combustion processes. However, this species' atmospheric lifetime is longer. Consequently, after emission the molecules will be in the air for a longer period of time and can be transported over larger distances. Nevertheless, the stations located near roads still show the highest average value and largest variance as can be seen in table 4.1 and figure 4.1. The levels observed in the area surrounding Schiphol are the second highest, but both the long term average and variance of the data show a similar pattern. The numbers show that average nitrogen dioxide levels in the vicinity of Schiphol are 2.7% above the average of all stations considered in this research.

Ozone follows a pattern opposite to nitrogen dioxide. The highest average values are observed at rural and urban background stations, while Schiphol and near road stations measure less ozone in those areas. This can be partly explained by atmospheric processes. Ozone is not directly emitted and is a so-called secondary pollutant. As a result meteorology and background concentrations of especially nitrogen oxides play an important role in its formation and depletion (Pison and Menut, 2004). Schiphol actually shows the highest variance in the data, but its average value is 44.13 $\mu g/m^3$ which is just 2.9% under the average of all stations.

Table 4.1: The average concentrations measured for nitrogen oxides, particulate matter and ozone in $\mu g/m^3$ for the four types of measurement locations. The measurement period contains hourly measurements from January 2014 until August 2020.

	NO	**NO_2**	**PM_{10}**	**$PM_{2.5}$**	**O_3**
Schiphol	7.09	24.06	18.55	12.51	44.13
Rural	3.21	15.5	17.76	10.81	48.84
Urban	5.52	23.53	19.70	10.95	46.15
Road	17.83	30.64	20.77	11.86	42.72

The ozone measurements are compared in the period from January 2014 until 7 June 2017, as this is the only time ozone is measured around Schiphol.

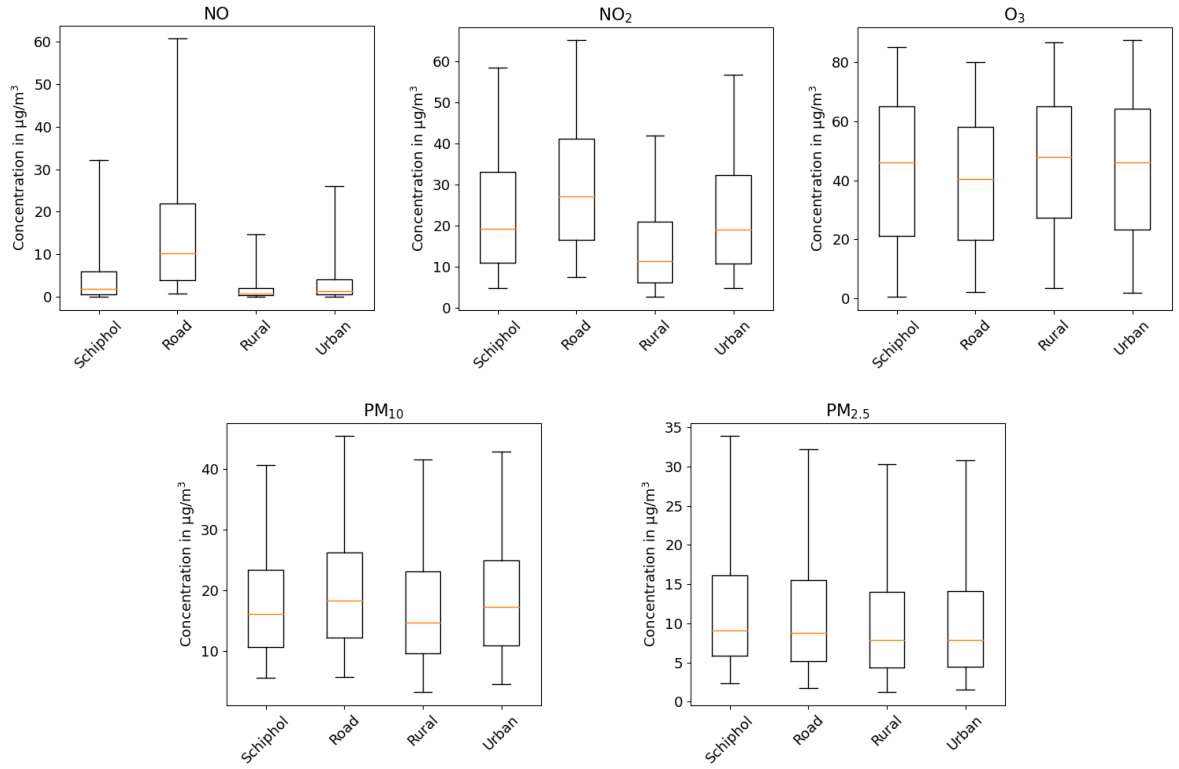

Figure 4.1: Box plots showing the air quality measurements from monitoring stations with different surroundings. The orange horizontal line shows the median of the data, the box shows the edges of the first and third quartiles and the whiskers show the edges of the 5th and 95th percentiles.

For particulate matter the data from table 4.1 shows that for PM_{10} road and urban stations measure the highest concentrations. The average concentrations measured at Schiphol are actually 3.4% below the overall average. However, around Schiphol the largest concentrations of $PM_{2.5}$ are observed. After NO, the relative difference regarding the overall average is largest for $PM_{2.5}$ as the station near Schiphol detected 8.48% more $PM_{2.5}$ compared to the mean of all stations. The variance in the data is similar for all background types.

4.2. Airport stations

There are three AQ measurement stations in the vicinity of Schiphol as shown in figure 3.5. Stations Hoofddorp, Badhoevedorp and Oude Meer are located North-West (but east of the Polderbaan), North and South-East with respected to the airport terminal building. A comparison between these stations is important as the direct surroundings of these stations are different. Station Oude Meer is located on a dike and is located at the edge of an industrial area with various warehouses and office buildings. On the other side there are some fields and a small marina. The measurement station is located 3.3 km from the airport's terminal building and 1.3 km from the Aalsmeerderbaan. The Hoofddorp station, on the other hand, is located only 440 meters

away from the start of the Polderbaan and is thus located significantly closer to the airport perimeter. However, the airport terminal building is 3.8 km away and there is a main highway between the airport terminal and the terminal building. The same goes for Badhoevedorp, actually two main highways are located within the terminal building and the measurement station. This station is located 2.8 km away from the airport terminal. Based on these different surroundings and the various orientations of stations relative to the airport the measurement results could be significantly different. This section will show the difference in measured AQ levels at the three stations closest to Schiphol.

The long term average values of the monitoring results are shown in figure 4.2. Only NO, NO_2 and PM_{10} are visible in this graph, as these are the only species with monitors at all three locations. The average levels of O_3 and $PM_{2.5}$ for the Schiphol stations shown in figure 4.1 are taken from Hoofddorp and Badhoevedorp, respectively. From figure 4.2 it follows that the highest levels of all three species are observed at Badhoevedorp. The absolute differences for NO between the highest value at Badhoevedorp and averages at Hoofddorp and Oude Meer are 2.93 and 3.82 $\mu g/m^3$, respectively. These differences are over 40 and 50 % of the area's average concentration of 7.07 $\mu g/m^3$. These percentages are lower for NO_2 and PM_{10}. Compared to Badhoevedorp, the average values for NO_2 are 5.81 and 4.75 $\mu g/m^3$, or 24.1 and 19.7 %, lower at Hoofddorp and Badhoevedorp, respectively. Subsequently, for PM_{10} the differences between Badhoevedorp and the other stations are 1.81 and 0.96 $\mu g/m^3$, or 9.8 and 5.2 % of the stations' overall average.

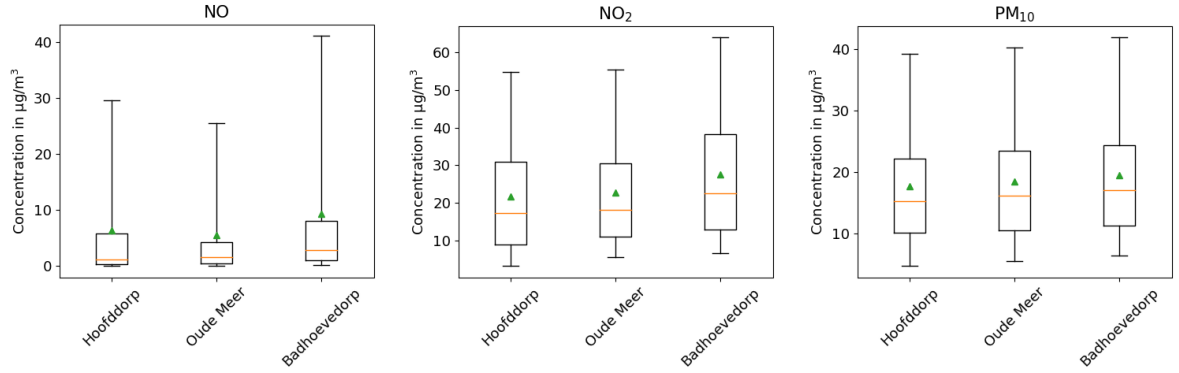

Figure 4.2: Box plots showing the air quality measurements from the three monitoring stations closest to Schiphol. The orange horizontal line shows the median of the data, the green triangle shows the mean, the box shows the edges of the first and third quartiles and the whiskers show the edges of the 5th and 95th percentiles.

Even though the relative differences for PM_{10} are lowest, they are still significant. For instance, when taking the values from Hoofddorp alone the results are almost the same as those of rural sites from figure 4.1. The results from Badhoevedorp, on the other hand, are closer to urban conditions. As mentioned before these relative differences between the stations are even higher for NO and NO_2. At Badhoevedorp, the average concentration of NO_2 approaches the value of road stations while at Hoofddorp the average is 1.76 $\mu g/m^3$ lower than the long term average of all urban sites. However, all stations still show significantly higher averages than rural background sites. Relative differences are highest for NO. At Oude Meer, the results are similar to those of urban locations while Hoofddorp and Badhoevedorp are higher than rural and urban sites but more than 8 $\mu g/m^3$ lower than near-road monitoring sites.

The aforementioned results show that there are significant differences between the long term averages of pollution levels at the three monitoring stations around Schiphol. These differences highlight the importance of taking multiple measurement locations into account and analyzing the results of all three stations and pollutants one by one. Therefore the subsequent chapters will always analyse the data sets from these three stations separately.

4.3. Conclusion and discussion

The results from the different types of monitoring sites have been presented in this chapter. These results show that for NO_2 the median and variance around Schiphol are higher than those observed at rural and

urban sites, but lower than road stations. The long term mean concentration of NO_2 is 0.63 $\mu g/m^3$, or 2.7% higher than the overall average. In contrast, for NO the mean at Schiphol is 1.32, or 16%, below average. This is mainly due to the very high average from road monitoring stations. Compared to rural and urban background sites, the average at Schiphol is actually 3.88 (121%) and 1.57 (28%) $\mu g/m^3$ higher, respectively.

Besides differences between categories of monitoring sites, there are also strong deviations between the measurements taken at the three Schiphol stations. At Badhoevedorp, the average concentration of NO_2 approaches the value of road stations. While on the other hand Hoofddorp's average is 1.76 $\mu g/m^3$ lower than the value of urban sites. All three stations show higher average values than rural sites. The relative differences in terms of concentrations are largest for NO. The differences in concentrations can be up to 50% of the area's average NO level of 7.1 $\mu g/m^3$. At Oude Meer the results show similar behavior to urban background sites, while the data from Hoofddorp and Badhoevedorp lie 0.7 $\mu g/m^3$ and 2.23 $\mu g/m^3$ below and above the area's average value, respectively.

For O_3 the results show an inverse trend compared to nitrogen oxides. Highest mean values are linked to rural and urban monitoring sites, while the lower values are observed at Schiphol and near roads. The long term mean at Schiphol is 1.33 $\mu g/m^3$, or 2.9%, lower than the overall average. This is based on measurements taken between January 2014 and 7 June 2017. No comparison between locations around Schiphol could be made, as Hoofddorp was the only location with O_3 monitoring equipment.

Compared to the previous species, PM_{10} behaves differently as road and urban locations show the highest averages. The results from Schiphol show that the long term average from these three stations lies 0.65 $\mu g/m^3$, or 3.4 %, below the overall average. Of the three pollutants that could be compared at the three monitoring sites around Schiphol, the variations of long term average levels were lowest. The differences between the averages of the stations are less than 2% of the stations' averages.

The last pollutant discussed here is $PM_{2.5}$. This is the only pollutant for which the highest average is measured near Schiphol. At Schiphol the average is 0.98 $\mu g/m^3$, or 8.48%, higher than the overall mean. This value is remarkably similar to the case study for Atlanta Airport by Unal et al., 2005. Their research estimated that Atlanta Airport was responsible for an average increase of 1 $\mu g/m^3$ in the Atlanta area. When looking at these numbers one should take into account that Badhoevedorp is the only location near Schiphol where $PM_{2.5}$ is monitored. This site is also located close to some highways, so this could result in a larger difference to the mean than would be observed if the other locations near Schiphol monitored $PM_{2.5}$ as well. Besides the limitations due to the lack of multiple monitoring sites, $PM_{2.5}$ is also a secondary pollutant which means that long range transport could be another source that affects local measurements.

5

Air quality measurements versus wind conditions

Previous studies that investigated the effects of airports on local air quality have shown that correlations between wind parameters and AQ measurements are useful to assess airport contributions to ambient AQ levels. Therefore, this chapter investigates the correlation between these parameters based on the methodologies presented in section 3.3. The goal of this chapter is to determine both qualitatively as quantitatively if the airport has an effect on ambient AQ. Section 5.1 presents the results per station and in section 5.2 results for the background subtraction methods are presented. This chapter concludes with a discussion about the results in section 5.3.

5.1. The effect of wind conditions on AQ measurements per monitoring site

Based on the measurements from January 2014 until August 2020, polar plots for all pollutants for the three AQ measurement stations around Schiphol are created and shown in section 5.1.1. In order to interpret these results, it is important to consider the stations' locations relative to the airport as shown in figure 5.1. This section is divided in two parts. First, the polar plots based on all measurements taken between 6am and 10pm are discussed. Thereafter the sensitivity of the results with respect to time is discussed. The time frame for the first part is chosen based on flight activities at Schiphol.

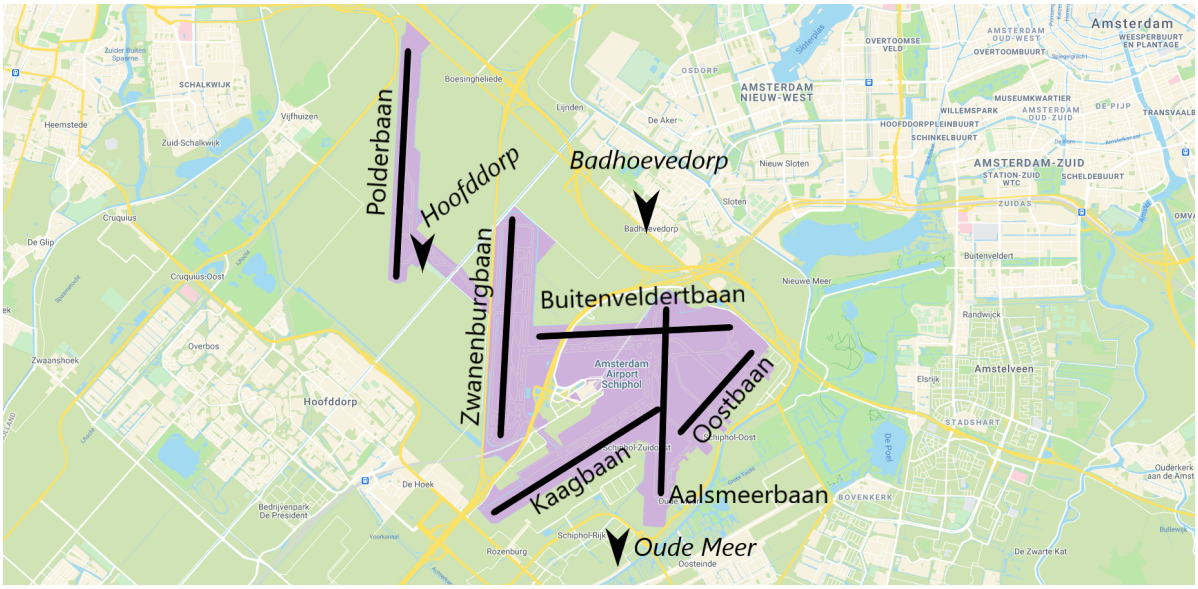

Figure 5.1: An overview of AQ monitoring sites and runways at Schiphol

5.1.1. Overall results

Around Schiphol ambient concentrations of NO, NO_2, PM_{10}, O_3, $PM_{2.5}$ and CO are monitored. The monitoring results versus local wind conditions are shown in figures 5.2, 5.3, 5.4 and 5.5. How these graphs should be interpreted and what the results say about the effect of Schiphol on AQ measurements will now be discussed in more detail.

To start, the graphs for NO are shown in figure 5.2. As at all three stations the highest concentrations appear at wind speeds lower than 4 m/s, which suggests that emissions from sources closer to the monitoring sites are dominant. NO has a short atmospheric lifetime, therefore at low wind speeds it will take too long to transport emissions from more distant sources to the AQ monitor in order to observe an effect on measured concentrations. Additionally, peaks observed at low wind speeds suggest that ground level sources such as emissions from road traffic are present (Yu et al., 2004). Inversely, peak values detected at higher wind speeds suggest that the pollutant is emitted through buoyant plumes from chimneys and, for example, aircraft. At Oude Meer, there is however no real peak pointing in the direction of the airport. So from graph 5.2c, it seems unlikely that airport related emissions play a significant role for NO concentrations measured at Oude Meer. On the other hand, for Badhoevedorp and Hoofddorp there are peaks pointing in the direction of the airport. Especially at Hoofddorp an increase in observed levels of NO with winds from the North-West is present. This coincides with the location of Schiphol's Polderbaan, suggesting that the higher levels of between 10 and 15 $\mu g/m^3$ are a result of aircraft moving at and near the Polderbaan. Compared to the overall average of 6.39 $\mu g/m^3$ observed at this measurement station as mentioned in section 4.2, this is a doubling of the concentration of NO when the station is located downwind from the Polderbaan. At Badhoevedorp, there is also a section in the South/South-East direction which indicates that a source is located in this direction. As this elevation is detected at higher wind speeds, this could be the effect of aircraft landing or taking-off from the Aalsmeerderbaan. Besides peaks at higher wind speeds, both figures 5.2a and 5.2b show that highest values are shown at low wind speeds and point, albeit weak, in the directions of nearby highways.

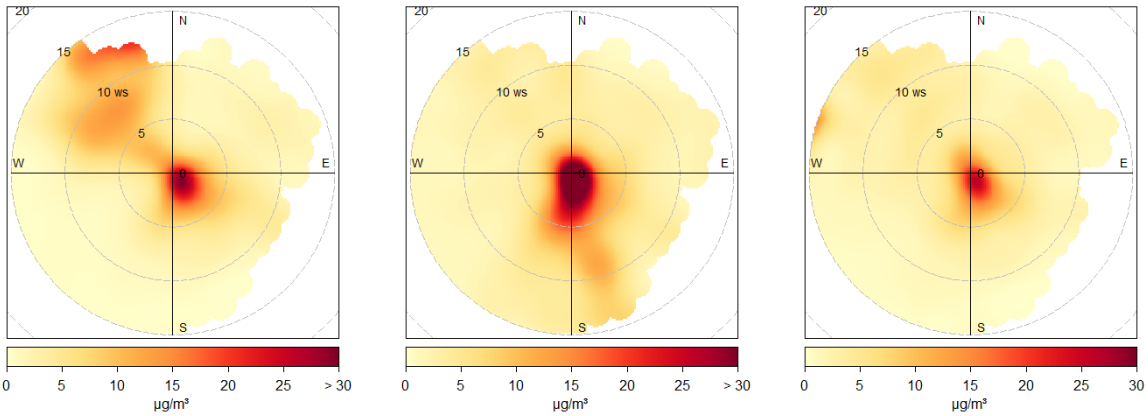

(a) Hoofddorp (b) Badhoevedorp (c) Oude Meer

Figure 5.2: Polar plots for NO.

Figure 5.3 shows the polar plots for NO_2 at the measurement stations closest to Schiphol. At first, the graphs seem to show similar behaviour to the ones for NO. However, there are some significant differences. For example, relatively speaking higher concentrations are observed at higher wind speeds. The directions of these elevated levels do however point in the same directions as the peaks in the graphs of NO. This indicates that the main sources of both NO and NO_2 are located at the same locations relative to the measurement stations. This is not unexpected, as both species are emitted through combustion of fossil fuels. Based on a similar analysis as for NO, at Hoofddorp main sources seem to be located in the directions of the Polderbaan and the A5 in South-Eastern direction. There is also a peak in Southern direction, even though there is only a relatively small national road 700 meters away from the monitoring station and the first other logical sources could be Hoofddorp and the to-roads for the A4 at 2 and 4 kilometers away, respectively. However, if Hoofddorp is a large source one would also expect to observe a peak in the direction of Amsterdam, especially at

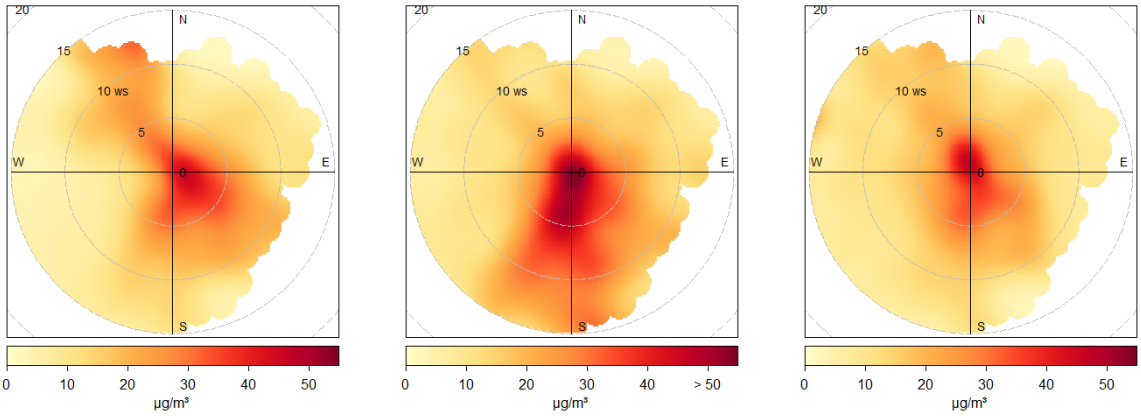

(a) Hoofddorp (b) Badhoevedorp (c) Oude Meer

Figure 5.3: Polar plots for NO_2.

Badhoevedorp, as this is a bigger city. Yet, Figure 5.3b does not show a similar peak in the North-East direction. At Badhoevedorp higher NO_2 levels originate from emissions South of the monitoring station. At wind directions between 135 and 225 degrees, where the peaks are observed, there are several large hypothetical sources such as the A4, A9, four runways and the airport's terminal building. Thus, determination of the exact cause of the boost of NO_2 for winds from this region is difficult. Nevertheless, at Badhoevedorp winds from the Southern region result in higher NO_2 pollution levels than winds from Amsterdam. At Oude Meer it is more difficult to determine whether elevated levels are observed with winds from the airport. At wind speeds lower than 5 m/s, the highest concentrations are observed for winds from the North-West. Whether this is due to the airport is uncertain, thus further investigation is required.

PM_{10} is the third and final pollutant that was measured from 2014 until 2020 at all three stations around Schiphol. Compared to the previous species, graphs 5.4a to 5.4c are relatively similar to each other. Actually, for concentrations above 20 $\mu g/m^3$ the measurement location relative to the airport does not seem to have an effect. At all three locations, peak values are observed at Easterly winds. The presence of nearby roads or the airport do not seem to affect the graph's lay-outs. Additionally, section 4.2 also showed that the relative differences between the three measurement stations around Schiphol are lowest for PM_{10}. Taking these results into account, these graphs do not suggest that local concentrations of PM_{10} increase if the measurement location is located downwind of the airport.

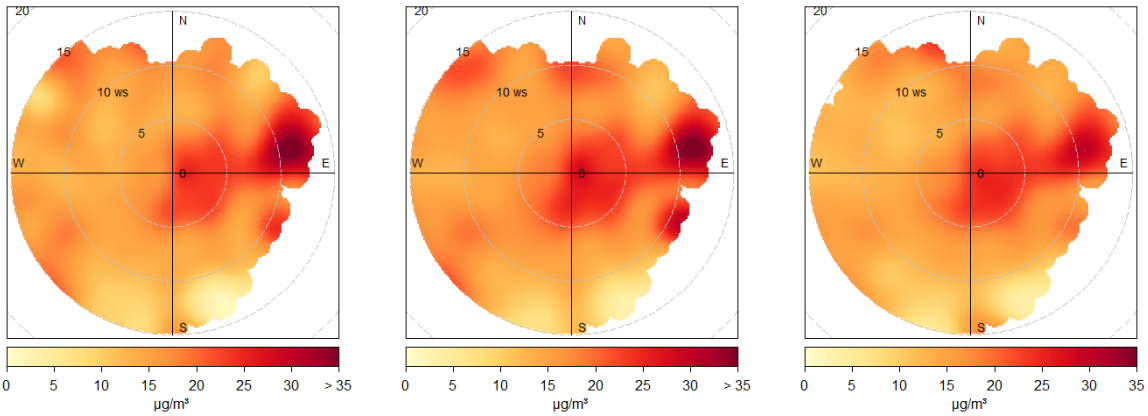

(a) Hoofddorp (b) Badhoevedorp (c) Oude Meer

Figure 5.4: Polar plots for PM_{10}.

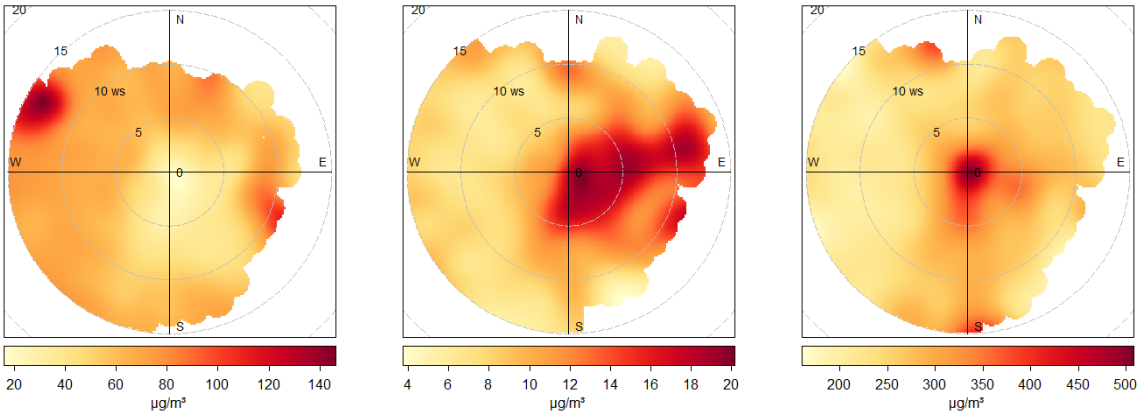

(a) Hoofddorp, O_3 (b) Badhoevedorp, $PM_{2.5}$ (c) Badhoevedorp, CO

Figure 5.5: Polar plots for O_3 measured at Hoofddorp and $PM_{2.5}$ and CO measured at Badhoevedorp.

The final three pollutants that are measured around Schiphol are O_3, $PM_{2.5}$ and CO. To start, the results for O_3 are shown in figure 5.5a. Unfortunately, for this pollutant only measurements from January 2014 until June 2017 are available. Nevertheless, it could still be interesting to analyse the data from this shorter period. Compared to nitrogen oxides and partly also particulate matter, O_3 is a secondary pollutant and is formed by atmospheric processes. Especially nitrogen oxides play an important role in its formation and depletion. Studies by Pison and Menut, 2004 and Song et al., 2015 have shown that even though nitrogen oxide emissions at airports lead to an increase in O_3 at downwind background sites, local concentrations can decrease due to O_3 depletion by NO emissions. The results from figure 5.5a show that lowest values are observed at conditions with low wind speeds or winds from the East to South. These lower values coincide with the peaks of NO_2 and the direction of the airport's terminal and runways, except for the Polderbaan. This could indicate that even though the graphs of NO do not show a similar correlation, the emissions of NO in the direction of the airport still play a role in the decrease of local O_3 levels as they are emitted by the same processes as NO_2 but have a shorter atmospheric lifetime of just minutes.

Figure 5.5b shows the results for $PM_{2.5}$ measured at Badhoevedorp. Similar to the graphs of PM_{10}, the highest concentrations are observed at strong winds from the East and also winds up to 5 m/s from the East to South. These peaks mainly point in the directions of Amsterdam, nearby highways and the airport. Unfortunately, the presence of just one measurement location makes it impossible to use a background subtraction method for $PM_{2.5}$. Nevertheless, the red peaks at wind speeds up to 5 m/s and the orange area towards the South indicate that there are elevated levels of $PM_{2.5}$ when air is blown from the airport towards the measurement station in Badhoevedorp.

Finally, graph 5.5c shows the results for CO measured at Badhoevedorp. It is clear that the highest levels are observed at low wind speeds. This could indicate the importance of the nearby highways and urban areas. There is, however, also a peak to the South with winds up to 5 m/s. On top of this peak seems to continue at higher wind speeds, albeit with lower concentrations. These Southern peaks point in the direction of the airport. Thus, these could indicate an effect from the airport on local concentrations of CO.

5.1.2. Time sensitivity

So far, the correlation between wind and measured AQ levels has only been analysed over the entire time period between 6am and 10pm. However, atmospheric concentrations and source activities vary throughout the day. As shown in figure 3.6, road traffic will be highest during morning and evening rush hours and shows relatively stable intensities during working hours. For aircraft activities, figure 3.6 shows that there is a morning peak in arrivals, after which the amount of take-offs and landings fluctuates throughout the day. Some specific times to keep track of in this analysis are between 8 and 9am, 11am and 10pm due to many landings, and two peaks in take-offs outside traffic rush hours, respectively. Especially considering the model that will be constructed in chapter 6, it is of interest to test the sensitivity of measurement results based on the time of

day parameter. Hence the time sensitivity is tested by creating separate graphs for every hour created by the same method as mentioned before. This results in 288 graphs, based on 24 hours times the combination of pollutants and stations, which is 12. The results are all shown in appendix B. The time sensitivity observed in these graphs will be discussed here.

Following the same order as the previous section, the results for NO are analysed first. In general, with respect to the orientation of peak values from figure 5.2 the hourly graphs do not show different results. What does change is the height of these peak values. For all locations the highest values are observed between 5 and 9 o'clock in the morning. Throughout the remainder of the day the graphs remain fairly stable, except for Badhoevedorp which shows some peaks again between 5pm and 10pm. During nights no region of increased values are present in the graphs. In the afternoon, between 11am and 4pm there is just a weak signal in the directions where peak values were observed in figure 5.2. An interesting observation in the results of Hoofddorp is the peak pointing in the direction of the Polderbaan, which is strong between 8am and 2pm. After this time period the peak decreases before they reappear in the measurements of 4pm and 9pm.

Similar observations are made regarding the graphs for NO_2. There is a strong sensitivity of the graphs with respect to time. Hours that show the characteristic shapes of the overall graphs are largely analogous to the times mentioned for NO. During morning and evening rush hours the patterns from figure 5.3 can be observed. Interestingly, a difference that can be identified is that the elevated concentrations in Hoofddorp in the North-West direction are visible throughout the day, but disappear completely during the night. The other spike in the South-East direction is visible at all times. In general, graphs of both NO and NO_2 show patterns similar to both flight movements and road traffic intensities.

Different conclusions were drawn for PM_{10}. The results from section 5.1.1 did not suggest that the airport has a large impact on local PM_{10} concentrations as all graphs were fairly similar. When analysing the results per hour, this conclusion is not refuted. During the day the wind directions and speeds responsible for peak values do not change.

As mentioned before, for O_3 measurements are only available from 2014 to 2017 at Hoofddorp. There are however some interesting characteristics present in the hourly polar plots for O_3. For example, the lower concentrations related to winds from the South-East are less evident in the afternoon between 12 and 4. In a similar time interval, from noon to 7pm, the overall concentrations seem higher in the area. Other than these two notes, there are no big changes detectable.

For $PM_{2.5}$ the overall results showed that winds from the East and South result in the highest concentrations in Badhoevedorp. When looking at the hourly pattern for this pollutant, all graphs share this result as no consistent peaks from other directions are visible. It is clear from figure 5.5b that the highest pollution levels are related to winds from the East and South. The orientation does vary slightly throughout the day, but no clear pattern is found in the results.

Finally, the results for CO are analysed per hour. In section 5.1.1 it was concluded that nearby highways could play an important role for the peak values observed at low wind speeds in graph 5.5c. The hourly results are shown in appendix B and support the previous conclusions. Between 5 and 10 am and 4 and 11 pm the highest concentrations of CO are observed at low wind speeds. These times partly coincide with rush hours. This, combined with the presence of nearby highways indicates that these roads play an important role in increasing local CO levels at Badhoevedorp. At other times the highest values are also measured during low wind conditions. Additionally, similar to graph 5.5c there are several lower peaks at winds from the South. These are observed between 6am and 10pm. This could indicate that the airport plays a role for these values, but the graphs are insufficient to draw strong conclusions.

This section has shown that the results from section 5.1.1 are not necessarily representative for all times of day. During the day the locations with respect to the measurement stations of the most prominent pollution sources can vary. Based on these results there are indications that the airport has an effect local concentrations of NO and NO_2. The same goes for O_3, $PM_{2.5}$ and CO, but this correlation is subject to larger uncertainties due to the lack of multiple measurement locations. As multiple measurement locations of NO, NO_2 and PM_{10} are available, the study of these species can go a step further. Depending on wind conditions, data

from other stations can be used to create background levels and to compare the observations of a station downwind of the airport with those from upwind locations. This method and the results will be presented in section 5.2.

5.2. Background subtraction

5.2.1. Overall results

Even though there are six species measured around the airport, only NO, NO_2 and PM_{10} are measured continuously at all three stations. As the background subtraction method allows a comparison between measurement locations, the results of this section will be more quantitative than the ones from previous sections. This way, a first quantitative estimation about airport effects on local concentrations of NO, NO_2 and PM_{10} can be made.

To start, figure 5.6 shows the results for NO. It is clear that the largest difference in measured concentrations is observed between Badhoevedorp and Oude Meer. At wind free and calm wind conditions the levels at Badhoevedorp are on average more than 20 $\mu g/m^3$ higher. Compared to this dissimilarity, at other wind conditions the differences are significantly lower. There is, however, still a difference of between 5 and 10 $\mu g/m^3$ in figure 5.6b for Southern winds up to 15 m/s. This peak does point in the direction of the airport. Interestingly, a similar peak for Northern winds is not present in figure 5.6c. It is important to consider the short atmospheric lifetime of several minutes when analyzing these graphs and the distance of several kilometers between the measurement locations. Comparing Badhoevedorp and Oude Meer, there is an important difference in their surroundings as Badhoevedorp is located just North of a large highway. Oude Meer, on the other hand, is located within office buildings and a semi-urban area to the South. This probably explains the difference at low wind speeds between these two stations. The peaks at higher wind speeds in figure 5.6b can be observed at Badhoevedorp, but not at Oude Meer, because the sources are located closer to Badhoevedorp and the NO will have disappeared before reaching the station in Oude Meer. Yet, On all graphs there are areas with weak positive differences in the directions of the airport terminal.

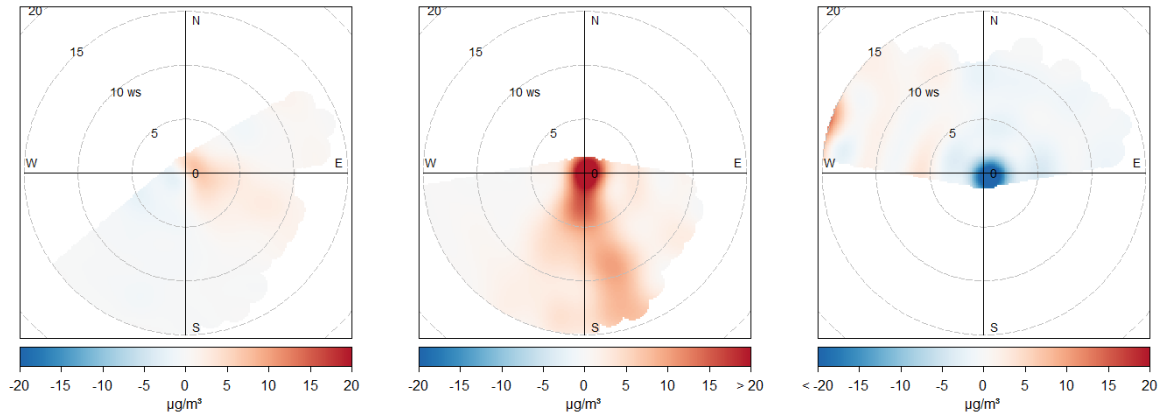

(a) Hoofddorp with background from Oude Meer subtracted.

(b) Badhoevedorp with background from Oude Meer subtracted.

(c) Oude Meer with background from Badhoevedorp subtracted.

Figure 5.6: Background subtraction plots for NO.

With respect to NO, the atmospheric lifetime of NO_2 is longer and can therefore be observed further away from the source. The results for this pollutant can therefore be more interesting than those of NO. Figure 5.7 shows the graphs for NO_2. When looking at these graphs it is immediately visible that for all stations there is an elevation of NO_2 of 5 $\mu g/m^3$ or more if the background station and the airport are located upwind of the monitoring site. Extreme values are present at Badhoevedorp, where the elevation is approximately 15 $\mu g/m^3$ and sometimes even more. For reference, the average concentration of NO_2 measured at this site over the entire measurement period is 27.58 $\mu g/m^3$. An increase of 15 $\mu g/m^3$ between Oude Meer and Badhoevedorp suggests that sources located between these two measurement stations are responsible for more than 50% of the ambient NO_2 at Badhoevedorp.

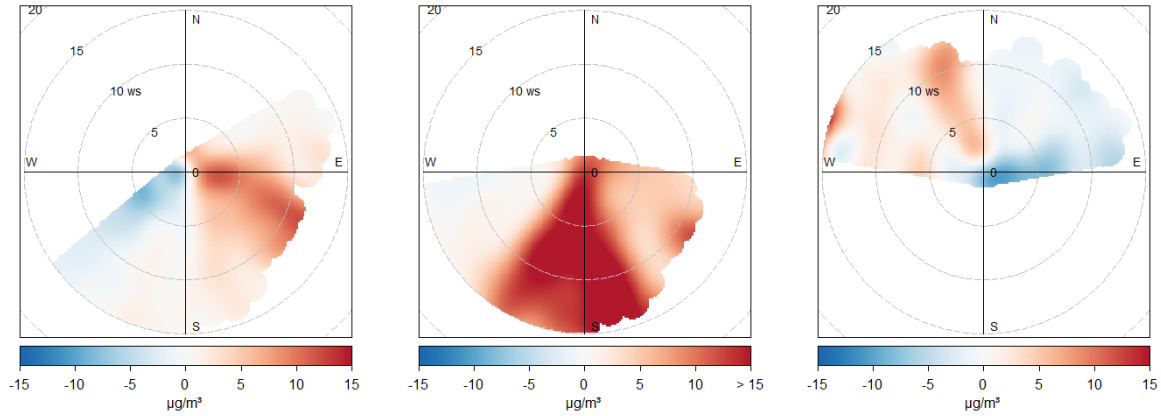

(a) Hoofddorp with background from Oude Meer subtracted.

(b) Badhoevedorp with background from Oude Meer subtracted.

(c) Oude Meer with background from Badhoevedorp subtracted.

Figure 5.7: Background subtraction plots for NO_2

At the other two graphs, 5.7a and 5.7c, the differences are not as high as the previous one. However, there is still a positive relation between winds from the airport and ambient NO_2 levels. The comparison between Hoofddorp and Oude Meer, as shown in figure 5.7a, shows that between both locations the atmospheric concentration of NO_2 increases. Between Southern and Eastern winds the difference is between 5 $\mu g/m^3$ and 12 $\mu g/m^3$. Similar to the other graphs for this pollutant in figure 5.7, the highest elevations are pointing in the direction of the airport terminal and the three runways closest to the terminal (Kaagbaan, Buitenveldertbaan and Zwanenburgbaan). At Oude Meer winds from these runways and the terminal building also result in a steady increase of NO_2. For both Hoofddorp and Oude Meer the peaks pointing towards these sources are present at high and low wind speeds, indicating that ground sources as well as higher sources such as aircraft and buoyant plumes from chimneys in the area affect the measurements. Increases of 5 and 12 $\mu g/m^3$ are equal to 23 and 55 % of the average ambient NO_2 levels at Hoofddorp. At Oude Meer, the peak at winds from the North/North-West results in elevations of 5 to 10 $\mu g/m^3$, which is equal to 22 and 44% of the station's average value, respectively.

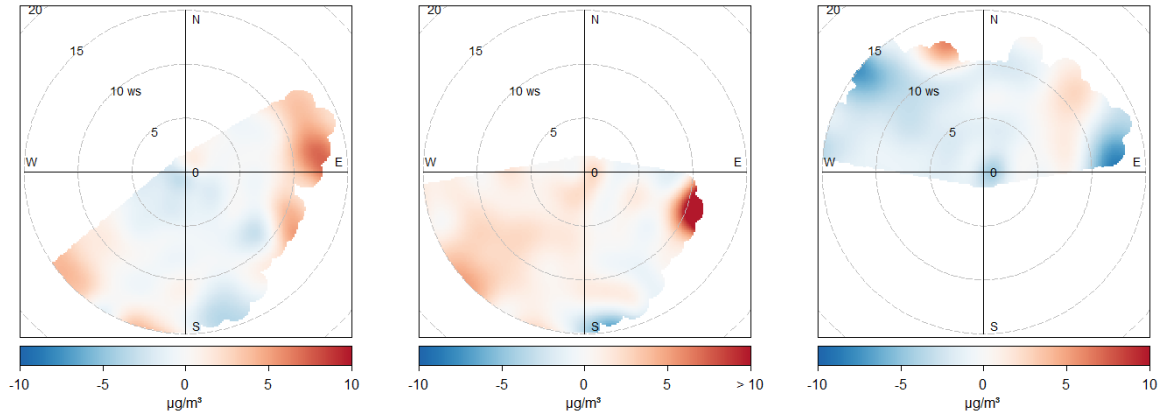

(a) Hoofddorp with background from Oude Meer subtracted.

(b) Badhoevedorp with background from Oude Meer subtracted.

(c) Oude Meer with background from Badhoevedorp subtracted.

Figure 5.8: Background subtraction plots for PM_{10}

Compared with the previous results, the graphs of PM_{10} shown in figure 5.8 are not as unambiguous as those of NO_2. At high wind speeds in the North/North-West direction figure 5.8c shows a peak of around 5 $\mu g/m^3$. Similarly to what was observed earlier at this station, this is in the direction of the airport's terminal. Nonethe-

less, at other wind directions and even at lower wind speeds this positive value turns negative. At Hoofddorp comparable behaviour is observed. With strong winds from the East and South-East the difference is positive, while values for weaker winds from the airport's direction are negative for this station as well. Finally, figure 5.8b shows a different pattern. Sources that have a positive effect are located between South and West of this station. This is partly pointing in the direction of airport, but the clearest peak is pointing in the directions of nearby fields and the closest highway. Adding the results of graphs 5.8a to 5.8c together does not result in an evident conclusion about the quantitative or qualitative effect of the airport on ambient PM_{10} concentrations.

5.2.2. Time sensitivity

In order to further investigate the effects of local sources on the trends mentioned in the previous section, the time sensitivity of the background subtraction method is analyzed in this section. By doing so, potential correlations between the AQ measurements and flight and road traffic trends will be deduced. All the graphs used to draw the conclusions in this section can be found in appendix C.

Similar to the other sections in this chapter, results for NO will be discussed first. At all three graphs of NO in figure 5.6 there are some positive differences between the main and background stations. When these graphs are decomposed into their hourly components, it becomes clear that the patterns shown in the overall graphs are not representative for all times of day. To start with Hoofddorp, figure 5.6a already showed a relatively weak effect. This graph's hourly pattern showed that at most times the difference with the background location is small. Only during morning rush hours there are some small differences and in general there is a small positive difference with winds from Oude Meer. At Badhoevedorp on the other hand, the patterns are more pronounced. Especially at morning there is an increase over the area, with an additional peak late in the evening between 7 and 10pm. The opposite is true for Oude Meer. At almost all times lower concentrations are measured at Oude Meer compared to Badhoevedorp. This result shows a limitation of this methodology for NO. This is a gas with a short atmospheric lifetime and therefore emissions far away from the monitoring site might already be transformed into NO_2. Analyzing the results of NO_2, which has a longer atmospheric lifetime, might therefore be more relevant.

Again starting at Hoofddorp, the pattern from figure 5.7a is present throughout the day. There are no fluctuations in the directional term, but only in magnitude. Highest increases are observed during morning peak hours for road and air traffic and later in the evening. From 4am until 10pm the minimum variation of 5 $\mu g/m^3$ is visible for winds from the airport, with peaks as high as 15 $\mu g/m^3$ at the earlier mentioned times of higher source activities. The comparison between Badhoevedorp and Oude Meer is almost unchanged during the day. Only at night the difference decreases. Finally, at Oude Meer the patterns are also relatively stable and highest variations compared to the reference station are observed during times of higher source activities. Interestingly, winds from the North-West still result in higher concentrations at Oude Meer compared to Hoofddorp, even though this is also a region that results in elevated concentrations of NO_2 in figure 5.3a. Nevertheless, the differences are not as pronounced as those seen at Badhoevedorp and still show some negative changes, especially in the morning. Between 6 and 9pm the peak from the airport terminal's direction shows an increase that ranges between 7 and 14 $\mu g/m^3$.

For PM_{10} the inconclusive patterns observed in figure 5.8 do not change according to a pattern. So these results indicate that there are no dominant sources of PM_{10} in the area in between the monitoring stations.

5.3. Conclusion and discussion

The goal of this chapter is to determine the qualitative and quantitative effect of the airport on ambient AQ. This was done using wind parameters and locally observed concentrations of NO, NO_2, PM_{10}, $PM_{2.5}$, O_3 and CO. In order to draw conclusions a separate analysis per pollutant was required, which in turn led to different conclusions per pollutant.

The clearest effect of the airport on AQ measurements was visible for nitrogen oxides. Both NO and NO_2 showed signs of elevated concentrations of these pollutants when measurements are taken downwind of the airport. For NO the highest levels are observed at low wind speeds, indicating that nearby roads are an important source. At Hoofddorp winds from the nearby Polderbaan also result in average measurements more than twice as high as the station's long term average of 6.39 $\mu g/m^3$. Similarly, at Badhoevedorp average values

for strong winds from the airport's direction are also higher than the local long term average, albeit a smaller difference. Comparing measurements with background levels also showed that at all stations a marginal increase due to the airport is seen at Hoofddorp and Oude Meer. Only at Badhoevedorp, the earlier mentioned peak at strong winds from the airport is also visible and shows a difference of up to 12 $\mu g/m^3$ compared to the background site. Interestingly though, this strong increase is not observed when the background and main sites are reversed. Taking the short lifetime of NO into account, this could mean that the elevation at Badhoevedorp is mainly caused by sources closer to Badhoevedorp such as major highways.

Taking the results of all NO_2 measurements between 6am and 10pm, the concentrations increase at least 5 $\mu g/m^3$ compared to background sites located upwind of the airport. At Hoofddorp and Badhoevedorp the elevation can be as high as 10 and 15 $\mu g/m^3$, respectively. At Oude Meer this can even increase to 14 $\mu g/m^3$ between 7 and 9pm. These results show that at Oude Meer, Hoofddorp and Badhoevedorp the observed increase of NO_2 due to sources between the monitoring sites increase by 22%, 46% and 53% of the stations' long term average values, respectively. In combination with the long term higher averages at Badhoevedorp and Hoofddorp for winds from the airport's direction and the results from background subtraction, this study shows that important sources are located in the area between the measurement stations. Consequently Schiphol could play an important role in increasing local NO_2 levels.

Opposite to the results for nitrogen oxides, PM_{10} does not show clear increases or decreases for winds from the airport. Actually, the long term measurement results show that at all three locations similar patterns are present. Underlining these inconclusive results with respect to the airport's effect are the results obtained using background subtraction. No stable relationship was observed using this methodology. So far, there are therefore no indications of a significant effect of the airport on local levels of PM_{10}.

Finally, for O_3, $PM_{2.5}$ and CO background subtraction methods could not be applied. Consequently, these species were analysed based on the measurements from individual stations. For O_3 the results of this study are in line with previous studies. At conditions with high NO_x levels the concentrations are lowest. Local emissions of NO_x are therefore likely to decrease ambient O_3. The hourly behaviour supports this assumption, as depletion is less significant in the afternoon when Schiphol and local roads are less active. However, studies by Pison and Menut, 2004 and Song et al., 2015 have shown that further downwind the negative effects of these emissions are reversed. Unfortunately no measurements at such locations are available, so this cannot be confirmed in this research.

$PM_{2.5}$ and CO are measured at Badhoevedorp and have shown peaks related to winds from the South. For $PM_{2.5}$, the results show that at wind speeds lower than 5 m/s the effect from the airport's direction is highest. The average concentration measured under these conditions varies between 14 and 20 $\mu g/m^3$. Those values are significantly higher than the station's long term average of 12.51 $\mu g/m^3$. At wind speeds higher than 5 m/s the concentrations are closer to the long term average. The measurement time does influence these results. CO levels show a similar behavior at winds from the South. At low wind speeds most CO is observed. It is therefore expected that the nearby roads are the most important sources. The times of highest pollution levels coincide with peak traffic, but also partly with increased air traffic. As a result, both the airport and nearby roads can be important sources.

The latter is actually an important note to all results from this chapter. The methodology used here is able to determine source locations and useful to estimate the quantitative effect of such sources if located between two monitoring locations. If potential sources behave as point or line sources this method is strongest. Schiphol, on the other hand, is spread out over a larger area and activities take place at different locations within the airport perimeter. As a result, there is not one single point to focus on in the graphs. Additionally, the presence of three large highways in between the measurement locations will influence the results as well. Road traffic emissions from these highways are potentially incorporated in estimated from this chapter and could result in overestimation of the effects of Schiphol on ambient AQ. This limitation was also observed in previous studies by Yu et al., 2004 and Carslaw et al., 2006. In order to further investigate how Schiphol affects local AQ levels and to overcome this limitation, the next chapter presents the results of regression modelling based on all available data sets.

6

Regression Modelling

The results from chapters 4 and 5 have shown the differences in observed AQ levels and investigated the effect of wind parameters on measured concentrations, respectively. Even though this provides an estimate of long term effects of the airport on local AQ and locations of main pollution sources per species, the analysis did not include parameters for airport activities. This chapter presents the results from the models per pollutant species. Models are selected using the methodology from section 3.4 and the average mean square errors from table 6.1. Models with the lowest prediction errors are not always chosen to generate the final estimates. This is a result of anomalies in the regression parameters. What this means will be explained per pollutant. Once the models are chosen, two different cases were treated as the data offered information about the unique situation of decreased airport activities in 2020. First, the BAU case will be analyzed in this chapter, after which the effects of the COVID-19 situation from March to August 2020 are presented in chapter 7.

Table 6.1: The mean squared errors used to evaluate model performance. Bold values represent the models picked to generate the final estimates.

Station	Pollutant	1	2	3	4	5	6	7
Hoofddorp	NO	91.8	84.6	79.3	**82.4**	82.5	139.4	114.1
	NO_2	170.2	155.0	155.1	154.8	**154.4**	195.2	176.0
	PM_{10}	174.8	173.0	172.9	173.1	173.4	**172.6**	172.7
Oude Meer	NO	60,2	61.4	59.1	**59.9**	60.6	97.3	71.0
	NO_2	142.0	135.0	131.3	132.1	**131.9**	174.7	141.6
	PM_{10}	177.0	174.3	174.0	174.4	174.1	**172.9**	172.8
Badhoevedorp	NO	100.1	89.7	95.3	90.2	**89.6**	210.4	138.5
	NO_2	169.5	151.0	147.9	**148.2**	148.5	219.3	175.8
	PM_{10}	196.1	**192.7**	192.2	193.1	193.0	192.8	193.0
	$PM_{2.5}$	159.3	157.6	158.2	157.7	157.7	**156.3**	157.0
	CO	11459	**11291**	11250	11370	11361	11810	**11262**

6.1. NO_2

For NO_2, models 3 and 5 result in the lowest prediction errors according to table 6.1. Therefore, these were initially used to determine effects of Schiphol on the observed concentrations at the different monitoring sites. However, the regression coefficients for the models with separate parameters for the three highways show unexpected behavior. All parameters showed statistically significant contributions, but in the models of Badhoevedorp and Oude Meer the correlation between road traffic intensity at the A9 and the predictor were negative. This result is counter-intuitive, as the combustion processes in car engines generate NO and NO_2 emissions. Thus, despite showing the lowest prediction error these models were not considered suitable for further analysis. Instead models with a single road traffic parameter, i.e. 4 and 5, were used for stations

Badhoevedorp and Oude Meer, respectively.

In order to determine the effect of the airport on local concentrations the model was used to generate predictions on the local concentrations with and without take-offs and landings. The differences between overall predictions and those made without specific airport terms are shown in figure 6.1. According to the results from figure 6.1, at all stations the airport is responsible for an increase of between 0 and 10 $\mu g/m^3$ at the majority of time. At Badhoevedorp the absolute effect is largest and 50% of the results are between 2 and 10 $\mu g/m^3$. At Hoofddorp the values of the first and third quartiles are 1.2 and 8.7 $\mu g/m^3$, while they are 1.3 and 6.6 $\mu g/m^3$ for Oude Meer. Relative to the overall concentrations measured the effects are largest at Hoofddorp and lowest at Oude Meer. An unexpected observation is the larger effect of landings compared to take-offs at Oude Meer and Badhoevedorp. A possible explanation could be the stations' locations relative to the airport. Both Badhoevedorp and Oude Meer are located further away from the airport perimeter, while the other station is located just several hundred meters away from the Polderbaan. As a result, the station at Hoofddorp could be more sensitive to the actual aircraft activities on runways, while the other stations are more sensitive to taxiing aircraft and aircraft handling.

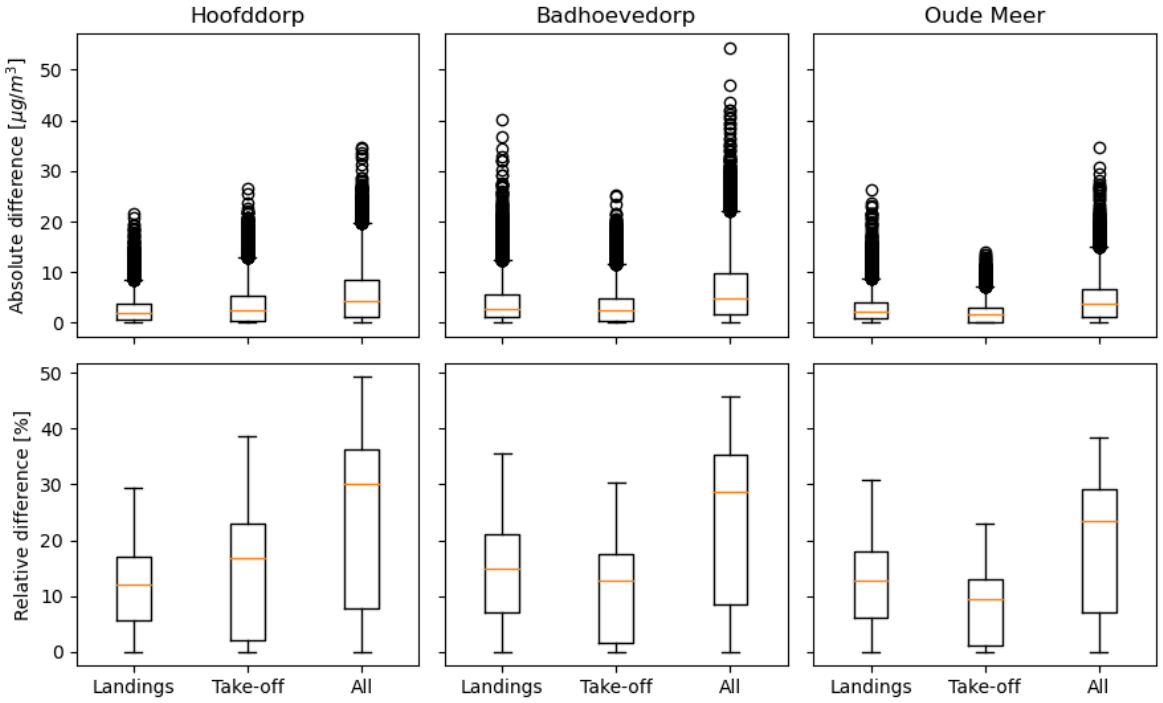

Figure 6.1: Modelling results that show the estimated contributions of aircraft take-offs and landings per hour at the three measurement locations of NO_2.

Compared to the expectations from the emission model, as presented in chapter 2, the results presented in this section are of the same order of magnitude. The expected deviations in $\mu g/m^3$ at all stations were expected to vary between 0 and 10 $\mu g/m^3$ most of the time. This is true for the model's results. At Hoofddorp the range of expected values also approximates the model's results and range from 0 to a maximum of about 37 $\mu g/m^3$. Similar behaviour is observed at Oude Meer and although some higher values are found by the model, these are considered outliers. The largest difference between expectations and results is observed at Badhoevedorp. While according to the predictions contributions of landings and take-offs should be lowest at Badhoevedorp, they are actually highest. There are two possible explanations for this. First, the simple box model used to estimate concentrations measured at the monitoring sites assumes equally distributed emissions over the area. Consequently, the predictions could be lower than the true values as emissions might be more concentrated near this station. Additionally, the smaller Δx in equation 2.2 also results in smaller predictions. Second, the nearby junction of the A4 and A9 could also result in higher values observed at this site. In turn, part of the highway's effect could still be present in the model's parameters for take-offs

and landings.

6.2. NO

Similar to the model selection process for NO_2, the best models are 3 and 5 according to table 6.1. But in the models of Hoofddorp and Oude Meer the regression parameter of the A4 is negative. For this reason the models with separate terms for all highways were replaced by the second best model (4 from table 3.8) in order to generate the results from figure 6.2. Thus, for Hoofddorp and Oude Meer the final models contain one road term, which is the traffic intensity of the nearest highway, while the model for Badhoevedorp uses the average traffic intensity of all three highways.

According to the models, there is a large variance in the contributions of LTO activities to NO measured at the monitoring sites. NO is directly emitted by combustion engines and has a short atmospheric lifetime of several minutes. In the atmosphere NO reacts into NO_2, but direct emissions from combustion processes contain more NO than NO_2. As a result, in the proximity of emission events large peaks in NO can be observed, while further downwind most of the NO can be transformed into NO_2. The data sets of NO show stable patterns with low concentrations, combined with sudden peaks that can be 100 times larger than the site's median.

Taking these properties into account the results from figure 6.2 should be interpreted with caution. At Hoofddorp the high relative effect due to LTO operations seems likely as the station is located near the Polderbaan. The other stations are located further away from the airport perimeter and therefore it is less likely that NO emitted on airport grounds are observed at these sites. Additionally, even though the A4 and A9 are closer to Badhoevedorp than the airport, the model still suggests that the airport occasionally is the main source of NO. Especially considering previous studies that suggest that road traffic is often the main source of NO_2, these results seem unlikely.

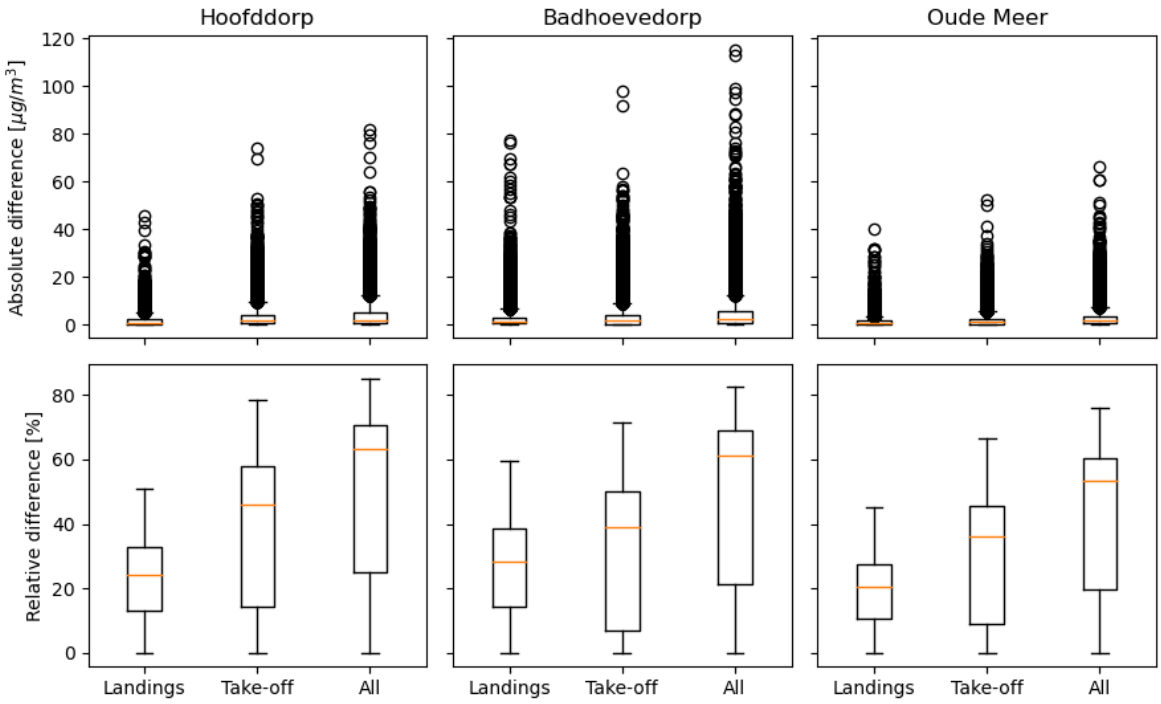

Figure 6.2: Modelling results that show the estimated contributions of aircraft take-offs and landings per hour at the three measurement locations for NO.

6.3. PM_{10}

The models with the smallest prediction errors for PM_{10} are 6, 7 and 3 for Hoofddorp, Oude Meer and Badhoevedorp, respectively. But again, these were not the final models used to generate the predictions for Oude

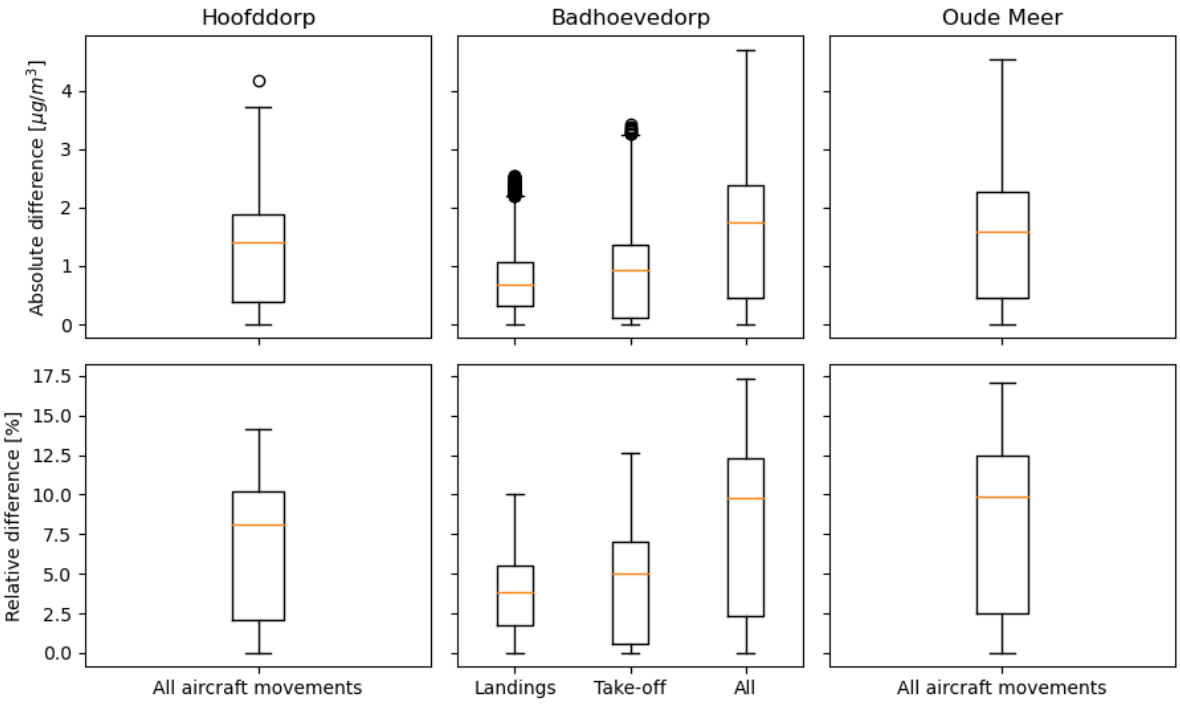

Figure 6.3: Modelling results that show the estimated contributions of aircraft take-offs and landings per hour at the three measurement locations for PM_{10}.

Meer and Badhoevedorp. The regression parameter for roads in model 7 turned out to be both negative and statistically insignificant. Therefore, the second best model from table 6.1 was chosen, namely model 6. This model did not contain a road term. The same holds for Badhoevedorp. At this station all three roads were included in the model separately, but the A9 showed a negative effect. This was especially remarkable as this is the closest highway. Again the second best model was chosen, also without a road term. As a result all models used to predict the airport contributions from figure 6.3 did not contain any road parameters.

Modelling results show that Schiphol's contributions to local concentrations of PM_{10} lie between 0 and 4.5 $\mu g/m^3$. At Hoofddorp the airport's contributions are smallest, while the largest effect is expected at Badhoevedorp followed closely by Oude Meer. The relative contributions are again very similar for the last two stations and can be up to 17% of the locally observed concentrations. At Hoofddorp this maximum value is 14.2%. Modelling thus suggests that the airport is not one of the main contributors to ambient PM_{10} at all three stations. Moreover, road traffic is statistically insignificant as a source of PM_{10} at the monitoring sites.

6.4. $PM_{2.5}$

The final two species, $PM_{2.5}$ and CO, are only measured at Badhoevedorp and their results are shown in figure 6.4. For $PM_{2.5}$, model 6 was best according to table 6.1 and therefore this model was used to generate the results.

Predictions show that the median of the contributions due to aircraft emissions is 1.1 $\mu g/m^3$, the first quartile is 0.3 and the third quartile equals 1.7 $\mu g/m^3$. These amounts are responsible for 3, 11.4 and 14.4% of the total ambient concentrations of $PM_{2.5}$ at those times. Peak values could be as high as 4.3 $\mu g/m^3$, which is about 20% of the ambient concentrations at those times. According to the models road traffic terms were not significant and did not decrease prediction errors.

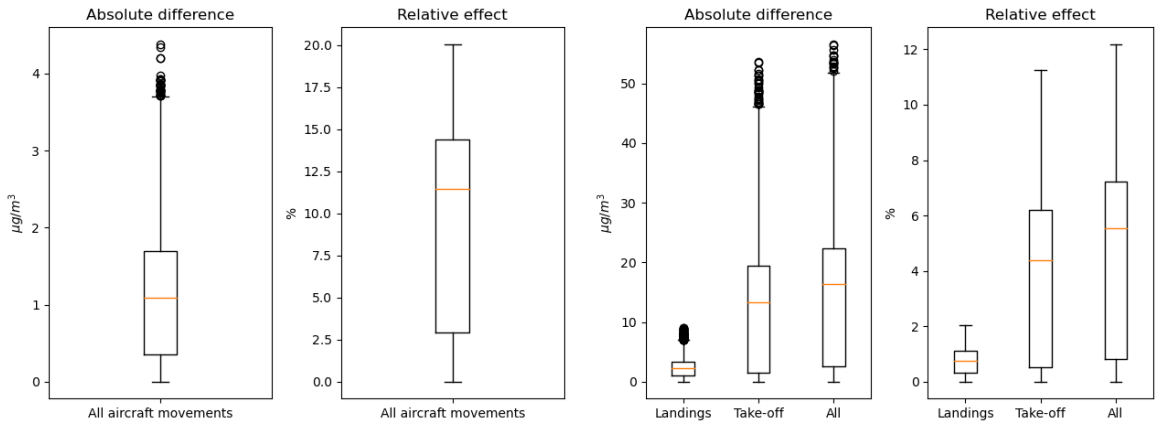

(a) $PM_{2.5}$ (b) CO

Figure 6.4: Modelling results that show the estimated contributions of aircraft movements on ambient $PM_{2.5}$ and CO at Badhoevedorp.

6.5. CO

Finally the results for CO are presented in figure 6.4b. In order to generate these results again the best model from table 6.1 was not used. This time, model 2 was taken as the configurations of numbers 3 and 7 showed similar peculiarities as those mentioned in the discussions of other pollutants in this section.

The results show that take-offs are significantly more important than landings and are responsible for the majority of the airport's effects on ambient CO. Overall LTO operations are responsible for a median increase of 16.3 $\mu g/m^3$ and maximum contribution of over 50 $\mu g/m^3$. These values are significantly larger than those calculated by the emission model in chapter 2. Even though these concentrations are higher than expected, relative effects are lower than 12.2%. The median of the relative effects equals 5.5%.

6.6. Conclusion and discussion

This chapter generated quantitative estimates for the effects of airport operations on local air quality. To do so, all pollutants were analyzed separately and different models to calculate the correlations were created. As could be expected, the effects of take-offs and landings on ambient AQ varies per pollutant species.

According to the modelling results the airport has the largest relative effect on NO levels. But after further inspection of these results they were considered unlikely. As a result the focus for nitrogen oxides was shifted to NO_2. At all stations the majority of contributions due to take-offs and landings lie between 0 and 10 $\mu g/m^3$. The largest increase in ambient NO_2 occurs at Badhoevedorp, followed by Hoofddorp and Oude Meer. Relative effects are largest at Hoofddorp, followed by Badhoevedorp and Oude Meer. The median relative contributions are 31, 29 and 24%, respectively. All final models used contained separate parameters for take-offs and landings and only one road parameter.

According to the final models the airport is responsible for a raise in ambient PM_{10} concentrations of between 0 and 4.5 $\mu g/m^3$ at all stations, with marginally lower values at Hoofddorp. The largest relative effects are 14.5, 17 and 17 % for Hoofddorp, Badhoevedorp and Oude Meer, respectively. Opposed to the models of nitrogen oxides, the final models used for PM_{10} did not consider road terms as they were either statistically insignificant or showed a negative correlation. These decisions decrease the reliability of the results and therefore they should be interpreted with caution. Especially considering that according to EEA, 2020, road traffic is a more important source of PM_{10} than aviation.

At Badhoevedorp the estimated median increase in ambient $PM_{2.5}$ in the measurement period is 1.1 $\mu g/m^3$. The first and third quartiles equal 0.3 and 1.7 $\mu g/m^3$. This corresponds to relative increases of 3, 11.4 and 14.4% for the first quartile, median and third quartile, respectively. Similar to the model used for PM_{10}, the model used for $PM_{2.5}$ did not contain road parameters and only used one term for aircraft activities at Schiphol. Finally, LTO operations are responsible for a median CO increase of 16.3 $\mu g/m^3$ and maximum

contribution of over 50 $\mu g/m^3$. Take-offs are the dominant source for this pollutant. Again a model without road parameters was used. This could be a reason for the larger effects compared to the predictions based on the emission model. It is likely that some road traffic effects are incorporated in the flight parameters, but the magnitude of these effects is unknown.

7

An intervention study based on the COVID-19 situation in 2020

When this study commenced a unique situation arose. In early 2020 COVID-19 emerged and spread over the globe, with unprecedented consequences. When the virus reached the Netherlands, the Dutch government introduced restrictions in order to prevent the virus to spread. Other countries had to do the same. The resulting situation had a large effect on both road and air traffic, which decreased significantly as shown in figure 7.1. Consequently, unique data was available towards the end of this study and despite not being present in the initial research plan, this opportunity could not be neglected. Therefore this final chapter was added, which focuses completely on the special data due to the COVID-19 situation. More specifically, data from March to August 2020 was used for this analysis. Section 7.1 presents the AQ measurements from this period, section 7.2 analyzes the polar plots from this period and finally the modelling results are presented in section 7.3.

Figure 7.1: Traffic intensities over time.

7.1. Air quality measurements

In order to provide an indication of the changes in measured concentrations of NO, NO_2, PM_{10} and $PM_{2.5}$ between 2019 and 2020, the measurement results for both years are shown in figures 7.2 and 7.3. A comparison between the results from 2019 and 2020 shows that the relative patterns are conserved and the same stations show the highest concentrations and largest variances. The magnitudes of the measurements, on the other hand, are different.

For NO the absolute values have decreased significantly, especially at monitoring sites around Schiphol and near roads. At the Schiphol stations the third quartile and median both decreased by about 1 $\mu g/m^3$. At sites near roads the median decreased by 1.5 $\mu g/m^3$ and the third quartile changed from 12 to 9 $\mu g/m^3$. At rural and urban sites the relative differences with respect to the median and third quartile decreased as well, but the magnitudes of these changes were lower. Comparing the measurements of NO_2 from 2020 with earlier measurements, all ambient concentrations of this pollutant have decreased as well. At Schiphol and near road sites the medians decreased by about one third and a quarter of the medians of 2019, respectively. In absolute terms the reductions were about 5 $\mu g/m^3$ for both sites. The differences were less pronounced at rural and urban sites, but these locations also showed a reduction in ambient NO_2.

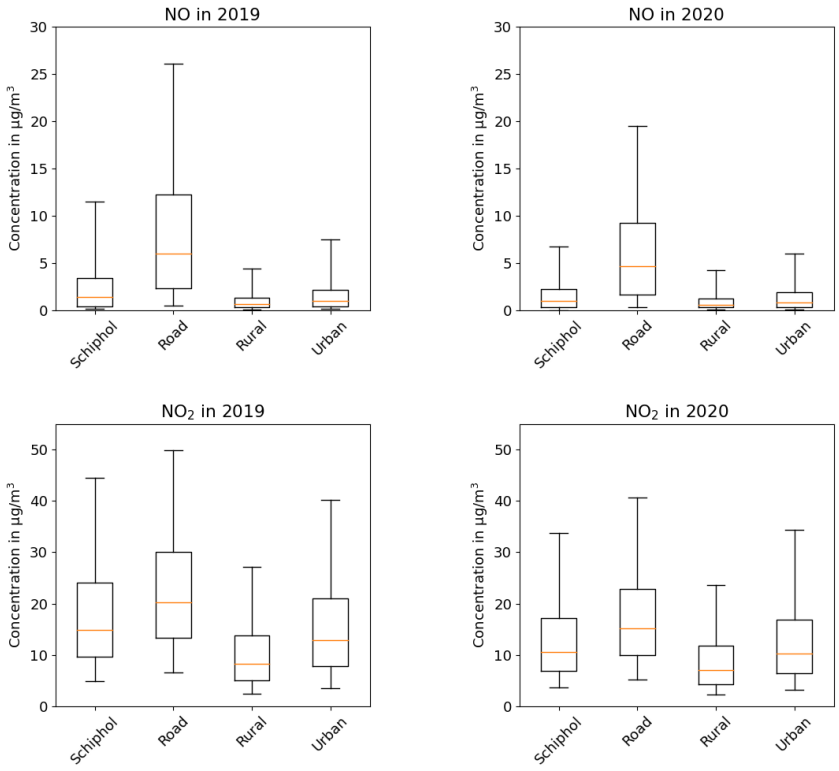

Figure 7.2: Box plots showing the NO and NO_2 measurements from March to August in 2019 and 2020.

The changes in particulate matter were different from those of nitrogen oxides. Lower limits of both PM_{10} and $PM_{2.5}$ are relatively unchanged. The same holds for the medians of PM_{10}, although the median of Schiphol decreased by approximately 1 $\mu g/m^3$. Rural and urban sites showed lower ambient concentrations, but the absolute changes were smaller. The median of $PM_{2.5}$ also decrease by about 1 $\mu g/m^3$. The levels measured at road sites are lower than those of rural sites in both years.

Additionally, the measurements taken during the special situation in 2020 were compared to the measurements of the same dates in 2014 to 2019. Table 7.1 shows that all species measured at the monitoring sites around Schiphol have decreased, except for CO. Thus, a clear effect of the lockdown can be observed. The largest decrease is detected in concentrations of NO, followed by NO_2 and PM_{10}. The next sections will further assess the correlations between reduced airport activities and local pollutant concentrations using the

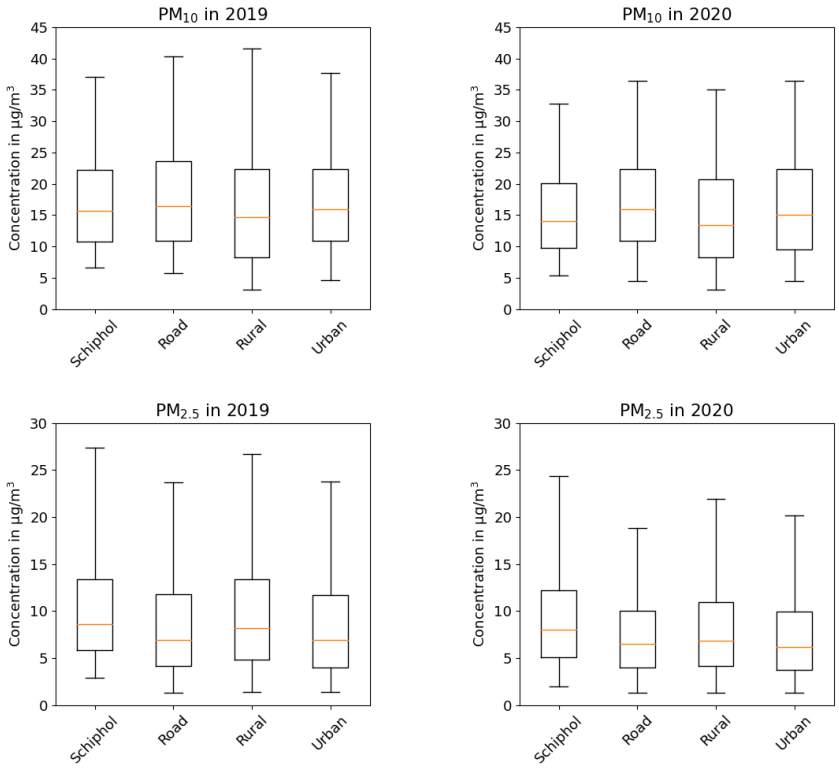

Figure 7.3: Box plots showing the PM_{10} and $PM_{2.5}$ measurements from March to August in 2019 and 2020.

methods presented earlier in this report.

Table 7.1: The relative change (%) between the measured concentrations of pollutant species during the COVID-19 situation in 2020 compared to the measurements of previous years (2014-2019).

Station	**NO**	**NO_2**	**PM_{10}**	**$PM_{2.5}$**	**CO**
Hoofddorp	-55	-33	-3		
Badhoevedorp Sloterweg	-46	-36	-11	-6	+32
Oude Meer	-40	-29	-11		

7.2. AQ measurements versus wind conditions

The previous section already showed that AQ improved in 2020 with respect to previous years. This section applies the methodology from chapter 5 in order to determine whether the change in traffic intensities also led to a change in main source locations. The graphs that are discussed in this section are similar to those from chapter 5 and can be found in appendix D. To start, polar plots with all measurements are discussed, after which the results of the background subtraction method are presented.

By maintaining the same scales changes are clearly visible in the graphs of NO, NO_2, $PM_{2.5}$ and CO. Starting with NO, peaks at low wind speeds have disappeared at all stations. The average values for almost all wind conditions are now similar to the lower values before the COVID-19 situation. In order to analyze the source distribution during this special period, the same data from 2020 with a scale more appropriate to these measurements was analyzed as well. At Hoofddorp the highest values are observed in the direction of the Polderbaan, as opposed to the South-East in the BAU case. This maximum during the new situation is about 8 $\mu g/m^3$, whereas this used to be between 10 and 15 $\mu g/m^3$. At Badhoevedorp the peak is also pointing in the same direction as before, namely towards the nearby A9 and the airport terminal building. The last station, Oude Meer, does not show consistent higher values pointing in the airport's direction.

Along with NO, the concentrations of NO_2 decreased for all wind directions. Nevertheless, some weak patterns are still visible in the graphs with old scales. Changing the scales results in patterns more in line with those of earlier years, albeit with concentrations that can be up to 20 $\mu g/m^3$ lower at peak locations. With regard to actual increments due to sources in the direction of the airport, background subtraction was performed as well. As mentioned before the short atmospheric lifetime of NO makes it tricky to draw conclusions. This method is more appropriate for NO_2. Inspection of the graphs showed that the main patterns from figure 5.3 with respect to the airport are conserved at Badhoevedorp. At the other stations the effects of sources in the airport's direction are still visible, but are less consistent. Especially at Oude Meer the results are hard to draw conclusions on, since the peak in the direction of the airport's terminal is right next to an area where concentrations decrease. The magnitudes of the increments between the main and background stations have also decreased by about 5 $\mu g/m^3$ or more at all stations.

For PM_{10}, the BAU case showed that the graphs of all three stations were very similar. This suggests that long distance transport of particles is dominant over local sources. Nevertheless, the PM_{10} graphs from the BAU case (figure 5.4) are different from those of the new situation. Especially at lower wind speeds the new situation shows lower values, indicating that the effects of local sources such as road traffic and the airport have decreased. However, still background subtraction plots do not show patterns indicating clear effects from the airport or nearby roads.

The last two species that can be compared are $PM_{2.5}$ and CO. The first behaves very similar to PM_{10}, as values at low wind speeds decrease significantly. For this pollutant only one site was available around Schiphol, so no background subtraction could be performed. The same goes for CO. Interestingly though, the concentrations of this pollutant increased during the new situation with respect to earlier years. The maximima at lower wind speeds decreased, but during the smart-lockdown concentrations observed at higher wind speeds in all directions have increased.

7.3. Modelling

The last methodology applied on the special case data is the modelling from chapter 6. Models from that chapter were used to predict the ambient concentrations at monitoring sites during the period of travel restrictions. By comparing these results with the conclusions from the BAU case, an indication of the impacts of diminished source activities should be created.

The first results are shown in figure 7.4 and confirm the change in airport contributions. The vast majority of increments during the period of traffic restrictions is below 2 $\mu g/m^3$, while there are moments where the airport is still responsible for more than 10 $\mu g/m^3$ at Hoofddorp and Badhoevedorp. Oude Meer has the lowest peak values, which are about 8 $\mu g/m^3$. The BAU case showed a range of increments about three times as high as those from figure 7.4. In terms of relative increments at the stations the magnitudes have decreased as well. Median values are 5 times lower at all sites, but the peaks are still as high as 35, 32 and 27% at Hoofddorp, Badhoevedorp and Oude Meer, respectively.

Predictions of PM_{10} are shown in figure 7.5. Before travel restrictions were introduced the effects of Schiphol on ambient PM_{10} was estimated to be up to 4,5 $\mu g/m^3$. The 2020 data from figure 7.5 ranges up to 2.7 $\mu g/m^3$. The median values decreased from 1.45, 1.75 and 1.6 to 0.3, 0.4 and 0.4 at Hoofddorp, Badhoevedorp and Oude Meer, respectively. Again this means that the absolute impacts have more than halved at all locations. Relative effects have also decreased at all locations.

Finally the results for $PM_{2.5}$ and CO are shown in figure 7.6. In absolute terms the median of $PM_{2.5}$ decreased from 1.1 to 0.2 $\mu g/m^3$ and the entire range of values is lower than 1.8 $\mu g/m^3$. The old peak values were higher than 4 $\mu g/m^3$. Relative effects have also decreased. The BAU case shows values up to 20%, while the new situation has a maximum of 13%. The median is 2%, which used to be 11.4% in the BAU situation. The last pollutant, namely CO, also shows a large decrease. Its median decreased from 16.3 to 2.5 $\mu g/m^3$ and the maximum value in the new situation was about 17 $\mu g/m^3$ lower. In relative terms the median changed from 5.5 to 1%, while the peak reduced to 8.5%.

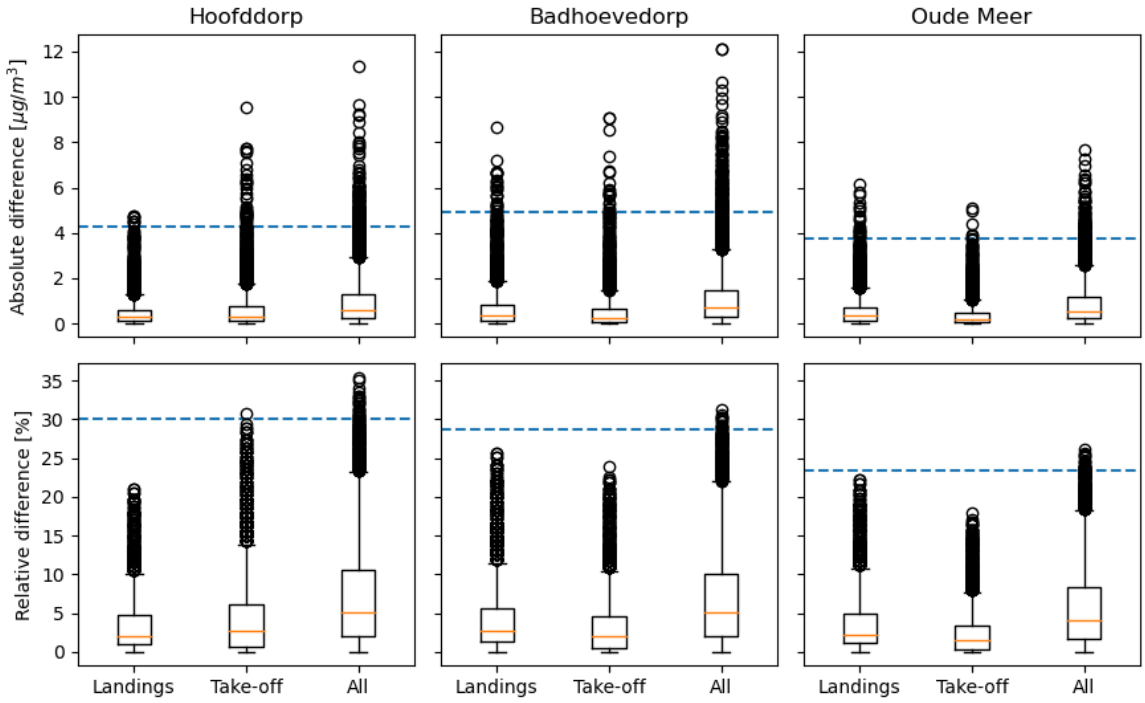

Figure 7.4: Modelling results that show the estimated contributions of aircraft take-offs and landings to NO_2 per hour at the three measurement locations during the COVID-19 situation in 2020. The dashed line shows the median of the estimated overall effect due to aircraft take-offs and landings for th BAU case.

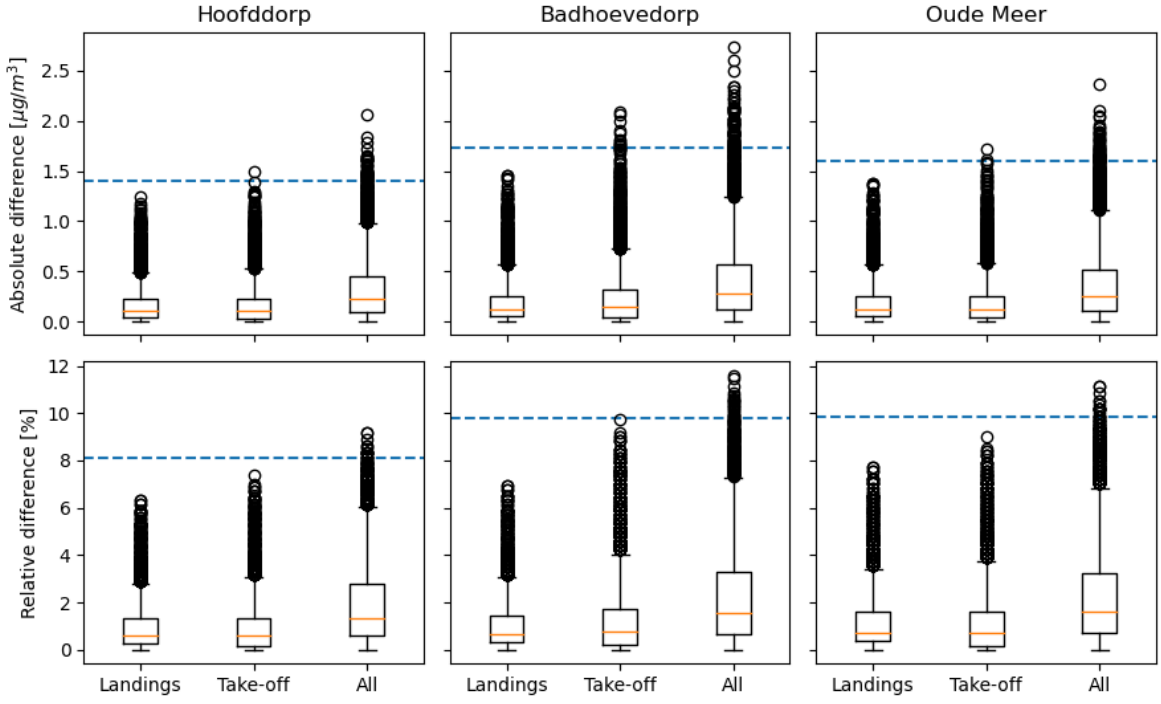

Figure 7.5: Modelling results that show the estimated contributions of aircraft take-offs and landings to PM_{10} per hour at the three measurement locations during the COVID-19 situation in 2020. The dashed line shows the median of the estimated overall effect due to aircraft take-offs and landings for th BAU case.

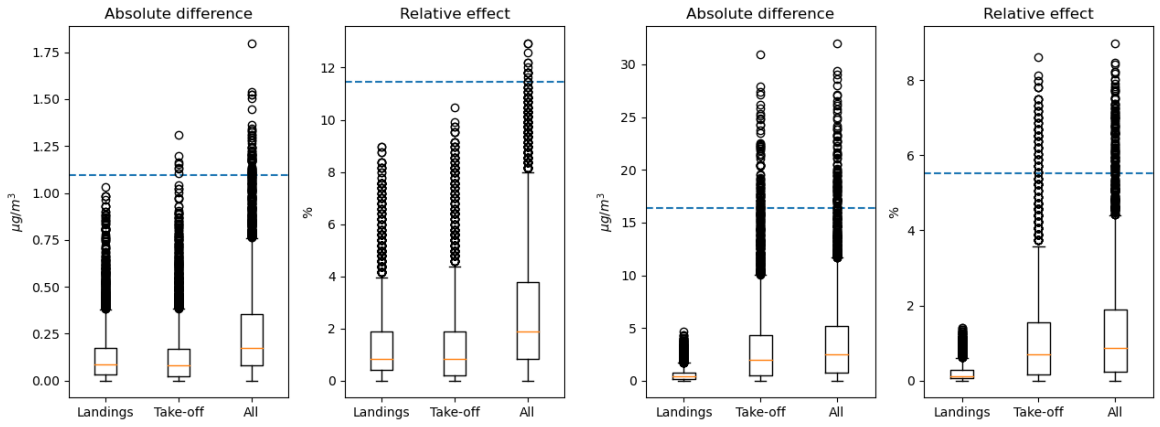

(a) $PM_{2.5}$ (b) CO

Figure 7.6: Modelling results that show the estimated contributions of aircraft movements on ambient $PM_{2.5}$ and CO at Badhoevedorp during the COVID-19 situation in 2020. The dashed line shows the median of the estimated overall effect due to aircraft take-offs and landings for th BAU case.

7.4. Conclusion and discussion

Concentrations of NO and NO_2 around Schiphol dropped with more than 40 and 29% when airport activities decreased. Additionally, the polar plots of NO showed that peaks related to low wind speeds became less important. At Hoofddorp the concentrations measured with winds from the Polderbaan decreased by 2 to 7 $\mu g/m^3$. This is a reduction of between 50 and 80% for measurements under these wind conditions. Other stations also showed lower concentrations, but determination of the airport's influence is more difficult at those sites due to nearby highways. Additionally, no modelling comparison was made as the results of NO did not seem very reliable as mentioned in chapter 6. Therefore the focus for nitrogen oxides will shift to NO_2.

The polar plots for this pollutant show that peak values have decreased by up to 20 $\mu g/m^3$. When background subtraction was applied, the increments between measurements at the two stations decreased by about 5 $\mu g/m^3$. Finally the models also showed that concentrations due to take-offs and landings decreased drastically. The BAU case showed airport contributions that were about three times higher than during the new situation. Medians of the relative effects became about five times smaller. Putting it all together all methods agree that part of the decrease in NO_2 is due to a reduction in air traffic. According to the general polar plots peaks decreased by about 10 $\mu g/m^3$, background subtraction suggests a decrease of 5 $\mu g/m^3$. The medians of the modelling results decreased by about 4 $\mu g/m^3$. Therefore, it is expected that the reduction in flights is responsible for about 4 to 5 $\mu g/m^3$ less NO_2 at the monitoring sites.

For PM_{10} it is estimated that the effects of take-offs and landings decreased by more than 1.2 $\mu g/m^3$ at all locations. Nevertheless, this is only based on the modelling results. Polar plots did show that average concentrations at the measurement sites were lower at low wind speeds, but background subtraction still did not generate clear patterns. For CO and $PM_{2.5}$ no background subtraction could be performed, but the polar plots of the latter showed similar results as those of PM_{10}. Based on the modelling both absolute and relative contributions of the airport decreased. The median decreased by 0.9 $\mu g/m^3$ and the new peak value was 1.8 $\mu g/m^3$, which is more than 2 $\mu g/m^3$ lower than the value of the BAU situation. The median of the relative effect of aircraft take-offs and landings changed from 12% to 2%. Despite these clear changes, the lack of road terms in the model and the presence of just one measurement station increases the uncertainty of these results. Finally, overall ambient CO increased, but the airport's contribution decreased.

8

Conclusion and discussion

The aim of this study was to estimate the effect of aviation activity of Schiphol Airport on local concentrations of NO_x, O_3, $PM_{2.5}$ and PM_{10}. Three different methods were applied in order to reach this objective, followed by an additional intervention study about the effects of decreased air travel in 2020. To conclude this report the results of these different methods are combined and discussed here.

Starting with NO, the various methods did suggest that concentrations increase based on airport activities. The long term average of this pollutant around Schiphol is 3.88 $\mu g/m^3$ (121%) and 1.57 $\mu g/m^3$ (28%) higher than rural and urban background sites, respectively. At the measurement site near the Polderbaan measurements twice as high as the station's long-term average of 6.39 $\mu g/m^3$ occur at winds from this runway. Background subtraction methods suggested that between Oude Meer and Badhoevedorp contentrations increased by about 12 $\mu g/m^3$. However, this was only observed with Southern winds which increased the uncertainty of these results. The final results from the modelling showed a large variance in the effects of the airport on ambient NO which showed extremes up to 115 $\mu g/m^3$. Despite the outcomes of these different methods the results are not considered robust due to the short atmospheric lifetime of this pollutant. The presence of highways close to the measurement stations, in combination with the higher values observed at highway stations located throughout the Netherlands, make it likely that part of the contributions estimated are actually due to nearby roads instead of the more distant airport.

More robust outcomes were observed for NO_2. In terms of measurement locations the long term mean concentration near Schiphol is 0.63 $\mu g/m^3$, or 2.7%, higher than the average of all monitoring stations. According to the second analysis concentrations of NO_2 increase by at least 5 $\mu g/m^3$ over the area between measurement sites. Maximum increments can even be as high as 10, 14 and 15 $\mu g/m^3$ at Hoofddorp, Oude Meer and Badhoevedorp, respectively. These peaks result in a rise of local concentrations of between 22 and 53% of the stations' long term average values. The final models also predicted that the medians of ambient concentrations increased between 24 and 31% due to hourly aircraft take-offs and landings, with peaks up to 48%. Combining all results the effects are similar to expectations and show that the airport is an important agent that can increase ambient concentrations significantly at monitoring sites located less than 1.5 kilometers away from the airport perimeter.

Results of other pollutants were less consistent. This was mainly due to the lack of multiple measurement sites or recent measurements. Average PM_{10} concentrations around Schiphol were 3.4% lower than the average of all measurement sites between January 2014 and August 2020. The second methodology also concluded that long term transport of particles is the main source of PM_{10}, as no patterns that pointed in the airport's direction were found. Models estimated that the airport was responsibe for maximum relative effects of 17% of the total ambient concentrations. But these results have to be interpreted with caution, as the models did not include road traffic parameters and are likely to incorporate road terms in the airport parameters. Similar conclusions are drawn for $PM_{2.5}$. Although this is the only species with the highest concentrations measured around Schiphol, the presence of only one monitoring site near Schiphol could distort the results. According to the regression model the largest impact of the airport was 4.3 $\mu g/m^3$, about 20% of the overall levels at that time. Most increments lie between 0.3 and 1.7 $\mu g/m^3$, which is 3 to 14.4% of the

overall ambient concentrations. Finally, O_3 could only be analyzed from January 2014 until 7 June 2017. As a result no modelling with flight parameters could be performed. The other methods showed that O_3 concentrations were 1.33 $\mu g/m^3$, which is equal to 2.9%, lower than the average of all monitoring sites. The polar plot showed some negative correlation between NO_x and O_3, but no quantitative values were generated.

With the main analysis finished, the intervention study was performed. The strong decrease in road and air traffic led to a drop in local concentrations of all pollutants monitored around Schiphol in 2020. Concentrations of NO and NO_2 around Schiphol reduced with more than 40 and 29%, respectively. Peaks of NO_2 have decreased by up to 20 $\mu g/m^3$ and background subtraction showed that the differences between stations decreased by about 5 $\mu g/m^3$. Adding the results of the various methods together the reduction in flights decreased ambient NO_2 by about 4 to 5 $\mu g/m^3$. Median ambient concentrations of PM_{10} and $PM_{2.5}$ reduced by 1.2 and 0.9 $\mu g/m^3$, respectively. These results are based on model predictions.

Overall this case study has analyzed the ambient air quality around Schiphol based on a combination of several data sets. These methods resulted in qualitative and quantitative estimates of correlations between the airport and ambient air quality, as desired. Nevertheless, improvements can be made with respect to the methodology. Limitations of this study are the lack of multiple AQ monitoring sites for $PM_{2.5}$, O_3 and CO. Also O_3 was only monitored until 2017. Ideally these monitoring sites could be changed to sites at the airport perimeter and would also provide information about wind speed and direction. Additionally, the flight data set was generated based on ADS-B data from the TU Delft and covers approximately 82.6% of the total aircraft activities from Schiphol. In order to improve the model accuracy the data set's accuracy should be improved. On top of that the data set can be made more detailed, by including aircraft types and runway information. Adding information about the mixing height is also likely to improve modelling results. In terms of future research there are two main aspects that are applicable for separate studies. First, the modelling could be extended and more complex models can be created.

Furthermore, while writing this report new data is available for the intervention study. This is also an interesting topic for a more in depth analysis. While writing this report restrictions are still in place. Taking into account that by now almost five months of extra data from this new situation is available, the study about the effects of the COVID-19 situation can be extended. On top of that, the COVID-19 analysis only applied the methodologies used earlier in this report. It would be interesting to further investigate the effects of the pandemic on ambient AQ around Schiphol using alternative methods. From March to August the traffic intensities fluctuate, thus investigating different periods separately would be an interesting addition to this study.

To conclude, this study has shown that Schiphol's effects on local air quality are largest for nitrogen oxides, while there is still some uncertainty with respect to particulate matter and ozone. The reduction of daily flights in 2020 had a positive effect on the area's air quality. Finally, the modelling has shown that adding a road traffic parameter to models of nitrogen oxides improves prediction accuracy.

Bibliography

Carslaw, D. C., Beevers, S. D., Ropkins, K., & Bell, M. C. (2006). Detecting and quantifying aircraft and other on-airport contributions to ambient nitrogen oxides in the vicinity of a large international airport. *Atmospheric Environment*, *40*(28), 5424–5434. https://doi.org/10.1016/j.atmosenv.2006.04.062

Carslaw, D. C., & Ropkins, K. (2012). Openair — An R package for air quality data analysis. *Environmental Modelling & Software*, *27–28*, 52–61. https://doi.org/10.1016/j.envsoft.2011.09.008

Dassen, A., Aben, J., Beck, J., Blom, W., Diederen, H., Folkert, R., Hoen, A., Jaarsveld, J., & Velze van, K. (2006). *De luchtkwaliteit rond Schiphol* (tech. rep. No. 500133001/2006). Milieu- en Natuurplanbureau (MNP). Bilthoven, The Netherlands. Retrieved December 29, 2020, from https://www.pbl.nl/sites/default/files/downloads/500133001.pdf

Davies, M. J. E. (2012). Chapter 12 - Air Quality Modeling in the Athabasca Oil Sands Region (K. E. Percy, Ed.). In K. E. Percy (Ed.), *Developments in Environmental Science*. Elsevier. https://doi.org/10.1016/B978-0-08-097760-7.00012-3

Diez, D. M., Dominici, F., Zarubiak, D., & Levy, J. I. (2012). Statistical Approaches for Identifying Air Pollutant Mixtures Associated with Aircraft Departures at Los Angeles International Airport [Publisher: American Chemical Society]. *Environmental Science & Technology*, *46*(15), 8229–8235. https://doi.org/10.1021/es3007172

Dodge, Y. (2008). *The Concise Encyclopedia of Statistics*. New York, Springer Science & Business Media.

Dodson, R. E., Andres Houseman, E., Morin, B., & Levy, J. I. (2009). An analysis of continuous black carbon concentrations in proximity to an airport and major roadways. *Atmospheric Environment*, *43*(24), 3764–3773. https://doi.org/10.1016/j.atmosenv.2009.04.014

Durre, I., Menne, M. J., Gleason, B. E., Houston, T. G., & Vose, R. S. (2010). Comprehensive Automated Quality Assurance of Daily Surface Observations [Publisher: American Meteorological Society]. *Journal of Applied Meteorology and Climatology*, *49*(8), 1615–1633. https://doi.org/10.1175/2010JAMC2375.1

EEA. (2020). *Air quality in Europe - 2020 report* (Publication No. 09/2020). Retrieved December 17, 2020, from https://www.eea.europa.eu/publications/air-quality-in-europe-2020-report

Feng, S., Hu, Q., & Qian, W. (2004). Quality control of daily meteorological data in China, 1951–2000: A new dataset [_eprint: https://rmets.onlinelibrary.wiley.com/doi/pdf/10.1002/joc.1047]. *International Journal of Climatology*, *24*(7), 853–870. https://doi.org/10.1002/joc.1047

Flightradar24. (2020). How flight tracking works [Date accessed: 2020-05-23 23:03]. Retrieved May 23, 2020, from https://www.flightradar24.com/how-it-works

Henry, R., Norris, G. A., Vedantham, R., & Turner, J. R. (2009). Source Region Identification Using Kernel Smoothing [Publisher: American Chemical Society]. *Environmental Science & Technology*, *43*(11), 4090–4097. https://doi.org/10.1021/es8011723

Janssen, N., Lammer, M., Maitland-Van De Zee, A., Van De Zee, S., Keuken, R., Blom, M., Van Den Bulk, P., Van Dinther, D., Hoek, G., Kamstra, K., Meliefste, K., Oldenwenning, M., Boere, A., Cassee, F., Fischer, P., Gerlofs-Nijland, M., & Houthuijs, D. (2019). *Onderzoek naar de gezondheidseffecten van kortdurende blootstelling aan ultrafijn stof rond Schiphol* (tech. rep.) [Publisher: RIVM]. Publisher: RIVM. Retrieved May 26, 2020, from https://rivm.openrepository.com/handle/10029/623133

Jonge de, D. (2020). *Datarapport Luchtkwaliteit Haarlemmermeer meetresultaten 2019* (tech. rep. No. 20-1127). GGD Amsterdam. Amsterdam.

Kim, B., Nakada, K., Wayson, R., Christie, S., Paling, C., Bennett, M., Raper, D., Raps, V., Levy, J., & Roof, C. (2015). *Understanding Airport Air Quality and Public Health Studies Related to Airports*. https://doi.org/10.13140/RG.2.1.1028.2086

KNMI. (2020). Uurgegevens van het weer in Nederland - Download. Retrieved August 2, 2020, from http://projects.knmi.nl/klimatologie/uurgegevens/selectie.cgi

Koulidis, A. G., Progiou, A. G., & Ziomas, I. C. (2020). Air Quality Levels in the Vicinity of Three Major Greek Airports. *Environmental Modeling & Assessment*. https://doi.org/10.1007/s10666-020-09699-6

Masiol, M., & Harrison, R. M. (2014). Aircraft engine exhaust emissions and other airport-related contributions to ambient air pollution: A review. *Atmospheric Environment*, *95*, 409–455. https://doi.org/10.1016/j.atmosenv.2014.05.070

NDW. (2020). Open Data Portaal. Retrieved December 1, 2020, from http://opendata.ndw.nu/

OAG. (2005). Flight Schedule Database [Library Catalog: www.oag.com]. Retrieved July 30, 2020, from https://www.oag.com/airline-schedules-data

Olive, X. (2019). Traffic, a toolbox for processing and analysing air traffic data. *Journal of Open Source Software*, *4*, 1518. https://doi.org/10.21105/joss.01518

Olive, X., Strohmeier, M., & Lübbe, J. (2020). Crowdsourced air traffic data from The OpenSky Network 2020 [type: dataset]. Zenodo. https://doi.org/10.5281/zenodo.4266938

Pinheiro, J., Bates, D., DebRoy, S., Sarkar, D., & Team, R. C. (2020). Nlme: Linear and Nonlinear Mixed Effects Models [R package version 3.1-149]. https://CRAN.R-project.org/package=nlme

Pison, I., & Menut, L. (2004). Quantification of the impact of aircraft traffic emissions on tropospheric ozone over Paris area. *Atmospheric Environment*, *38*(7), 971–983. https://doi.org/10.1016/j.atmosenv.2003.10.056

Popoola, O. A. M., Carruthers, D., Lad, C., Bright, V. B., Mead, M. I., Stettler, M. E. J., Saffell, J. R., & Jones, R. L. (2018). Use of networks of low cost air quality sensors to quantify air quality in urban settings. *Atmospheric Environment*, *194*, 58–70. https://doi.org/10.1016/j.atmosenv.2018.09.030

RIVM, DCMR, GGD-Amsterdam, ODRA, OMWB, & RUDZL. (2020). Luchtmeetnet.nl. Retrieved June 15, 2020, from https://www.luchtmeetnet.nl/

Schäfer, M., Strohmeier, M., Lenders, V., Martinovic, I., & Wilhelm, M. (2014). Bringing up OpenSky: A large-scale ADS-B sensor network for research, In *IPSN-14 Proceedings of the 13th International Symposium on Information Processing in Sensor Networks*. https://doi.org/10.1109/IPSN.2014.6846743

Schiphol. (2020). Verkeer- en vervoercijfers [Library Catalog: www.schiphol.nl]. Retrieved August 4, 2020, from https://www.schiphol.nl/nl/schiphol-group/pagina/verkeer-en-vervoer-cijfers/

Seinfeld, J. H., & Pandis, S. N. (2016). *Atmospheric Chemistry and Physics: From Air Pollution to Climate Change*. New York, UNITED STATES, John Wiley & Sons, Incorporated. Retrieved August 2, 2020, from http://ebookcentral.proquest.com/lib/delft/detail.action?docID=4462549

Simone, N. W., Stettler, M. E. J., & Barrett, S. R. H. (2013). Rapid estimation of global civil aviation emissions with uncertainty quantification. *Transportation Research Part D: Transport and Environment*, *25*, 33–41. https://doi.org/10.1016/j.trd.2013.07.001

Song, S.-K., Shon, Z.-H., & Kang, Y.-H. (2015). Comparison of impacts of aircraft emissions within the boundary layer on the regional ozone in South Korea. *Atmospheric Environment*, *117*, 169–179. https://doi.org/10.1016/j.atmosenv.2015.07.010

Stettler, M. E. J., Eastham, S., & Barrett, S. R. H. (2011). Air quality and public health impacts of UK airports. Part I: Emissions. *Atmospheric Environment*, *45*(31), 5415–5424. https://doi.org/10.1016/j.atmosenv.2011.07.012

Sun, J., Ellerbroek, J., & Hoekstra, J. (2017). Flight Extraction and Phase Identification for Large Automatic Dependent Surveillance–Broadcast Datasets [Publisher: American Institute of Aeronautics and Astronautics]. *Journal of Aerospace Information Systems*, *14*(10), 566–572. https://doi.org/10.2514/1.I010520

Tiwari, S., & Agrawal, M. (2018). *Tropospheric Ozone and its Impacts on Crop Plants*. Cham, Springer International Publishing. https://doi.org/10.1007/978-3-319-71873-6

To70. (2016). *Analyse gebruik luchthaven Schiphol* (tech. rep.). To70: Aviation Consultants. Den Haag. https://www.onderzoeksraad.nl/nl/media/attachment/2018/7/10/a2f01c57ef9720161220_4b_b4_5_veiligheid_schiphol_bijlage_rapport_to70_analyse_ge.pdf

Unal, A., Hu, Y., Chang, M. E., Talat Odman, M., & Russell, A. G. (2005). Airport related emissions and impacts on air quality: Application to the Atlanta International Airport. *Atmospheric Environment*, *39*(32), 5787–5798. https://doi.org/10.1016/j.atmosenv.2005.05.051

van Zoest, V. M., Stein, A., & Hoek, G. (2018). Outlier Detection in Urban Air Quality Sensor Networks. *Water, Air, & Soil Pollution*, *229*(4), 111. https://doi.org/10.1007/s11270-018-3756-7

Wolfe, P. J., Yim, S. H. L., Lee, G., Ashok, A., Barrett, S. R. H., & Waitz, I. A. (2014). Near-airport distribution of the environmental costs of aviation. *Transport Policy*, *34*, 102–108. https://doi.org/10.1016/j.tranpol.2014.02.023

Wood, S. N. (2003). Thin-plate regression splines. *Journal of the Royal Statistical Society (B)*, *65*(1), 95–114.

Wood, S. N. (2017). *Generalized Additive Models: An Introduction with R* (Vol. 2). Chapman; Hall/CRC.

Woody, M. C., Wong, H. .-.-W., West, J. J., & Arunachalam, S. (2016). Multiscale predictions of aviation-attributable PM2.5 for U.S. airports modeled using CMAQ with plume-in-grid and an aircraft-specific 1-D emission model. *Atmospheric Environment*, *147*, 384–394. https://doi.org/10.1016/j.atmosenv.2016.10.016

Wu, H., Tang, X., Wang, Z., Wu, L., Lu, M., Wei, L., & Zhu, J. (2018). Probabilistic Automatic Outlier Detection for Surface Air Quality Measurements from the China National Environmental Monitoring Network. *Advances in Atmospheric Sciences*, *35*(12), 1522–1532. https://doi.org/10.1007/s00376-018-8067-9

Yim, S. H. L., Lee, G. L., Lee, I. H., Allroggen, F., Ashok, A., Caiazzo, F., Eastham, S. D., Malina, R., & Barrett, S. R. H. (2015). Global, regional and local health impacts of civil aviation emissions [Publisher: IOP Publishing]. *Environmental Research Letters*, *10*(3), 034001. https://doi.org/10.1088/1748-9326/10/3/034001

Yu, K. N., Cheung, Y. P., Cheung, T., & Henry, R. C. (2004). Identifying the impact of large urban airports on local air quality by nonparametric regression. *Atmospheric Environment*, *38*(27), 4501–4507. https://doi.org/10.1016/j.atmosenv.2004.05.034

Zuur, A., Ieno, E. N., Walker, N., Saveliev, A. A., & Smith, G. M. (2009). *Mixed Effects Models and Extensions in Ecology with R* [Google-Books-ID: vQUNprFZKHsC]. Springer Science & Business Media.

A

An example data set

This appendix shows an example data set. The data shown in table A.1 shows data from January 1st, 2018. Similar data sets are also used for the regression modelling from chapter 6. The measurements shown for CO are taken at monitoring site Badhoevedorp. The meteorological data originates from the KNMI station mentioned in section 3.2.

Table A.1: Example data frame for measurements of carbon monoxide,

Timestamp measured	Measured concentration [$\mu g/m^3$]	A4	A5	A9	Take-offs	Landings	Windx [m/s]	Windy [m/s]	Wind speed [m/s]	Wind direction [°]	T [°C]	Precipitation [mm]
2018-01-01 01:00:00+00:00	206.7	1170	354	653	0.0	2.0	-6.5	-11.26	13.0	210.0	8.0	0.5
2018-01-01 02:00:00+00:00	201.0	3474	1578	2566	0.0	1.0	-9.19	-7.71	12.0	230.0	7.9	0.5
2018-01-01 03:00:00+00:00	177.0	3169	1276	2063	0.0	1.0	-12.8	-2.26	13.0	260.0	7.8	0.5
2018-01-01 04:00:00+00:00	166.4	1865	643	1014	0.0	2.0	-10.34	-3.76	11.0	250.0	7.7	0.5
2018-01-01 05:00:00+00:00	170.2	1256	421	740	0.0	11.0	-10.34	-3.76	11.0	250.0	7.3	0.0
2018-01-01 06:00:00+00:00	170.4	1126	408	751	9.0	12.0	-7.79	-4.5	9.0	240.0	6.7	0.0
2018-01-01 07:00:00+00:00	207.1	1208	399	789	29.0	35.0	-5.14	-6.13	8.0	220.0	5.9	0.0
2018-01-01 08:00:00+00:00	254.6	1116	321	860	18.0	47.0	-4.0	-6.93	8.0	210.0	6.0	0.0
2018-01-01 09:00:00+00:00	219.5	1027	312	744	31.0	21.0	-4.5	-7.79	9.0	210.0	6.6	0.0
2018-01-01 10:00:00+00:00	211.3	1133	427	1036	50.0	29.0	-5.0	-8.66	10.0	210.0	6.8	0.0
2018-01-01 11:00:00+00:00	226.2	1960	904	1994	31.0	28.0	-4.5	-7.79	9.0	210.0	7.2	0.0
2018-01-01 12:00:00+00:00	231.7	3227	1640	3506	38.0	31.0	-4.5	-7.79	9.0	210.0	7.3	0.0
2018-01-01 13:00:00+00:00	268.6	4925	2537	5286	37.0	26.0	-2.39	-6.58	7.0	200.0	6.7	0.0
2018-01-01 14:00:00+00:00	288.4	6362	3548	6650	36.0	22.0	-2.05	-5.64	6.0	200.0	6.9	0.0
2018-01-01 15:00:00+00:00	278.9	7338	3965	7610	30.0	35.0	-0.87	-4.92	5.0	190.0	6.9	0.0
2018-01-01 16:00:00+00:00	310.3	7315	3897	7304	32.0	22.0	0.52	-2.95	3.0	170.0	6.9	0.5
2018-01-01 17:00:00+00:00	322.8	6498	3379	6386	32.0	19.0	-0.52	-2.95	3.0	190.0	6.3	2.0
2018-01-01 18:00:00+00:00	292.7	5277	2543	4972	14.0	40.0	-2.3	-1.93	3.0	230.0	6.0	3.0
2018-01-01 19:00:00+00:00	304.8	4243	1863	3342	25.0	45.0	-2.82	-1.03	3.0	250.0	6.1	1.0
2018-01-01 20:00:00+00:00	268.0	4176	2034	3321	23.0	26.0	-3.46	-2.0	4.0	240.0	6.4	0.5
2018-01-01 21:00:00+00:00	267.0	4097	1961	3072	57.0	17.0	-3.46	-2.0	4.0	240.0	6.7	0.5
2018-01-01 22:00:00+00:00	242.5	3242	1541	2390	13.0	20.0	-4.92	-0.87	5.0	260.0	6.8	0.0
2018-01-01 23:00:00+00:00	213.6	2799	1208	1694	0.0	8.0	-4.7	-1.71	5.0	250.0	6.9	1.0
2018-01-02 00:00:00+00:00	195.4	1696	644	1026	0.0	2.0	-5.0	-0.0	5.0	270.0	5.6	3.0
2018-01-02 01:00:00+00:00	191.8	861	333	527	1.0	0.0	-2.6	-1.5	3.0	240.0	5.2	1.0
2018-01-02 02:00:00+00:00	193.4	579	218	287	0.0	0.0	-3.94	-0.69	4.0	260.0	4.2	0.0
2018-01-02 03:00:00+00:00	196.9	335	158	191	0.0	2.0	-3.94	-0.69	4.0	260.0	5.5	0.5
2018-01-02 04:00:00+00:00	210.5	369	214	282	0.0	3.0	-4.0	-0.0	4.0	270.0	6.2	2.0
2018-01-02 05:00:00+00:00	238.2	694	489	601	1.0	11.0	-5.64	2.05	6.0	290.0	6.6	5.0
2018-01-02 06:00:00+00:00	208.1	1498	1251	1530	6.0	15.0	-6.89	1.22	7.0	280.0	6.2	0.0
2018-01-02 07:00:00+00:00	228.8	4467	3398	4320	31.0	35.0	-5.64	2.05	6.0	290.0	6.3	0.0
2018-01-02 08:00:00+00:00	244.4	8478	4742	7621	26.0	53.0	-5.91	1.04	6.0	280.0	6.0	3.0

B

Hourly polar plots

This appendix is an addition to the time sensitivity analysis presented in section 5.1.1. All figures in this appendix show the hourly variations of the correlation between observed pollution levels and wind parameters. As a result, this appendix contains 12 figures with 24 graphs each. These graphs need to be read from top left to bottom right as you would read normally from left to right and top to bottom. The top left graph in each figure shows the results for measurements taken at 1am, then the second graph on the top row shows the results for 2am, etc.

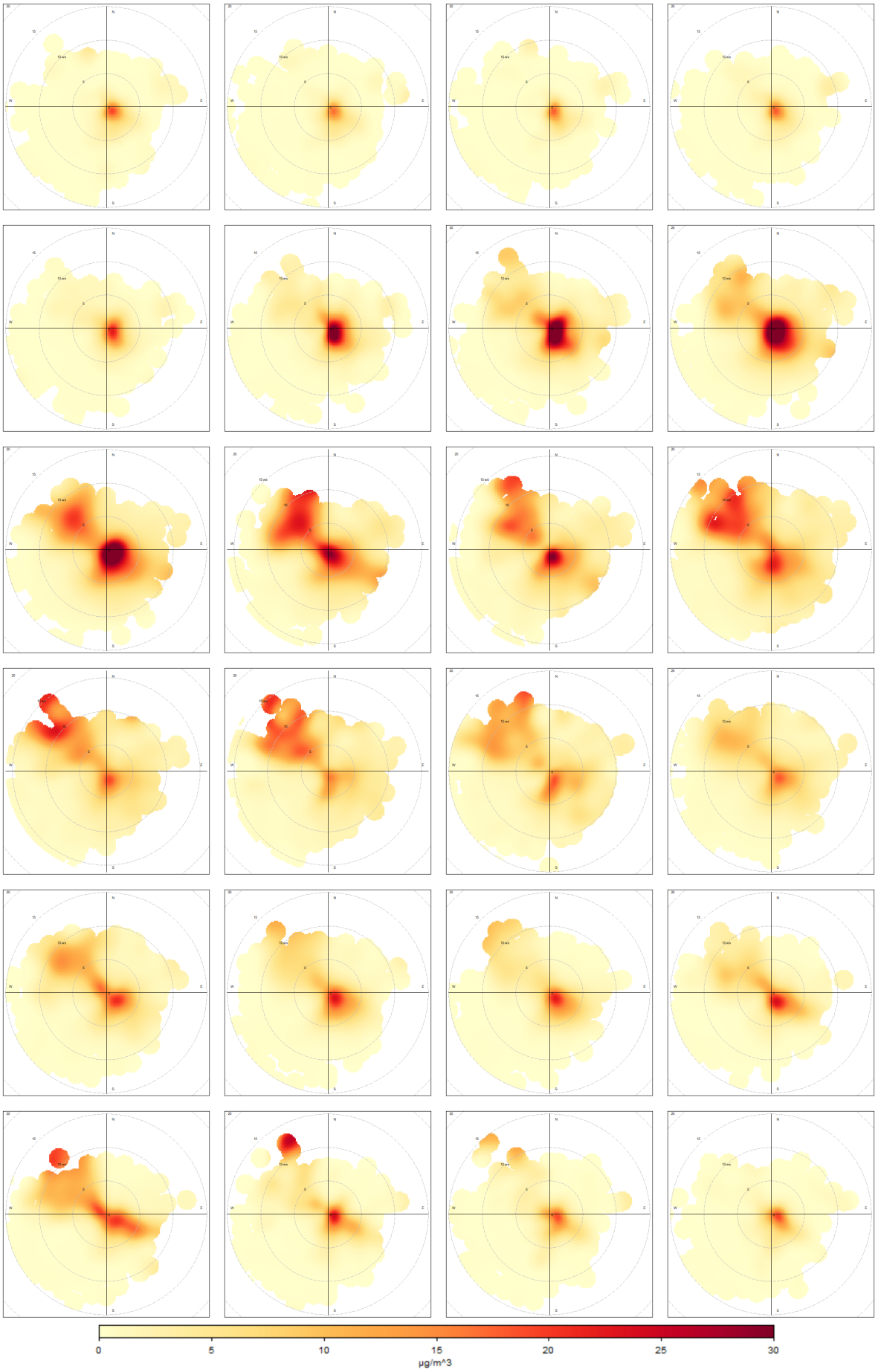

Figure B.1: Hoofddorp - NO

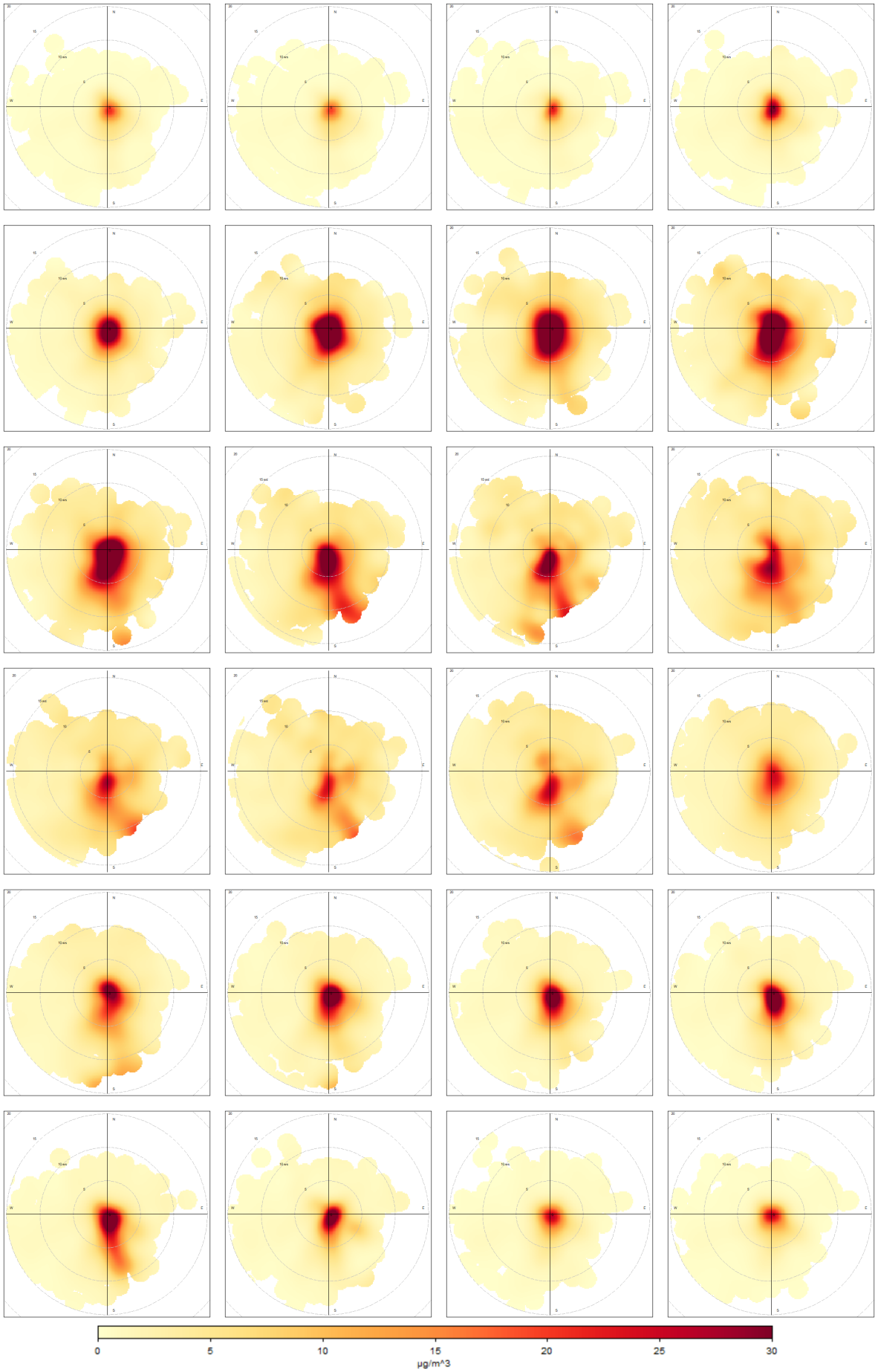

Figure B.2: Badhoevedorp - NO

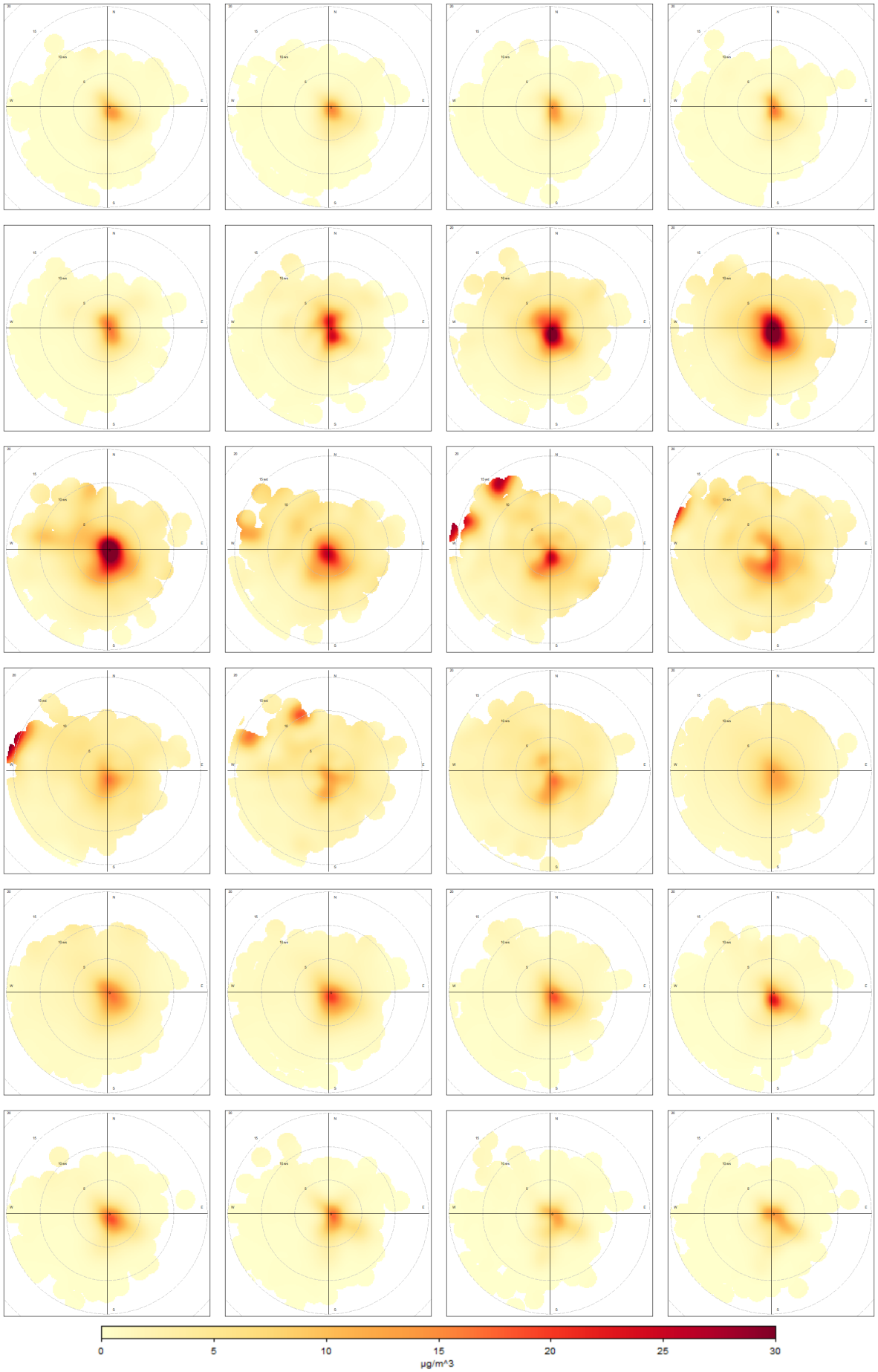

Figure B.3: Oude Meer - NO

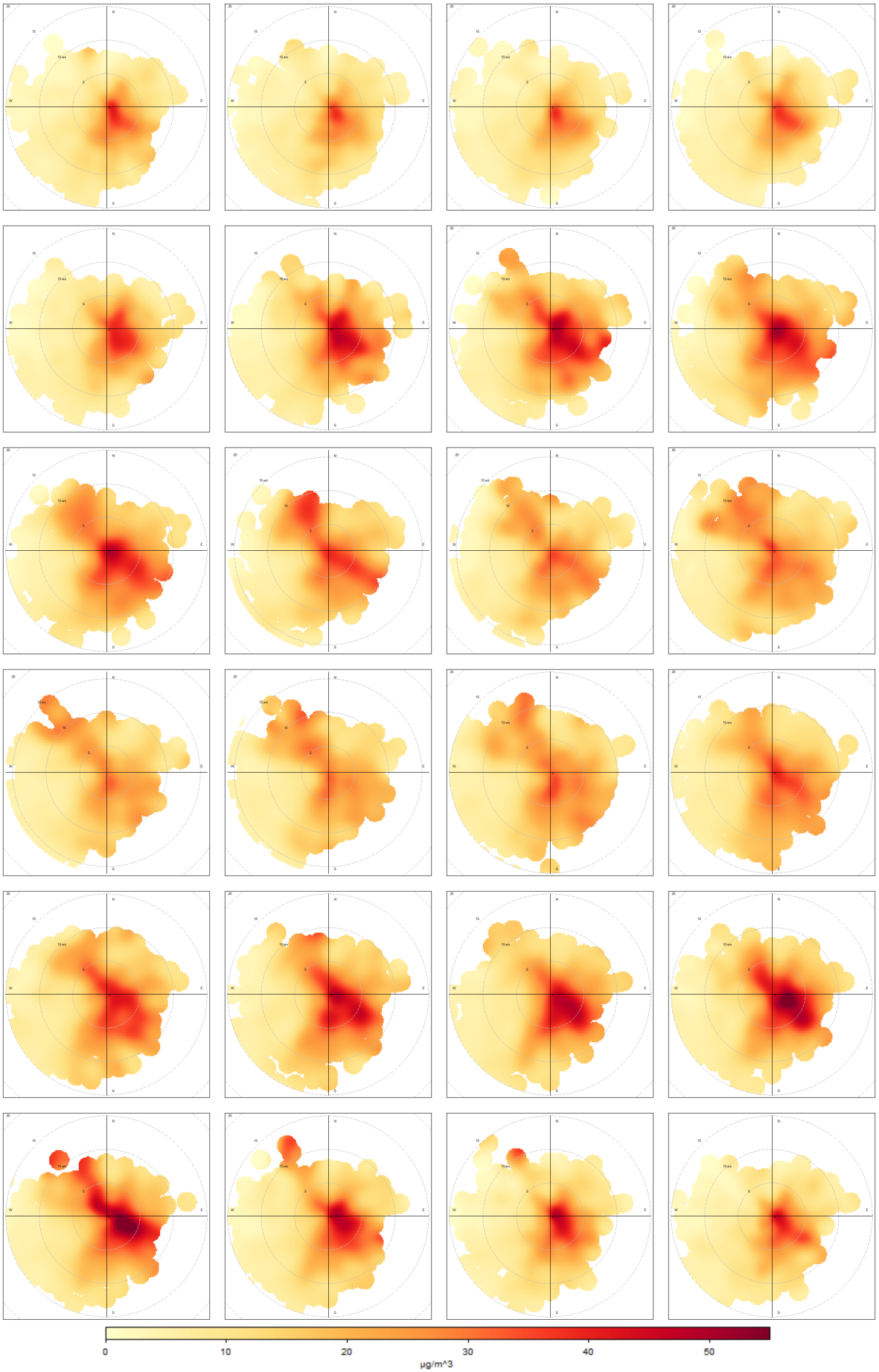

Figure B.4: Hoofddorp - NO_2

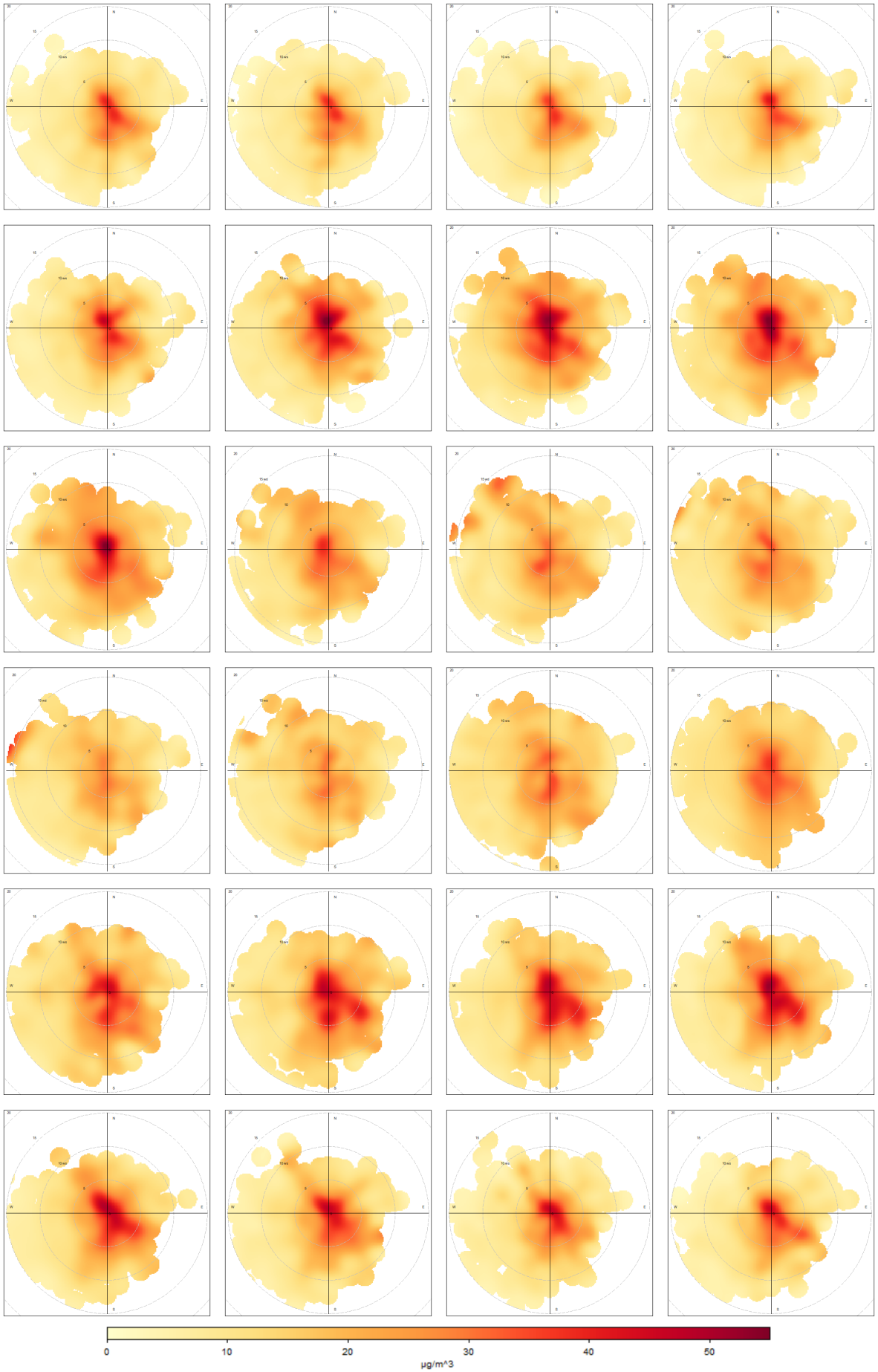

Figure B.5: Badhoevedorp - NO_2

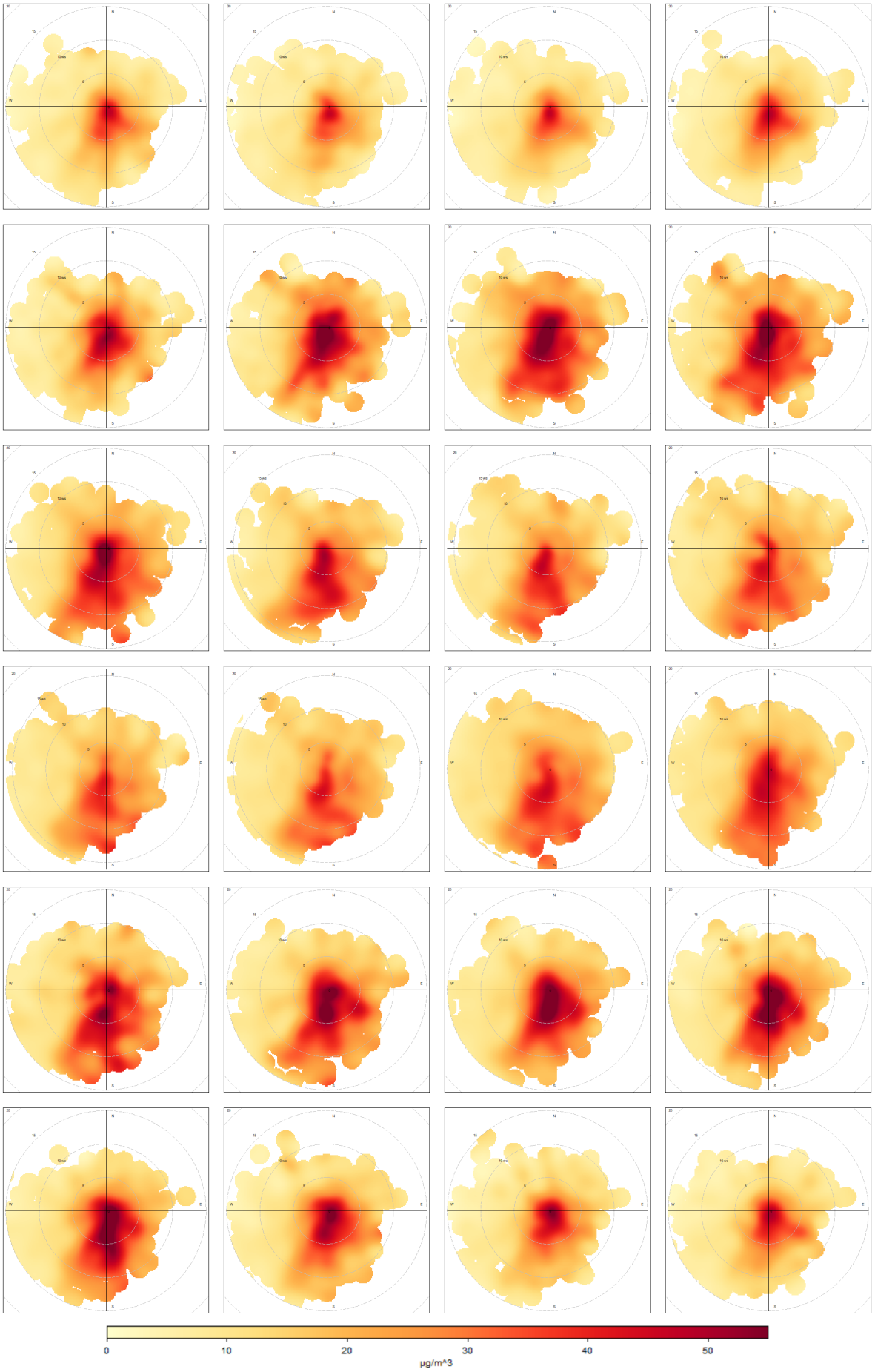

Figure B.6: Oude Meer - NO_2

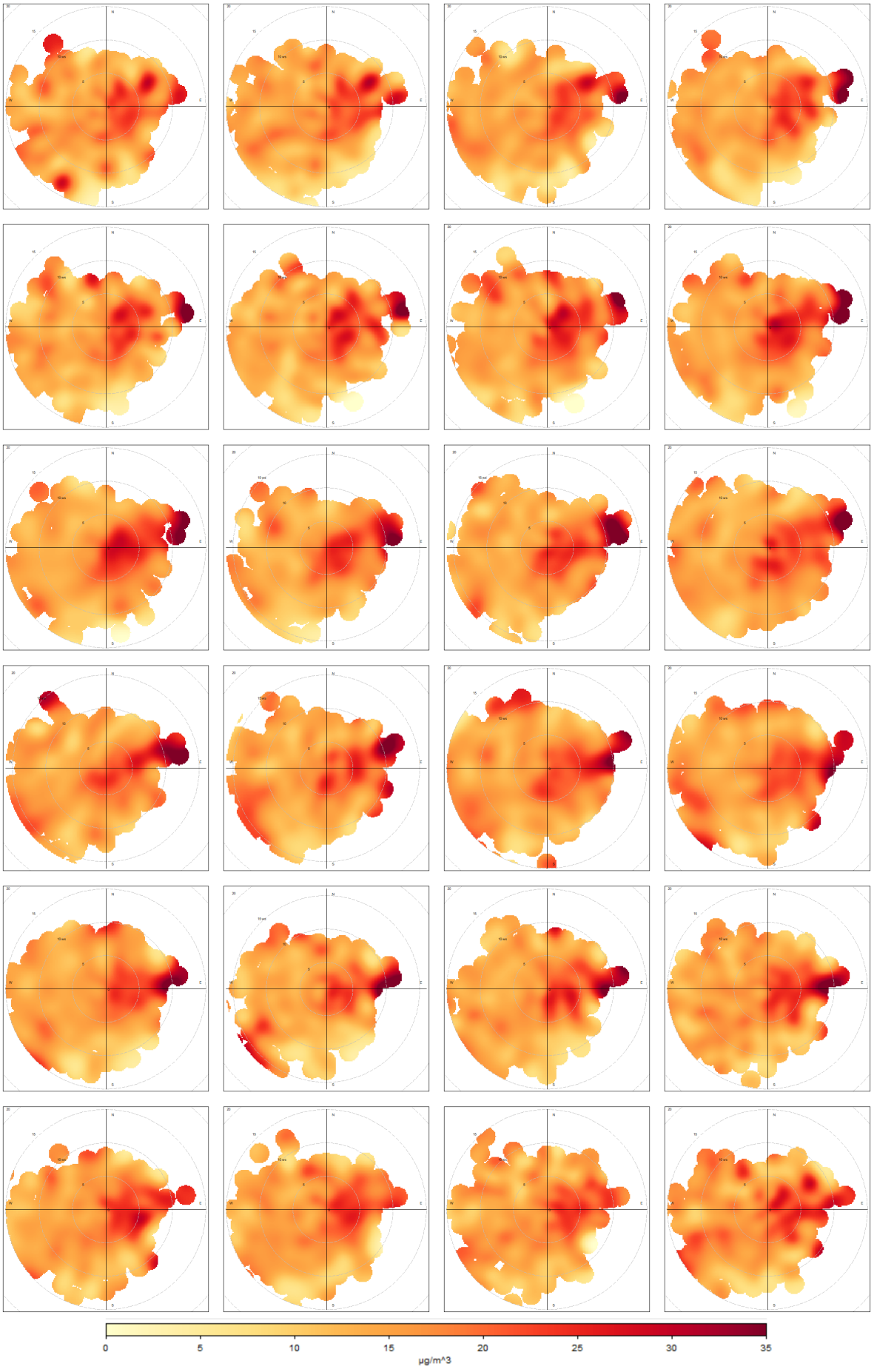

Figure B.7: Hoofddorp - PM_{10}

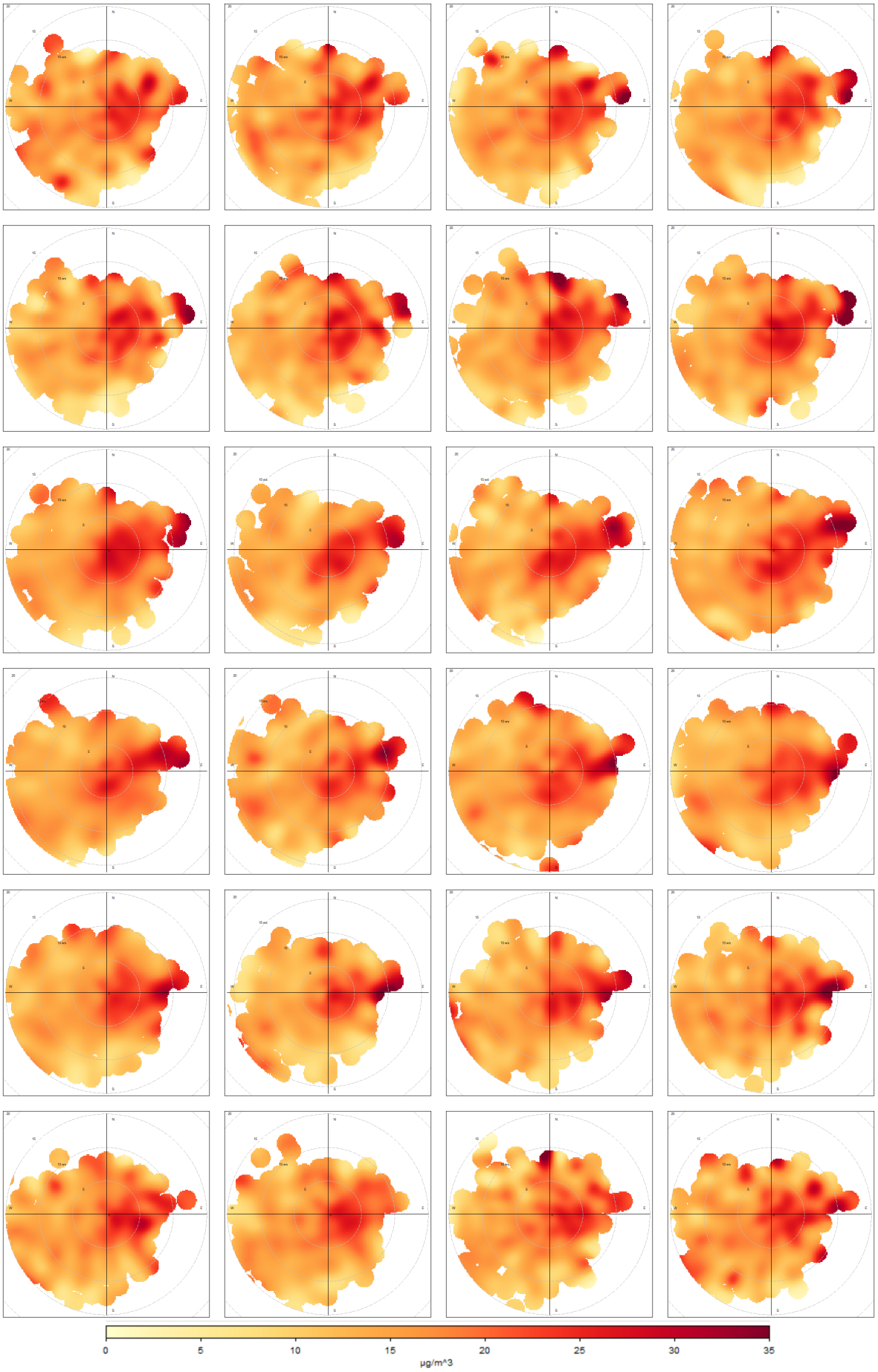

Figure B.8: Oude Meer - PM_{10}

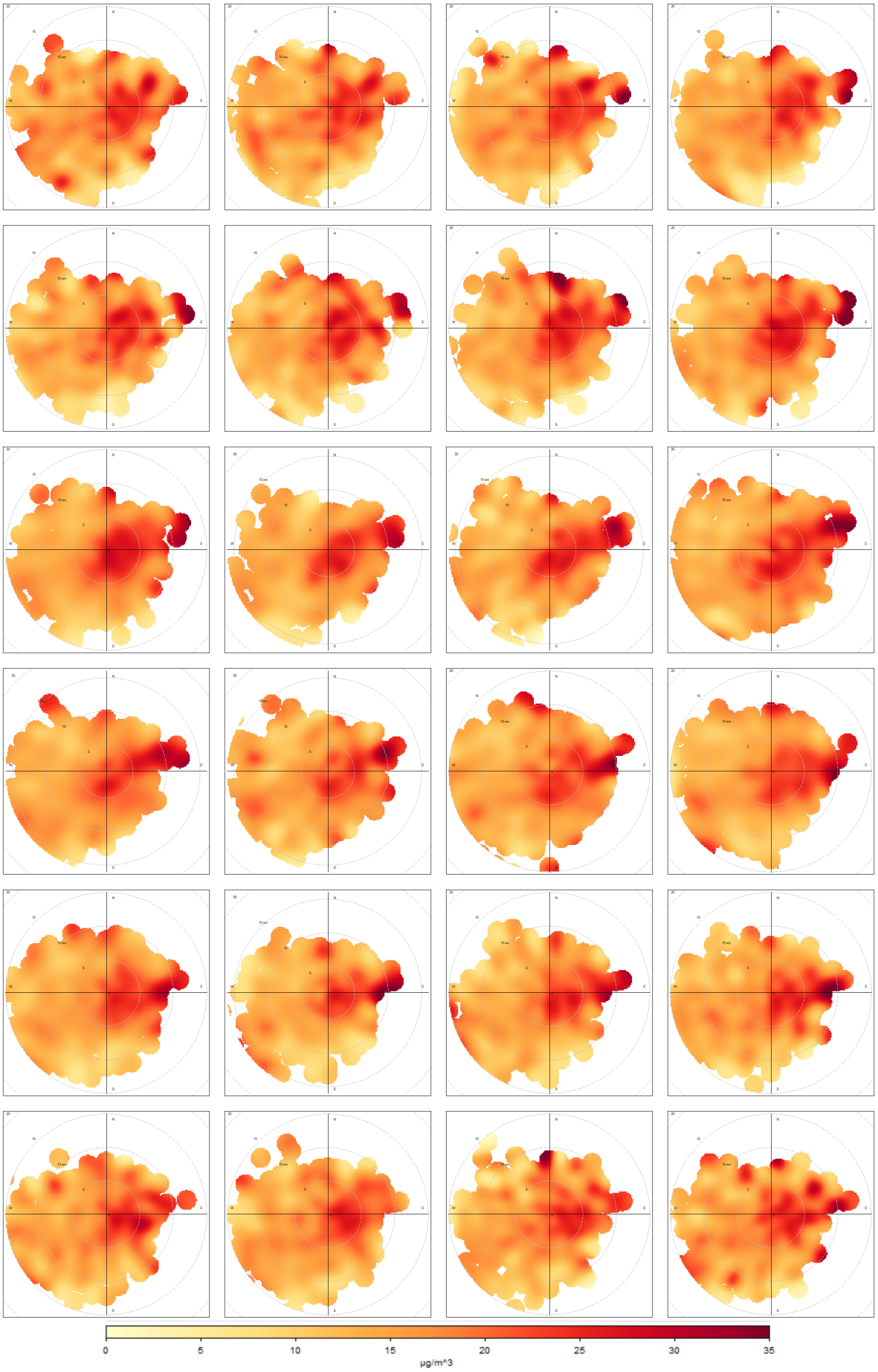

Figure B.9: Badhoevedorp - PM_{10}

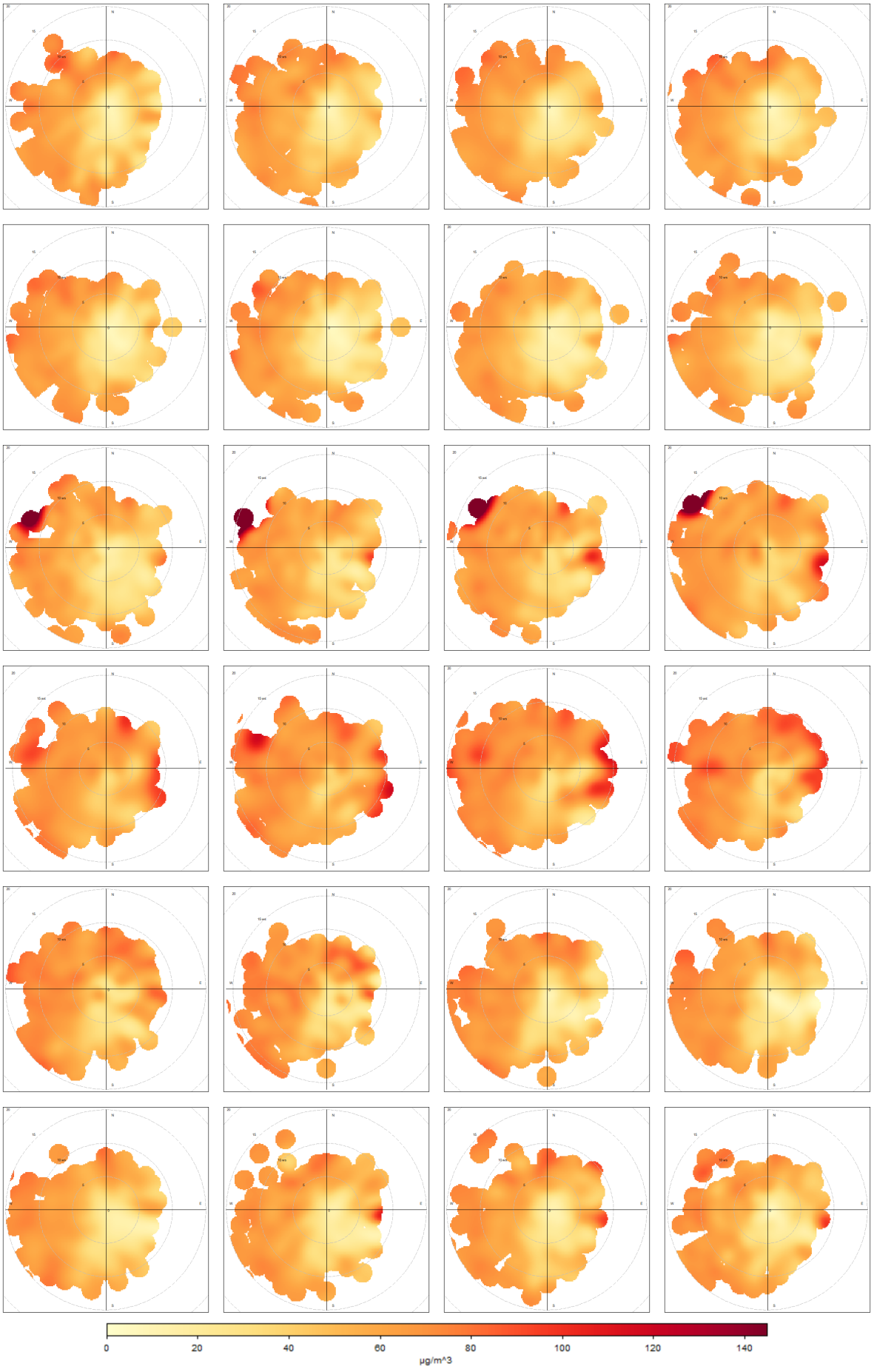

Figure B.10: Hoofddorp - O_3

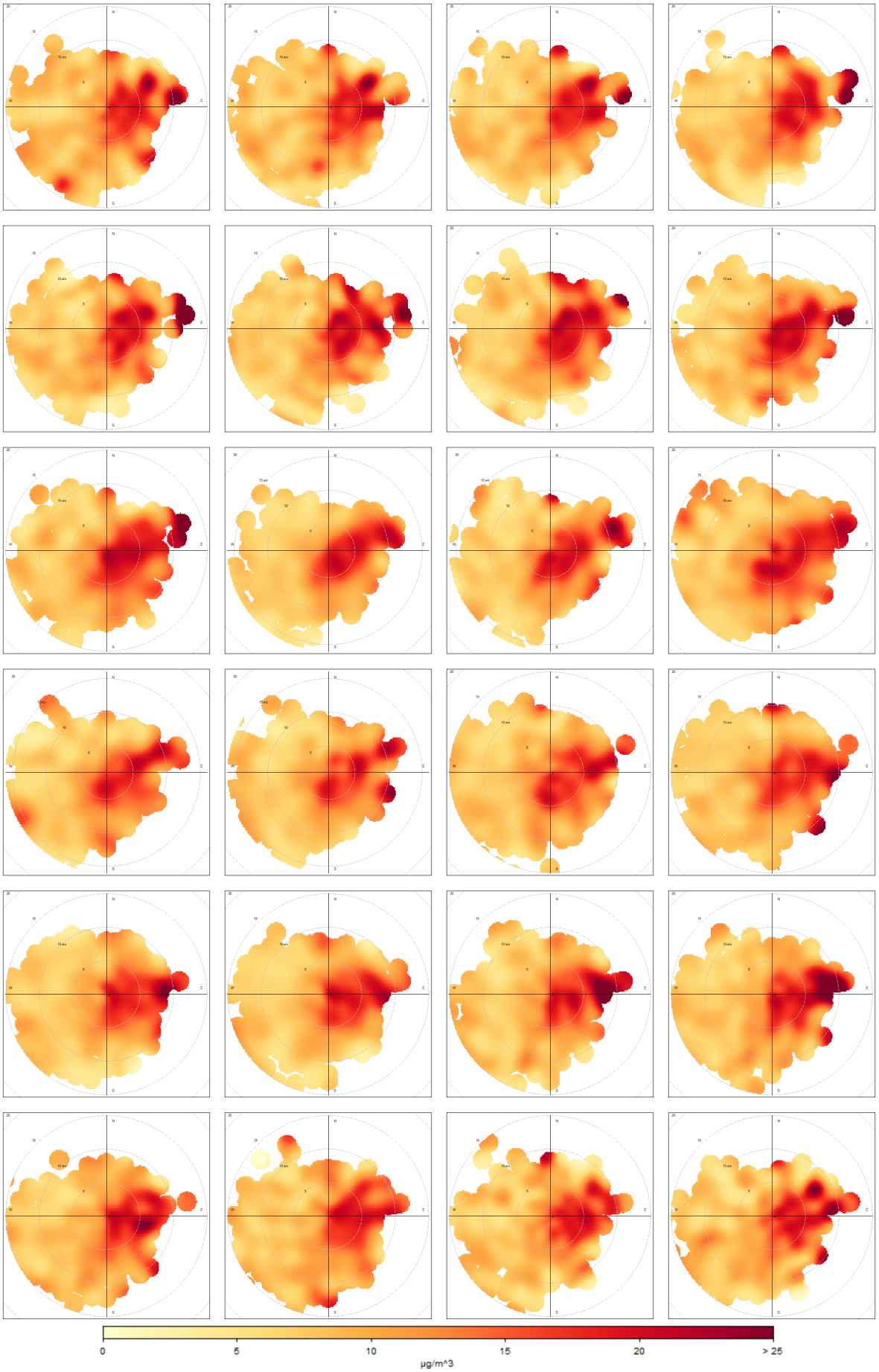

Figure B.11: Badhoevedorp - $PM_{2.5}$

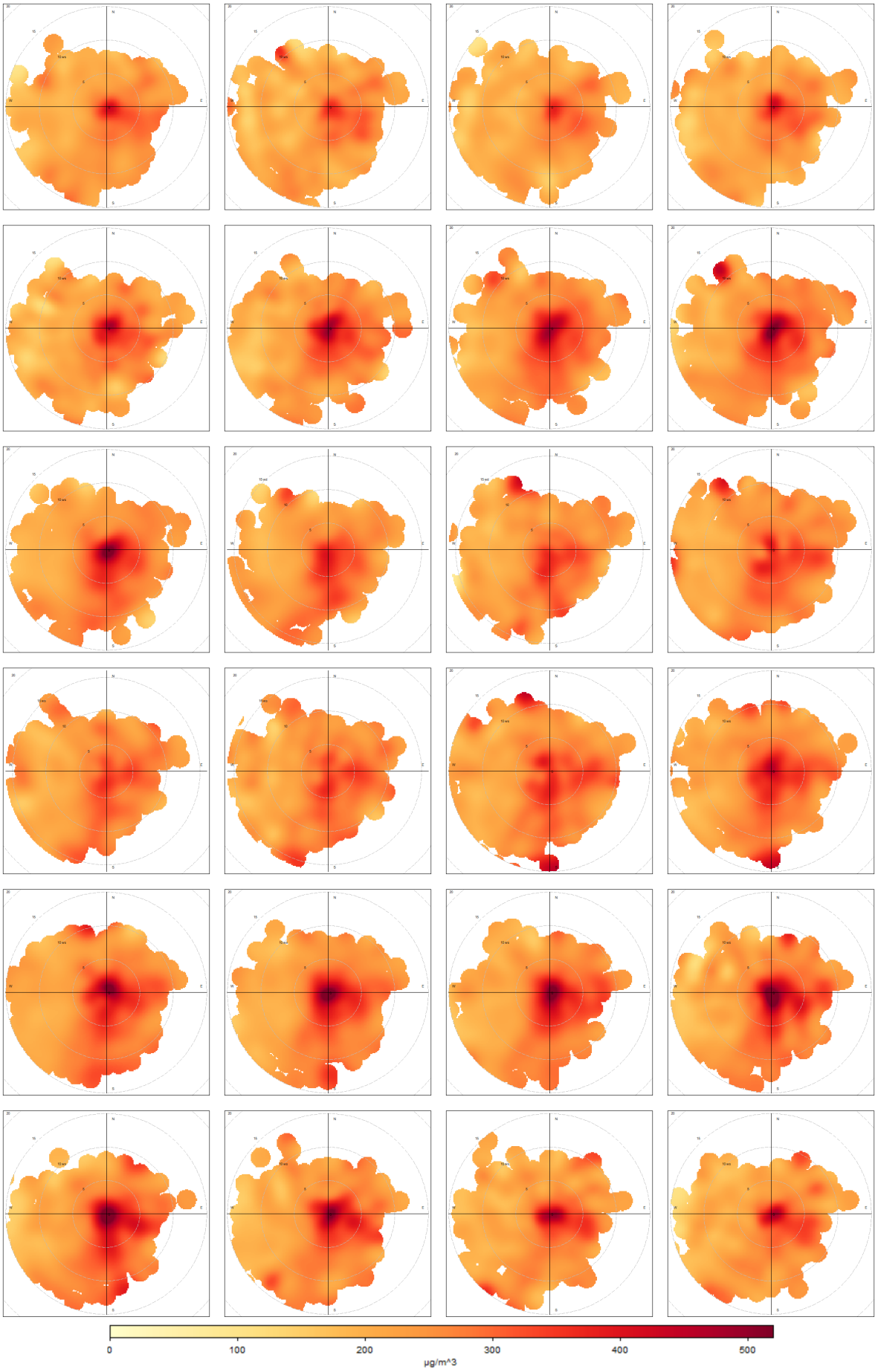

Figure B.12: Badhoevedorp - CO

C

Hourly polar plots with background subtraction

Similar to appendix B, this appendix is an addition to the time sensitivity of the background subtraction graphs from section 5.2.2. All figures in this appendix show the hourly variations of the graphs from that section. As a result, this appendix contains 9 figures with 24 graphs each. These graphs need to be read from top left to bottom right as you would read normally from left to right and top to bottom. The top left graph in each figure shows the results for measurements taken at 1am, then the second graph on the top row shows the results for 2am, etc.

Figure C.1: Hourly variations of NO at Hoofddorp with Oude Meer as background

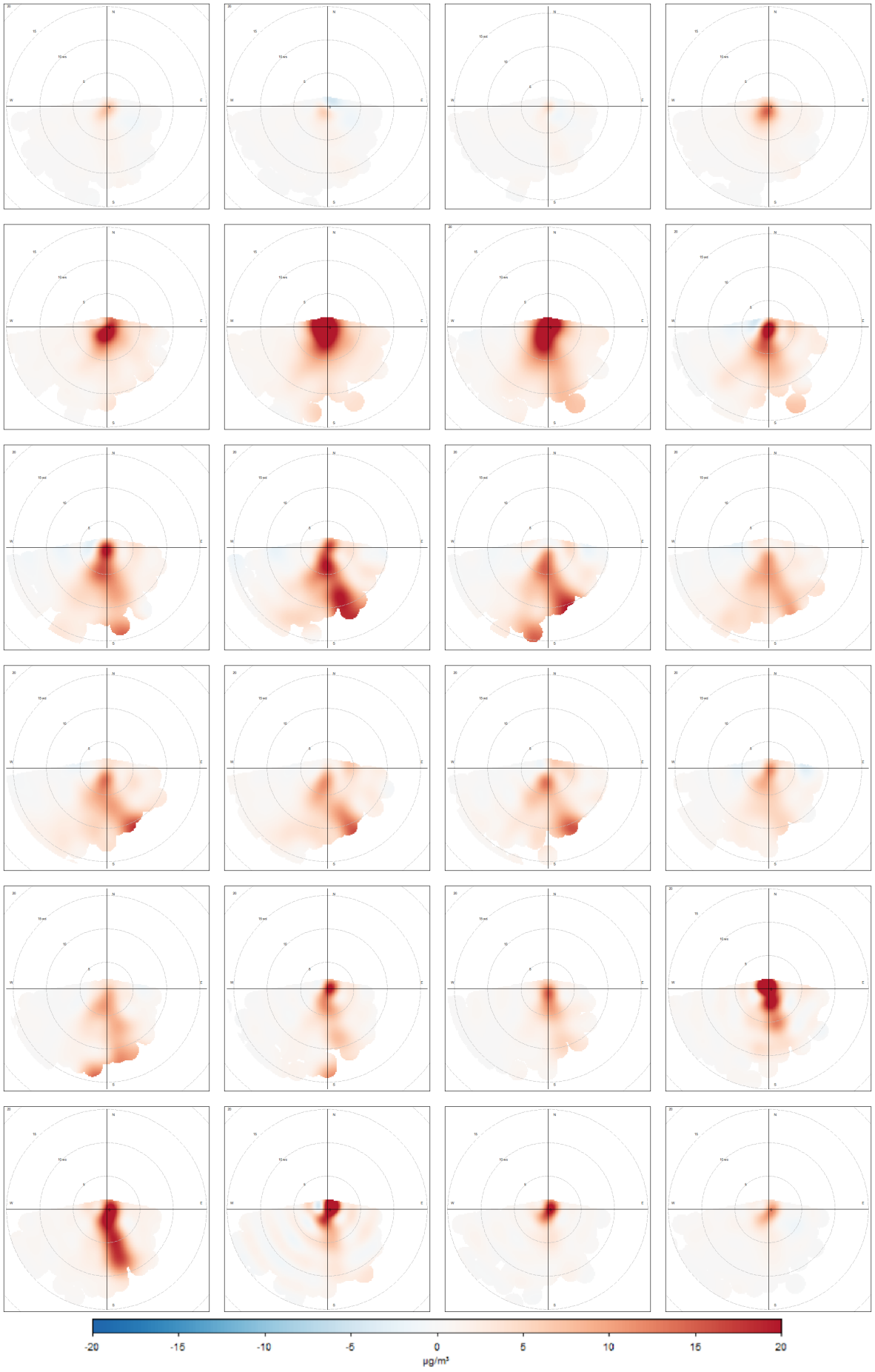

Figure C.2: Hourly variations of NO at Badhoevedorp with Oude Meer as background

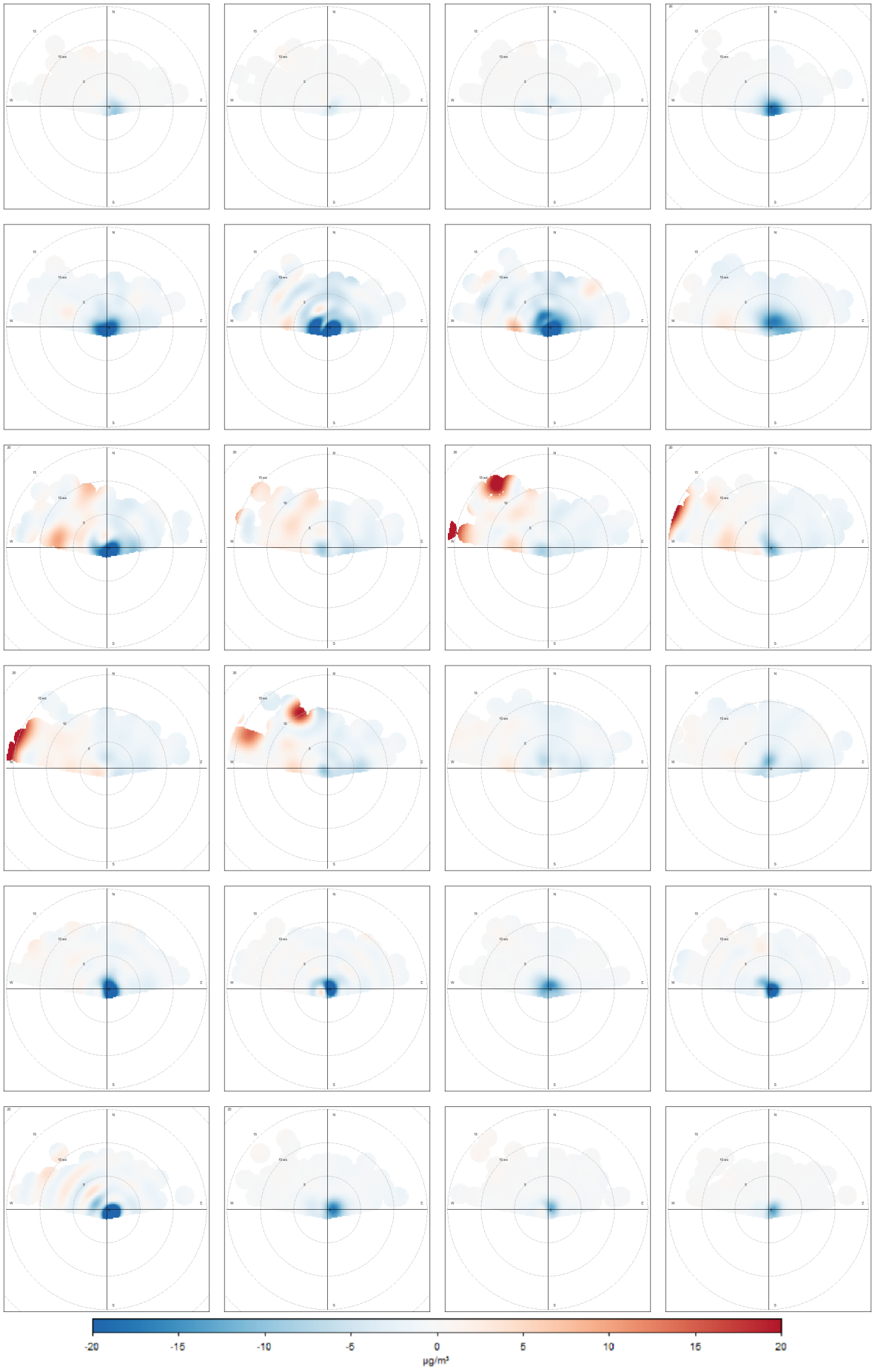

Figure C.3: Hourly variations of NO at Oude Meer with Badhoevedorp as background

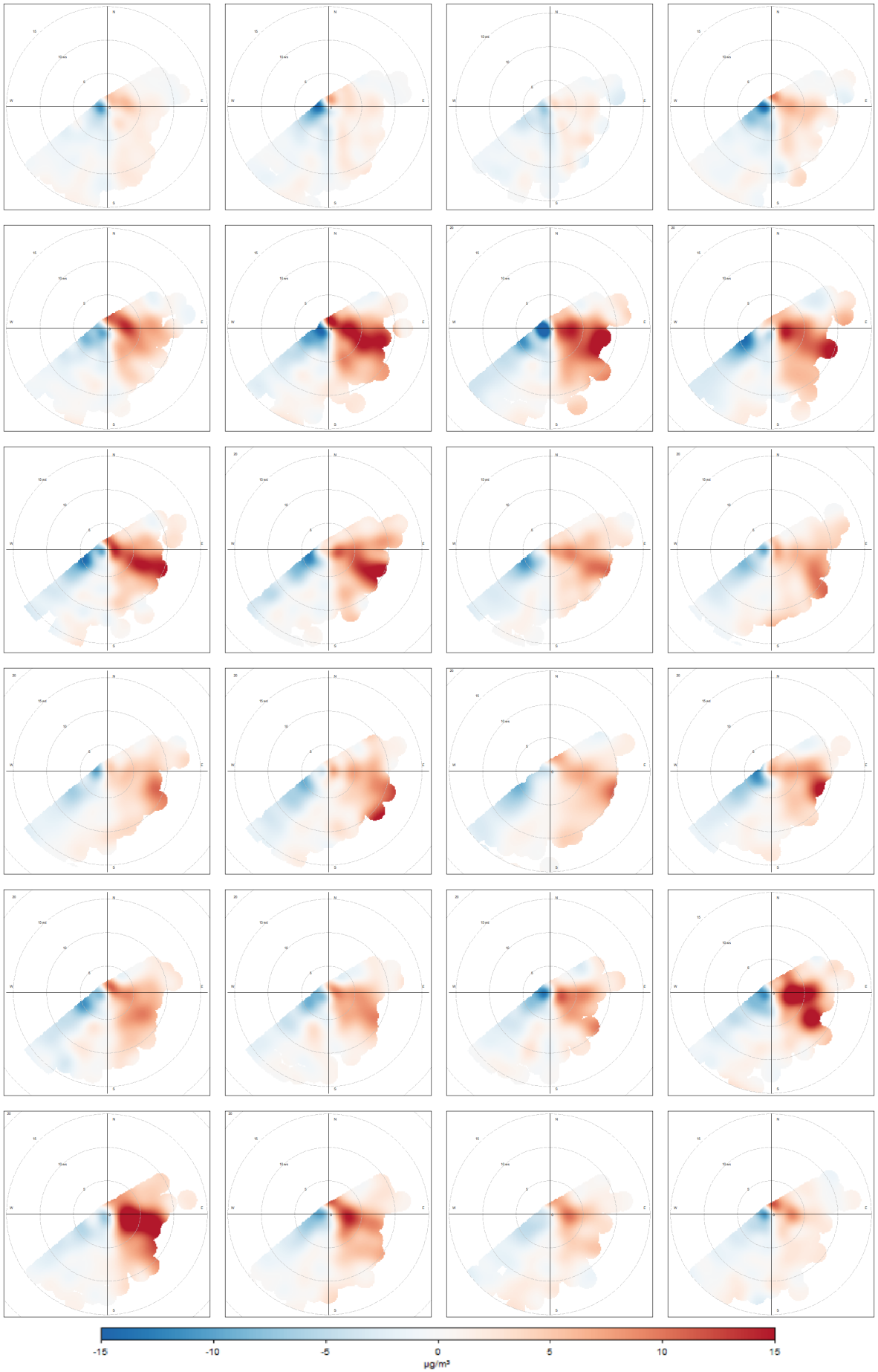

Figure C.4: Hourly variations of NO_2 at Hoofddorp with Oude Meer as background

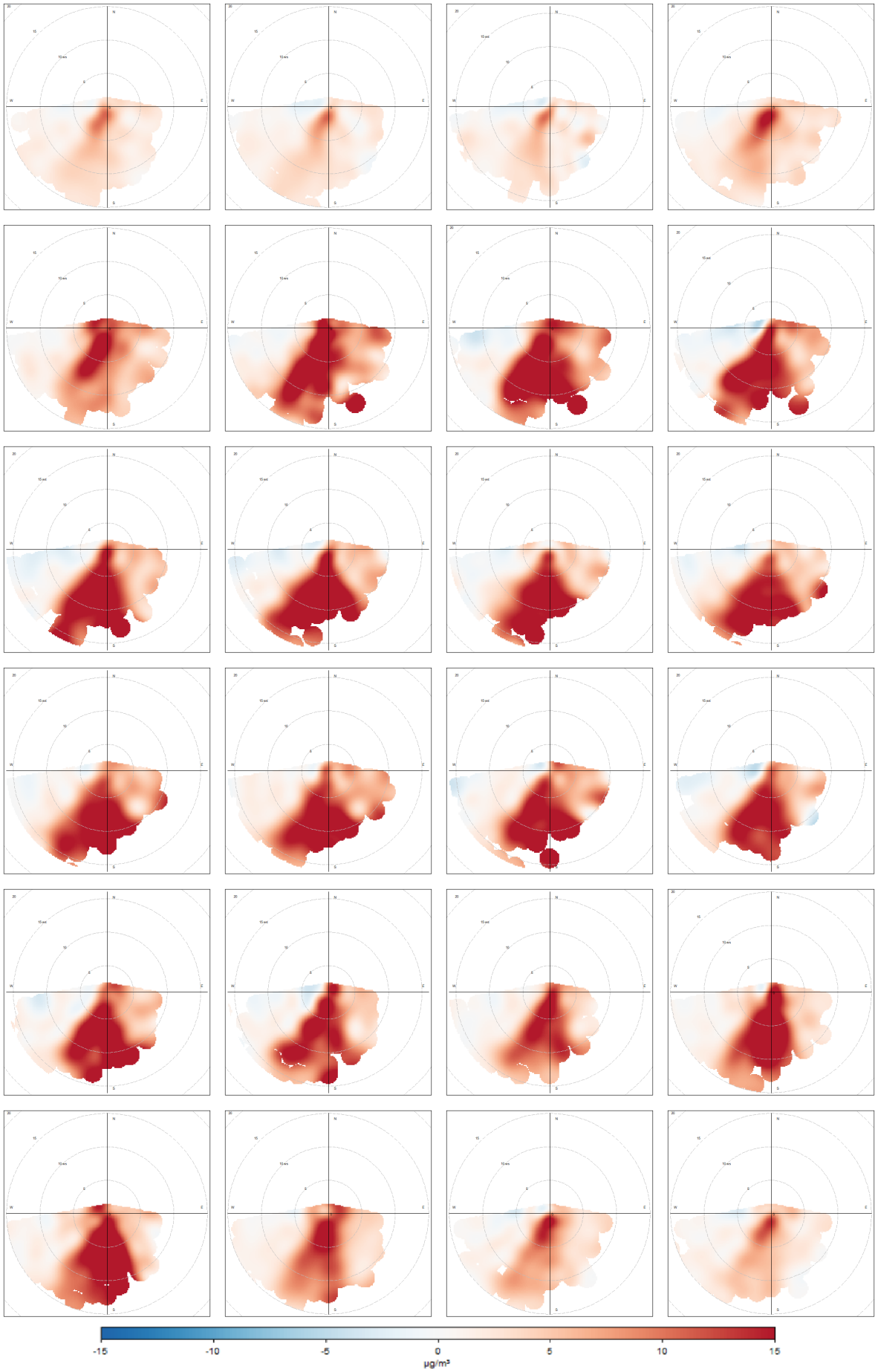

Figure C.5: Hourly variations of NO_2 at Badhoevedorp with Oude Meer as background

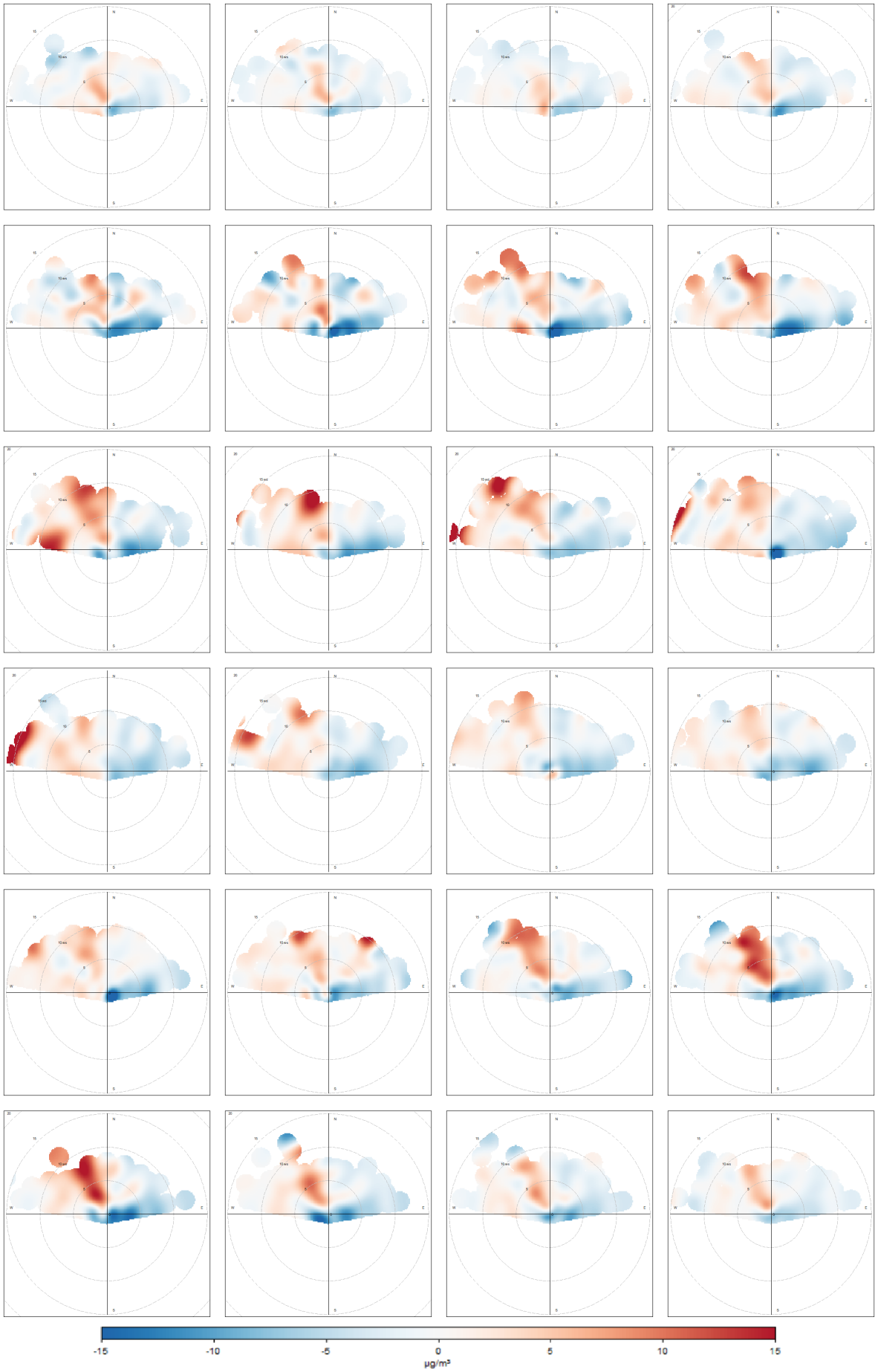

Figure C.6: Hourly variations of NO_2 at Oude Meer with Badhoevedorp as background

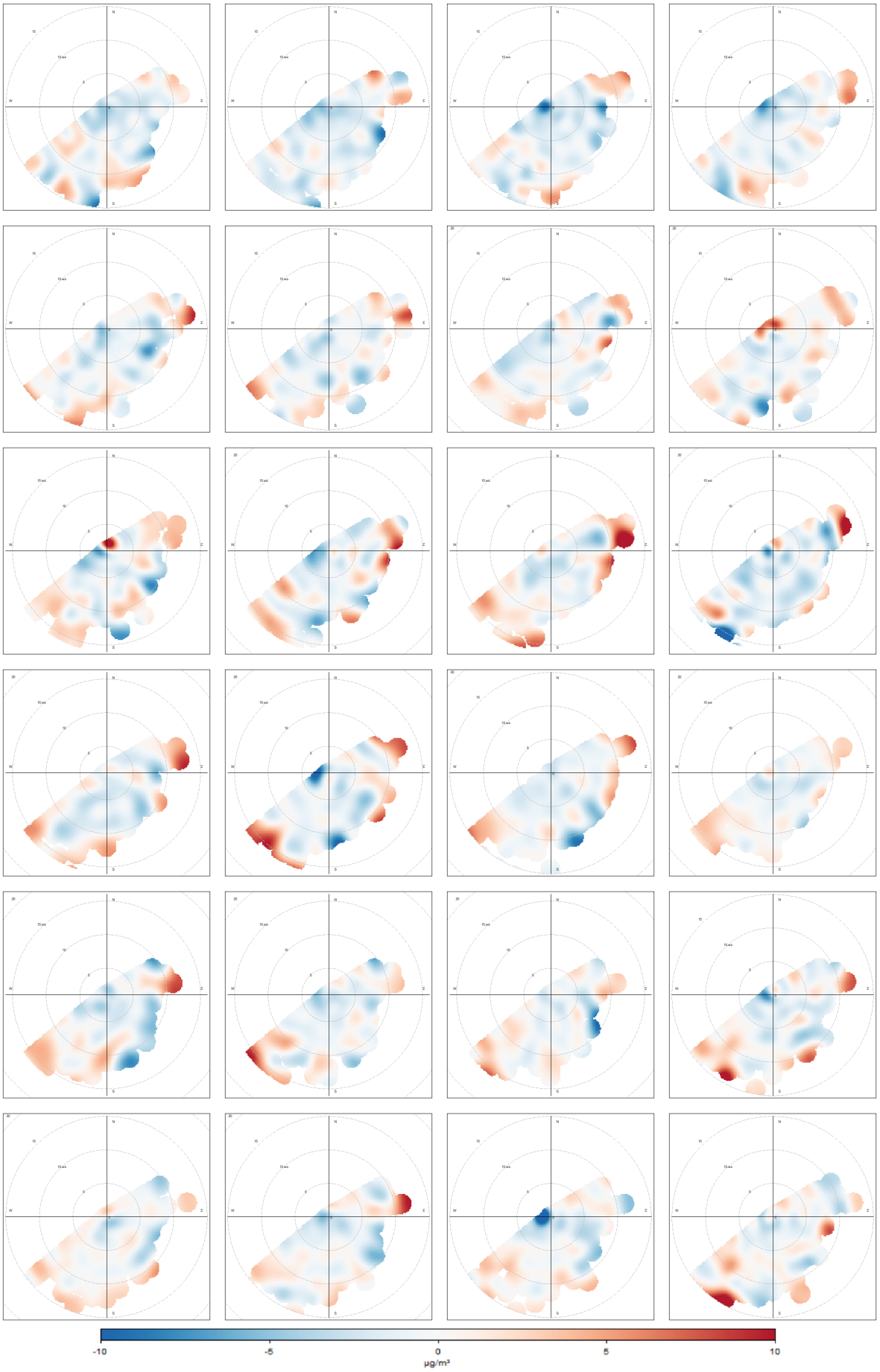

Figure C.7: Hourly variations of PM_{10} at Hoofddorp with Oude Meer as background

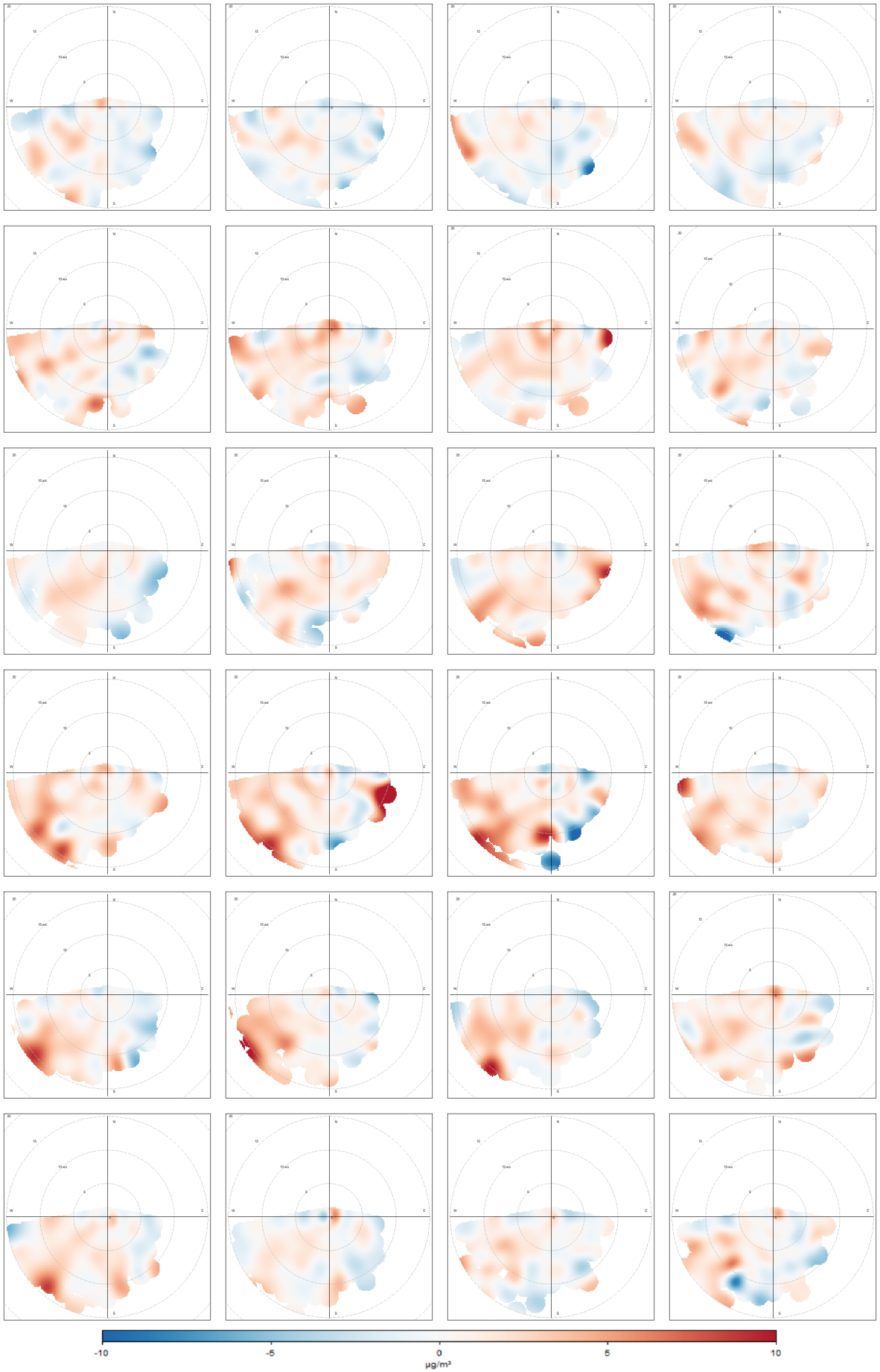

Figure C.8: Hourly variations of PM_{10} at Badhoevedorp with Oude Meer as background

Figure C.9: Hourly variations of PM_{10} at Oude Meer with Badhoevedorp as background

D

Polar plots with data from March to August 2020

This appendix is an addition to section 7.2. Three different figures are presented here. First, the polar plots with the same scales as those in section 5.1.1 are generated for data from 27 March to 16 August 2020. The second figure shows the same graphs again, but with lower scales. By doing so directions of sources in this new situation can be evaluated. Finally, figured with background subtraction similar to section 5.2.1, but with data from this new situation, is presented.

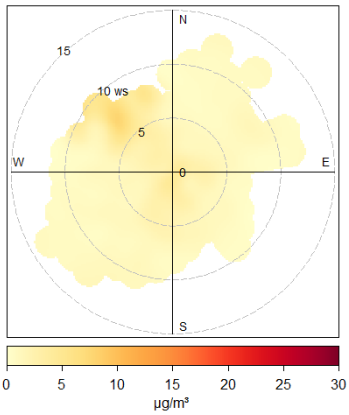

(a) Hoofddorp, NO

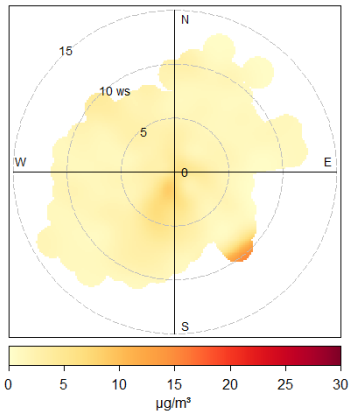

(b) Badhoevedorp, NO

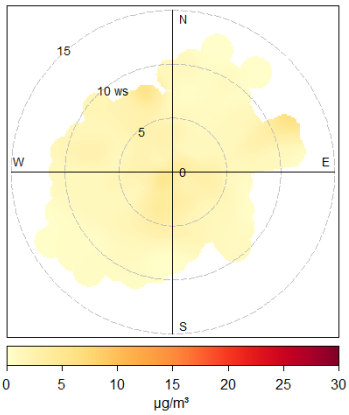

(c) Oude Meer, NO

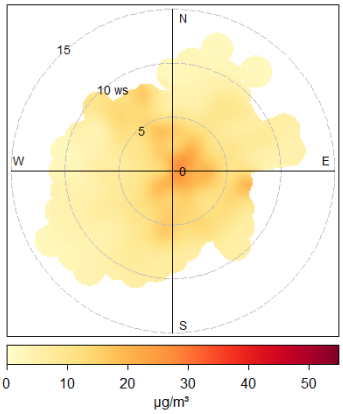

(d) Hoofddorp, NO_2

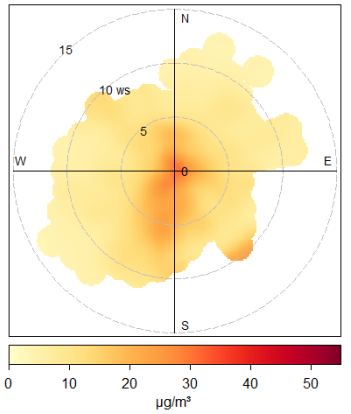

(e) Badhoevedorp, NO_2

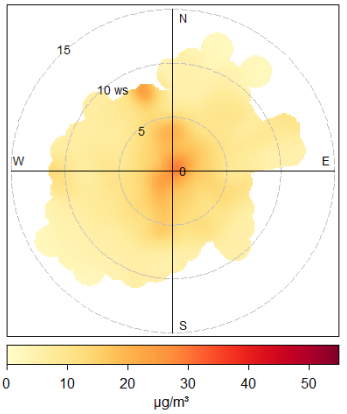

(f) Oude Meer, NO_2

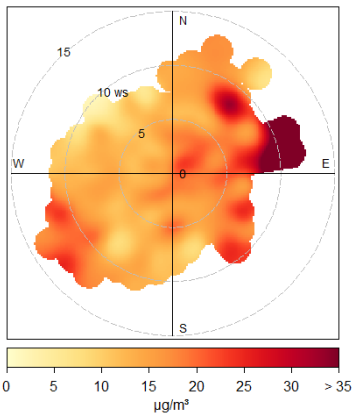

(g) Hoofddorp, PM_{10}

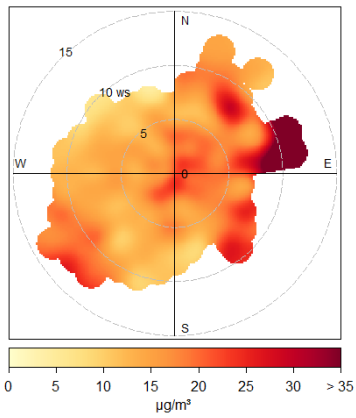

(h) Badhoevedorp, PM_{10}

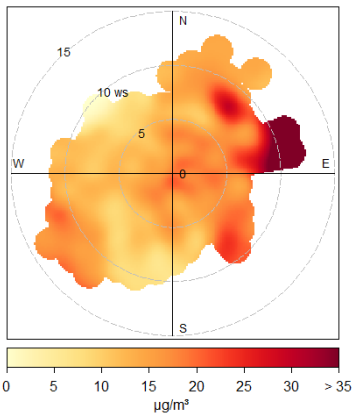

(i) Oude Meer, PM_{10}

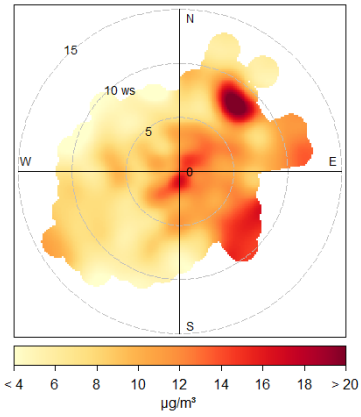

(j) Badhoevedorp, $PM_{2.5}$

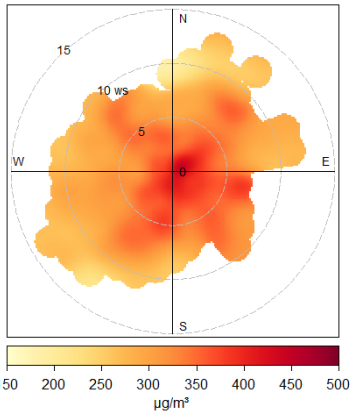

(k) Badhoevedorp, CO

Figure D.1: A graphical representation of wind speed and direction versus the measured pollutant concentrations at various ground stations. All graphs are created using measurements taken between 6am and 10pm from 27 March 2020 until 16 August 2020. The scales are the same as those in section 5.1.1

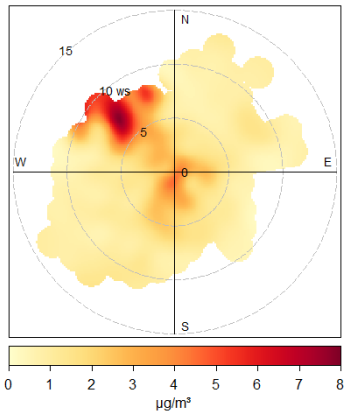

(a) Hoofddorp, NO

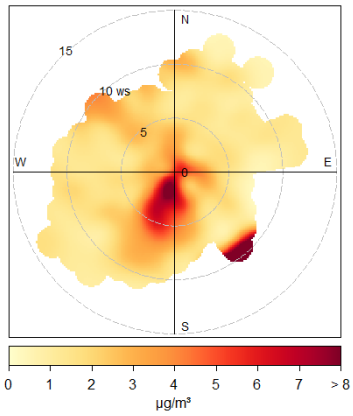

(b) Badhoevedorp, NO

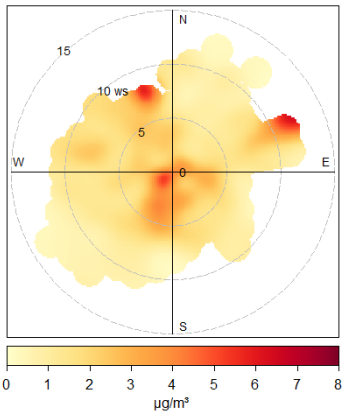

(c) Oude Meer, NO

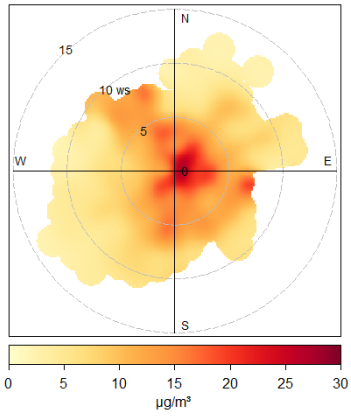

(d) Hoofddorp, NO_2

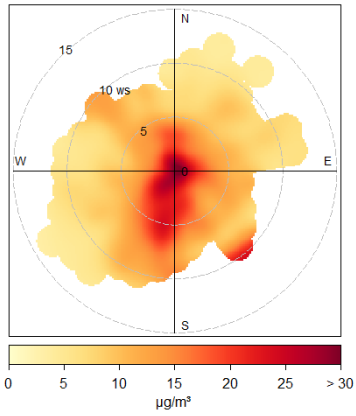

(e) Badhoevedorp, NO_2

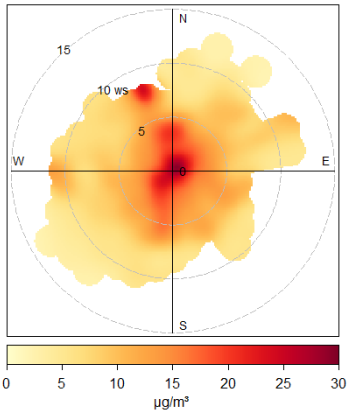

(f) Oude Meer, NO_2

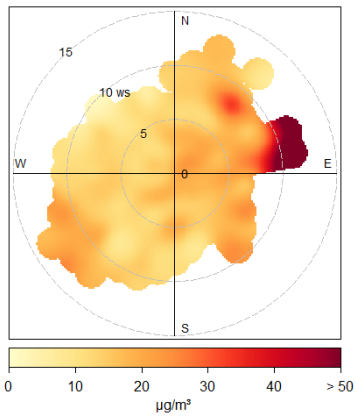

(g) Hoofddorp, PM_{10}

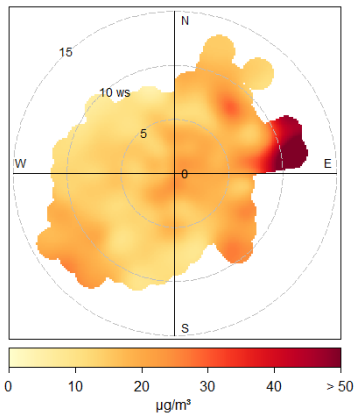

(h) Badhoevedorp, PM_{10}

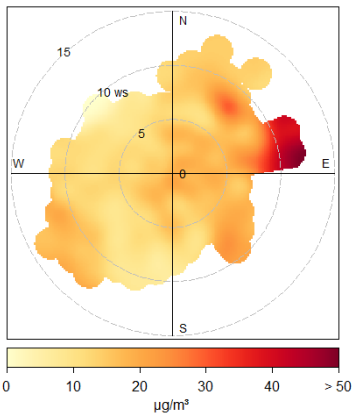

(i) Oude Meer, PM_{10}

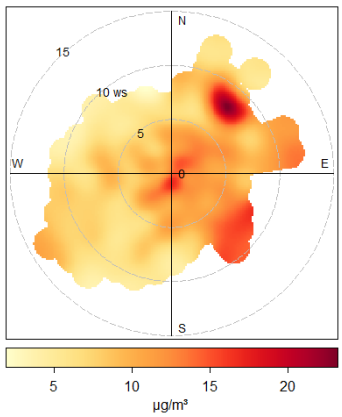

(j) Badhoevedorp, $PM_{2.5}$

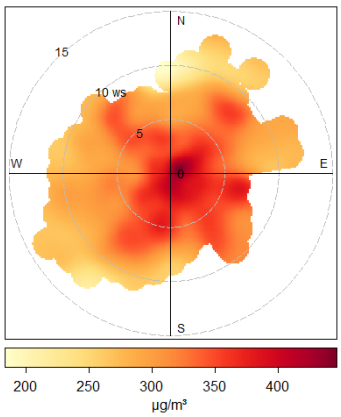

(k) Badhoevedorp, CO

Figure D.2: A graphical representation of wind speed and direction versus the measured pollutant concentrations at various ground stations. All graphs are created using measurements taken between 6am and 10pm from 27 March 2020 until 16 August 2020.

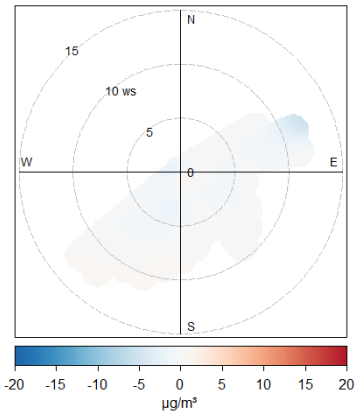

(a) Hoofddorp with background from Oude Meer subtracted, NO

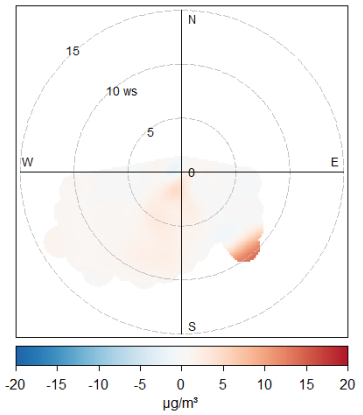

(b) Badhoevedorp with background from Oude Meer subtracted, NO

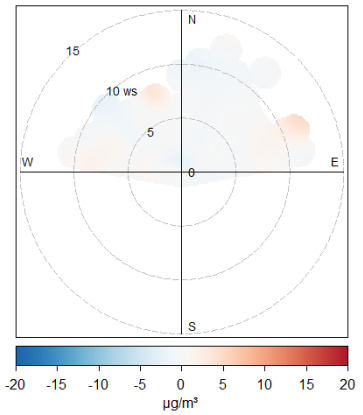

(c) Oude Meer with background from Badhoevedorp subtracted, NO

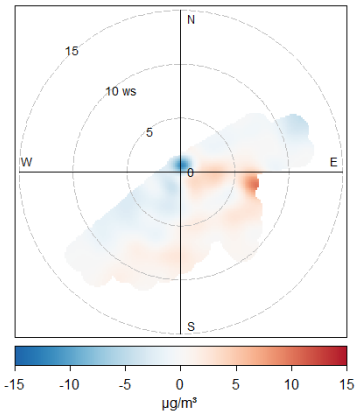

(d) Hoofddorp with background from Oude Meer subtracted, NO_2

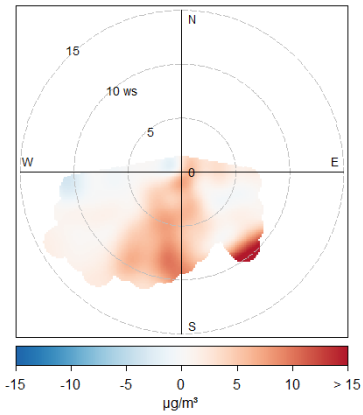

(e) Badhoevedorp with background from Oude Meer subtracted, NO_2

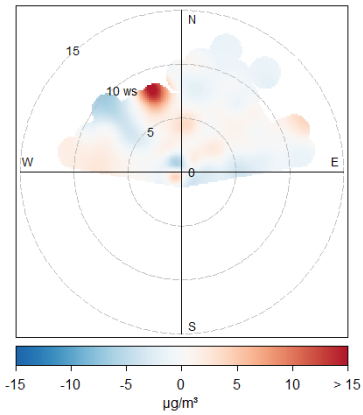

(f) Oude Meer with background from Badhoevedorp subtracted, NO_2

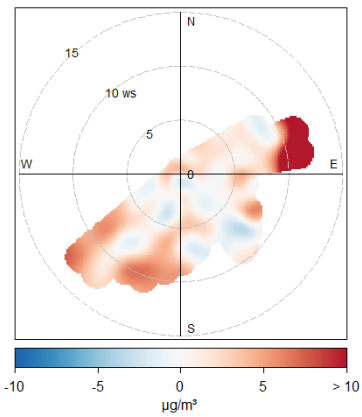

(g) Hoofddorp with background from Oude Meer subtracted, PM_{10}

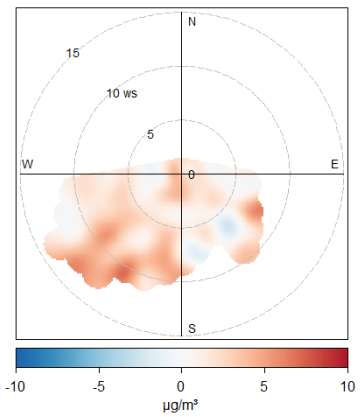

(h) Badhoevedorp with background from Oude Meer subtracted, PM_{10}

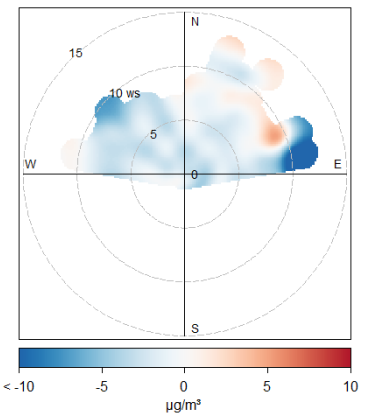

(i) Oude Meer with background from Badhoevedorp subtracted, PM_{10}

Figure D.3: Polar plots with background concentrations subtracted for measurements taken between 6am and 10pm from 27 March 2020 until 16 August 2020.